Master Thesis

Validation of the Suitability of a Zeolite-Salt Composite for its Use in Thermochemical Energy Storage Applications

Providing body:

Chair of Thermal Processing Technology

Submitted by: **Supervisors:**
Christoph Ponak, BSc   Dipl.-Ing. Daniela Meitner
1135277   Univ.Prof. Dipl.-Ing. Dr.techn. Harald Raupenstrauch

Leoben, June 30, 2016

EIDESSTATTLICHE ERKLÄRUNG

Ich erkläre an Eides statt, dass ich diese Arbeit selbstständig verfasst, andere als die angegebenen Quellen und Hilfsmittel nicht benutzt und mich auch sonst keiner unerlaubten Hilfsmittel bedient habe.

AFFIDAVIT

I declare in lieu of oath, that I wrote this thesis and performed the associated research myself, using only literature cited in this volume.

_____   _____

Ort und Datum/Location and date   Unterschrift/Signature

Danksagung

Mein aufrichtiger Dank gilt meiner Betreuerin Dipl.-Ing. Daniela Meitner. Ohne sie wäre diese Arbeit nicht zustande gekommen. Mein Dank gilt ihr nämlich nicht nur für die großartige Betreuung, das Korrekturlesen meiner Arbeit, die Begleitung meiner Forschungstätigkeit und jegliche Hilfestellung dabei, sondern auch dafür, dass sie mich vor mehr als einem Jahr ins Boot geholt hat.

Dieses Boot, der Lehrstuhl für Thermoprozesstechnik an der Montanuniversität Leoben, wird von meinem Begutachter und Betreuer Univ.-Prof. Dipl.-Ing Dr.techn. Harald Raupenstrauch geleitet. Ihm gilt mein herzlichster Dank für die Aufnahme in sein Team, seine Unterstützung, die Lektüre meiner Arbeit und die Förderung meiner Arbeit mit allen Mitteln.

Auch dem Rest des Teams, das mich teils mit Rat, teils unter schwerstem körperlichen Einsatz – und mit Kuchen – unterstützt hat, danke ich vielmals.

Vor allem gilt mein Dank aber meinen Eltern, Susanne und Norbert Ponak. Sie ebnen seit jeher meinen Weg, der ohne ihre bedingungslose Unterstützung niemals so sorgenfrei und erfolgreich hätte sein können. Jeder Beistand und jedes Verständnis für meine noch so ungewöhnlichen Vorhaben war für sie selbstverständlich. Mein Erfolg ist der meiner Eltern.

Acknowledgement

I would like to express my gratitude to my supervisor Dipl.-Ing. Daniela Meitner. Without her, this thesis would not exist. My gratitude is not only for the great supervision, the proof-reading of my thesis, the support of my research and any form of assistance, but also for getting me on board of this ship more than a year ago.

This ship, the Chair of Thermal Processing Technology at the Montanuniversität Leoben, is led by my evaluator and supervisor Univ.-Prof. Dipl.-Ing. Dr.techn. Harald Raupenstrauch. I would like to thank him for bringing me in, for his support, the perusal of my thesis and the promotion of my work by all available means.

Thanks also to the rest of the team, which supported me partly by giving advice and partly by showing severe, physical effort – and with cake.

Last but not least, I would like to particularly thank my parents, Susanne and Norbert Ponak. They have always paved my way, which would not have been so successful and free from worries without their support. To them, every form of backup and being sympathetic about my various exceptional plans was taken for granted. My success is that of my parents.

Kurzfassung

Das Ziel dieser Arbeit ist die Validierung der Eignung eines Calciumchlorid-Klinoptilolith-Kompositmaterials für dessen Einsatz in Anwendungen zur thermochemischen Langzeitenergiespeicherung.

Der experimentelle Teil der Arbeit umfasst zwei Teilaufgaben. Zuerst wurde ein vorhandener Versuchsaufbau optimiert. Die Möglichkeit der exakten Einstellung der relativen Feuchtigkeit der verwendeten synthetischen Luft ist dabei die größte Neuerung. Im Anschluss wurden der reine Klinoptilolith, der synthetisch hergestellte Zeolith 13XBF sowie Komposite mit unterschiedlichen Salzgehalten und Hydrophobierung in demselben Desorptions-Adsorptions-Zyklus untersucht. Die Ergebnisse werden mithilfe einer umfassenden Literaturrecherche auf den komplexen Vorgang im Sorptionsreaktor zurückgeführt.

Es zeigt sich, dass sich die Salzimprägnierung eignet, um die thermischen Eigenschaften der reinen Zeolithe zu verbessern. Die Hydrophobierung stellt überdies ein geeignetes Mittel dar, um das Salz an der Zeolithoberfläche zu fixieren. Probleme, welche die Eignung der Kompositmaterialien für deren Einsatz zum jetzigen Zeitpunkt noch nicht tragbar machen, werden aufgezeigt und analysiert, um der weiteren Forschung eine Richtung zu geben.

Abstract

The aim of this thesis is to validate the suitability of a clinoptilolite-calcium chloride composite material for its use in thermochemical energy storage applications.

The practical part of this thesis involves two subtasks, one of which was that an existing experimental setup was optimised. The biggest improvement is the possibility to accurately adjust the relative humidity of the used synthetic air. Subsequently, pure clinoptilolite, the synthetic zeolite 13XBF as well as composites with different mass fractions of salt and hydrophobicity treatment were studied in the same desorption-adsorption cycle. With the help of thorough literature research, the results are ascribed to the complex process in the sorption reactor.

It shows that the salt impregnation is able to improve the thermal properties of the pure zeolite. The hydrophobicity treatment turns out to be a suitable way of stabilising the salt on the zeolite surface. Problems, which make the applicability of the composite materials unviable at this time, are explained and analysed in order to lead the way for future research.

Table of Contents

List of Abbreviations

General Abbreviations

DPT   dew point temperature

EU   European Union

PM   Paltentaler Minerals GmbH

RH   relative humidity

SBU   secondary building unit

Si-Al-ratio   ratio of silicon and aluminium atoms in zeolites

Chemical Formulae

$CaCl_2$ calcium chloride

$CaCl_2 \cdot 6\,H_2O$ calcium chloride hexahydrate

CO_2 carbon dioxide

$[AlO_4]^{5-}$ aluminate ion

$[SiO_4]^{4-}$ silicate ion

Formula Symbols

A	cation species (ion exchange)	
B	cation species (ion exchange)	
b	coefficient in BET-isotherm	[-]
c	heat capacity	$[Jkg^{-1}K^{-1}]$
d	diameter	[m]
e	vapour pressure	[hPa]
f	relative humidity	[%]
h	height	[m]
m	mass	[kg]
$\dot{m}$	mass flow	$[kgs^{-1}]$
p	pressure	[Pa]
Q	heat	$[MJm^{-3}]$
T	temperature	[K]
t	time	[s]
V	volume	[m³]
$\dot{V}$	volume flow	$[m^3s^{-1}]$
X	loading	[-]
z	valence	[-]
ΔT	temperature difference	[K]
Δt	time difference	[s]
φ	specific humidity	[-]
ρ	energy density (index Q)/density	$[MJm^{-3}]/[kgm^{-3}]$

Formula Indices

A	cation species (ion exchange)
a	adsorptive
air	air
B	cation species (ion exchange)
b	material bed
calc	calculated
e	equilibrium/end (regarding temperature)
i	control variable
lift	temperature lift
m	mean
max	maximum
meas	measured
mon	monolayer
p	isobaric
Q	index of energy density
r	room
rel	relative
s	saturated/start (regarding temperature)
sorb	sorption
th	thermostat
tot	total
use	usable
w	water
0	starting point
1	terminal point (integral)/lower humidity or temperature sensor
2	upper humidity or temperature sensor

Material Labels

13XBF	synthetic zeolite
H4	suffix to hydrophobised materials
Mono	natural zeolite
Multi 5-20	$CaCl_2$-impregnated and hydrophobised composite with salt amount
Multi 5 S	natural zeolite with 5% (w/w) salt impregnation only

List of Illustrations

List of Tables

1 Problem Outline

We live in a world of growth. The 20th century and the 21st century have been marked by increase. On average, the world population becomes richer. According to the World Bank, the GDP per capita increased from 7,738.3 US$ in 2006 to 10,738.8 US$ in 2014. Data published by the United Nations Population Division shows a world population of some 2.5 billion people in 1950, some 7.3 billion people in 2015 and a further tendency to rise in a variety of scenarios. These growth trends also bring an increased raw material consumption with them. In only 20 years, from 1994 to 2014, the world raw material production increased from 10,445,669,005 t to 17,434,662,951 t. [1–3]

It is a logical consequence that the world energy consumption rises accordingly. From 1973 to 2013 the world primary energy supply increased from 6,100 Mtoe to 13,541 Mtoe. The share of fossil fuels (natural gas, oil, coal) decreased only from 86.7% to 81.4%. [4]

The same situation is reflected in data on the European Union (EU). It is a part of the core targets of the EU for 2020 to lower the green house gas emissions by 20% compared to 1990, increase the amount of renewable energy to 20% and to increase the energy efficiency by 20%. [5]

Austria has a high share of renewable energy sources of the whole energy production (31% in 2010). Yet, the energy consumed consists of 70% energy from fossil fuels. It is remarkable that private households account for 26% of the total energy consumption of the country (2010). This is about the same value as the EU average. Therefore, it becomes obvious that the household sector has a huge potential for energy efficiency increase and green house gas emission reduction tasks. [6]

Said potential is exactly where thermochemical energy storage applications come into play. Sorption storage systems can be "loaded" in summer and used for heating purposes in winter with hardly any losses and without local green house gas emissions. If combined with photovoltaic systems, these inter-seasonal heating applications can immensely reduce the amount of gas or oil needed for heating purposes. [7]

Emission-free heating sounds utopic. Yet, the mentioned systems are expected to be highly promising by researchers worldwide. Unfortunately, the implementation of these systems in households is still hindered by several problems. On the one hand, the integration into the heating system of a house is difficult, on the other hand, available sorption materials are either expensive or not sufficiently performant. This thesis is placed in the material development field of research.

1.1 Statement of Task

Synthetic zeolite sorption materials show a high performance in said systems already. Due to their high prices, affordable, natural minerals are investigated. In order to enhance their suitability for sorption energy storage applications, they are improved by methods such as salt impregnation or hydrophobicity treatments.

The task of the research conducted in the course of this thesis is to investigate the thermal behaviour of a salt-zeolite composite material in order to validate if it is suitable for the applications mentioned. Furthermore, the effects of the different treatments shall be analysed and used to reason and explain why the material seems to be suitable or not.

1.2 Research Relevance

The idea of chemically enhancing the performance of sorption materials by impregnating them with a salt is commonly praised in respective literature. Very often, experiments described are conducted under laboratory conditions that are not viable for implementation in households. One of the main problems is the instability of the salt. In order to tackle this problem, the material analysed was hydrophobised. The hydrophobicity layer is supposed to stabilise the composite.

The relevance of the conducted research lies in the validation of the qualification of the treatment methods used and in the demonstration and explanation of potential problems that are often neglected in related research.

1.3 Objectives

In the following, the research questions are presented as well as the methodology that is used to answer them.

1.3.1 Research Questions

- How does the adjustment of the relative humidity (RH) using gas washing bottles, deionised water and dew point temperature settings work?
- How do the synthetic and natural zeolites (13XBF and Mono) behave during the adsorption process?
- How does the hydrophobicity treatment influence the thermal behaviour of the zeolites Mono, 13XBF and the composite materials (Multi 5-20)?
- Does the calcium chloride ($CaCl_2$) impregnation improve the suitability of the natural zeolite to be used in sorption storage systems? If so, in what way? If not, why?

1.3.2 Methodology

In order to measure the thermal behaviour of the zeolite materials, the existing experimental setup is advanced so that the temperature and humidity settings work exactly.

Subsequently, all relevant materials (13XBF, Mono, 13XBF H4, Mono H4, Multi 5, Multi 10, Multi 15, Multi 20 and Multi 5 S) are measured in the same desorption-adsorption-cycle.

With the help of Microsoft Office Excel, the data is analysed and the performance of the materials is compared.

Based on these experiments and the findings of a fundamental literature research, the results are reflected and the thesis is concluded.

1.3.3 Motivation

Well-performing sorption storage systems using a material that exists abundantly all over the planet appear to provide an auspicious opportunity to reduce carbon dioxide (CO_2) emissions tremendously. It might be hard to conceive of a serial production of such storage devices now, but every piece of research represents a small step towards this long-term goal and it is exciting to be given the chance to make a contribution.

2 Theoretical Fundamentals

This chapter contains the theoretical fundamentals needed to comprehend the following experiments, including their analysis and its interpretation.

At first, the materials used are described. The composite material of interest to this thesis consists of the zeolite clinoptilolite and the salt $CaCl_2$. Therefore, both components are presented as well as the composite itself, including its production and hydrophobicity treatment.

Next, the basics of thermochemical energy storage systems are shortly discussed. The mechanism in the sorption reactor is highly complex. In order to comprehend, all necessary fundamentals are explained.

As a last point, the theoretical part is concluded by the consideration of the humidity of air. The definition is complemented by simple equations in order to be able to understand the setting of the relative humidity discussed in chapter 3.

2.1 Materials

This part of the thesis is to present the materials relevant to the described field of research. It contains general information about the zeolite and the salt as well as specific information about the composite used in the experiments described in the practical part (chapter 3ff.), including their production and treatment.

2.1.1 Zeolites/Clinoptilolite

Zeolites are a group of materials with a huge variety of important applications. For example, they are used in the petrochemical industry as well as in agriculture, which shows how broad their range of applications is. Also, there are a lot of different zeolite types. Yet, the fundamental framework they all consist of is always the same. Zeolites are crystalline minerals consisting of aluminosilicates. Silicate ions ($[SiO_4]^{4-}$) and aluminate ions ($[AlO_4]^{5-}$) form a three-dimensional structure of polyhedra. In their physical configuration, these polyhedra share their oxygen-corners to create channels and cavities, which are responsible for the materials' precious properties. [8]

Zeolites received their name from the immense loss of water that occurs when the materials' temperature is increased, after the Greek word for boiling stone. Yet, other materials show the same behaviour. Also, some aluminosilicates are amorphous – not crystalline – and other materials, such as aluminium phosphates, show a similar structure of regular arrays of pores. Hence, even though the definition of zeolites might seem convoluting at first, the term usually refers to all crystalline aluminosilicates with a porous structure of regular arrays of pores and apertures. [8]

Natural zeolites can be of volcanic or saline lake origin, occur in soils or open flowing systems with high pH values and have also been discovered in marine deposits or as the products of burial diagenesis. Even though they were thought of as something rare in the 18th and 19th centuries, zeolites are actually amongst the most abundant minerals on earth. [8]

Today, in addition to the natural types of zeolites, a huge number of synthetic ones is available. The process of creating perfectly regular structures of channels and cavities is well-controlled. Therefore, structures of any desired channel diameter and specific surface area that do not occur in nature can be manufactured. [8]

Basically, all zeolites consist of so-called coordination polyhedra of $[SiO_4]^{4-}$ and $[AlO_4]^{5-}$ ions, whose oxygen atoms share the corners of identical unit cells (s. **Illustration 2-1**).
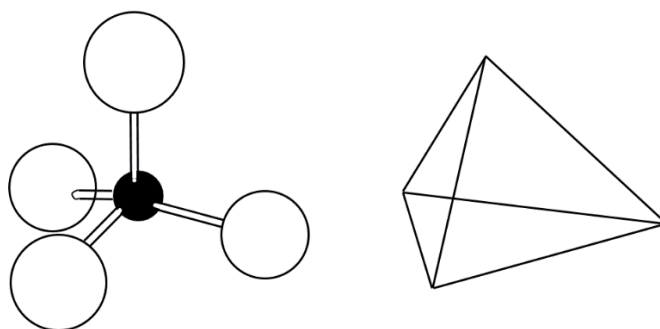
Illustration 2-1: Coordination polyhedra. [8]

In order to classify different types of zeolites, secondary building units (SBU) are defined, which commonly recur throughout the material. With the help of only seven SBU classes, the most common zeolite structures can be defined. It is important to keep in mind that this model does not consider additional polyhedral units, which are often part of silicate materials. Also the classification system using seven groups of zeolites was already introduced in 1974 by Breck and has not been updated since. **Illustration 2-2** shows an example of a T_5O_{10} SBU, whereby T stands for a Si or, respectively, an Al atom. [9]
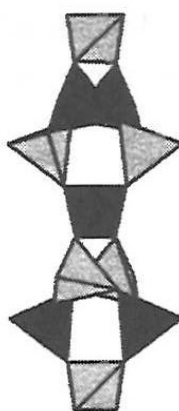
Illustration 2-2: T_5O_{10} SBU. [9]

In addition to the pore structure, the ratio of silicon and aluminium atoms (Si-Al-ratio) in that very structure has an enormous effect on the properties of the zeolite. When trivalent aluminium is substituted by tetravalent silicon, it leaves the oxygen frame with a single, negative charge. Those negative charges attract cations to attain electroneutrality. Therefore, the Si-Al-ratio determines the amount of cations present in the zeolite structure and in turn the amount of water molecules incorporated. [8]

The zeolite used in the composite that is observed in this thesis is clinoptilolite. It is found in marine deposits in all three oceans as well as in open flowing systems. Its structure is far

more complex than the single four ring structure shown before. Clinoptilolite consists of group seven SBUs, which create oxygen frames with windows consisting of either eight or ten oxygen atoms. The windows consisting of ten oxygen atoms are elliptical and, naturally, larger than the ones consisting of only eight oxygen atoms. Yet, their width along one axis is about the same size as the diameter of the circular, eight-membered windows (s. **Illustration 2-3**). [8, 9]
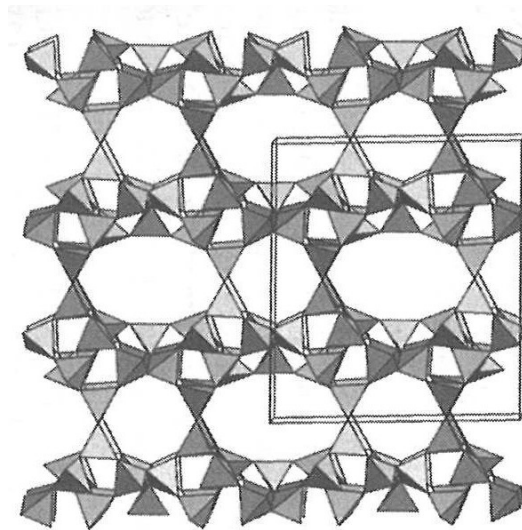
Illustration 2-3: Clinoptilolite structure. [9]

The zeolite has a high Si-Al-ratio of four and its channels and cavities contain a large amount of alkali metals (especially sodium and potassium). This explains the material's suitability for its use as an ion exchanger. **Formula (2-1)** shows the chemical formula describing the mineral. [8, 9]

$$(Na, K)_6 [Al_6 Si_{30} O_{72}] \cdot 20 H_2 O \qquad \textbf{(2-1)}$$
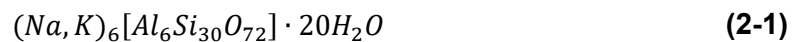
Other applications of zeolites in general include their use as catalysts and gas separators. For one thing, the variable diameter of different zeolites makes them work like molecular sieves. Smaller molecules in gases can pass through the structure whilst bigger ones are held back. Also, reactants in the form of ions can be brought inside the zeolite's array of pores. When reactions occur within the material, some reaction products might be too big to leave the channels and cavities, while others can. With the help of synthetic zeolites, this selectivity can be deliberately altered. [8]

Illustration 2-4 and **Illustration 2-5** show the natural zeolite clinoptilolite and the synthetic zeolite 13XBF as used in the experiments conducted in the course of this thesis.

Illustration 2-4: Clinoptilolite grains.

Illustration 2-5: 13XBF bulk.

13XBF consists of almost perfectly spherical grains in a particle size range from 1.6 mm to 2.5 mm. The clinoptilolite bulk consist of smaller grains in a range from 0.3 mm to 1.0 mm.

2.1.2 Calcium Chloride

$CaCl_2$ has been used for over 200 years. Its first scientific application is reported to be its use by Davy in 1808, who separated pure Ca from fused $CaCl_2$ using the salt in electrolytic

processes. The salt's melting point is at roughly 780°C. Pure Ca melts at some 800°C. Its use poses a safety risk for it burns at over 800°C if surrounded by moist air. [10]

The salt's synthesis is a part of other industrial processes. It occurs during the recovery of ammonia in the production process of sodium carbonate (**Formula 2-2**) and on a laboratory scale during the CO_2 release when marble and hydrochloric acid react (**Formula 2-3**). [11]

$$2\,NH_4Cl + Ca(OH)_2 \rightarrow CaCl_2 + 2\,NH_3 + 2\,H_2O \qquad \textbf{(2-2)}$$

$$2\,HCl + CaCO_3 \rightarrow CaCl_2 + CO_2 + H_2O \qquad \textbf{(2-3)}$$
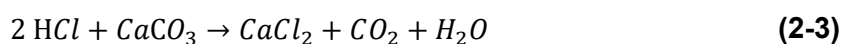
The product is colourless and in its pure form it is a crystalline powder. It is also odourless and contains over 90% calcium chloride hexahydrate ($CaCl_2 \cdot 6\,H_2O$) at standard temperature and pressure. If heated over 260°C, the anhydrous form can be obtained. [12]

$CaCl_2$ exits in more hydrate forms than the anhydrous one and the hexahydrate. Next to those, mono-, di- and tetrahydrates are known. This causes a lot of problems when it comes to the application in thermochemical energy storage systems. The hydration of $CaCl_2$ to $CaCl_2 \cdot 6\,H_2O$ is highly exothermic but not all transitions between the hydrate forms are. Also, the melting points of the hexa- and tetrahydrates are below the desorption temperature used in the experiments described later (29.9°C and 45.3°C). Furthermore, the solution of the hexahydrate in water is endothermic with a heat of solution of 17.2 cal/g or 72.0 kJ/kg. In comparison, the heat of the exothermic solution of pure $CaCl_2$ is -176.2 cal/g or -737.7 kJ/kg. [13]

Therefore, the hydration, dehydration, adsorption and desorption processes observed in the experiments described in the practical part will differ from the ideal processes described in literature. The melting, dissolution and hydrate form transition phenomena have to be considered. In order to understand the system $CaCl_2$ – water, **Illustration 2-6** shows the phase diagram of said system. [13]
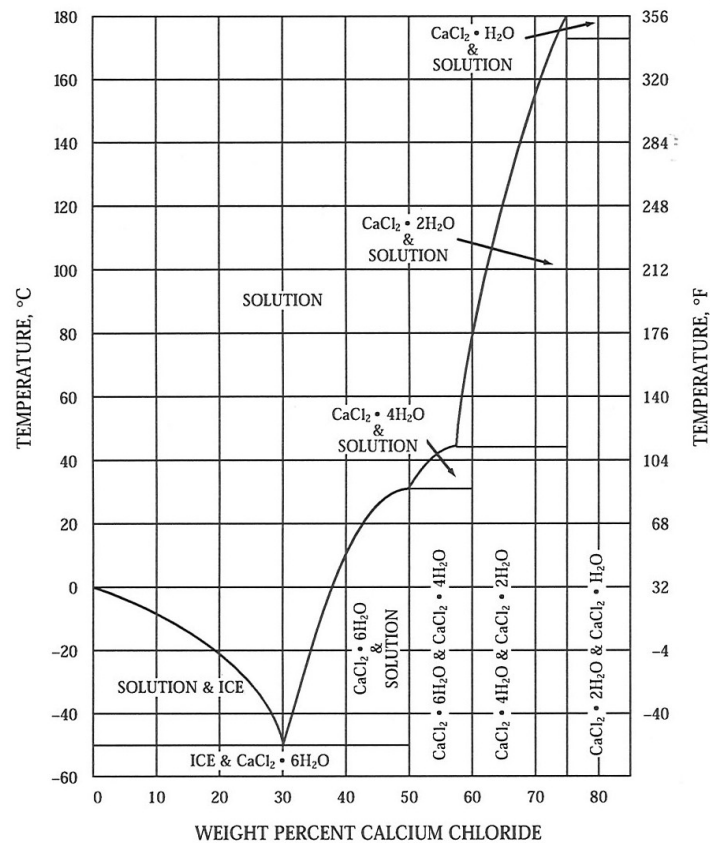
Illustration 2-6: Phase diagram of $CaCl_2$. [13]

Due to the discussed phenomena, there are a lot of phase transitions during the desorption/dehydration at 80°C and the adsorption/hydration at room temperature.

Furthermore, the salt is highly soluble in water and hygroscopic. It is therefore used as a desiccant. Also it is used in frost protection agents, as a thawing salt, in heating baths (because a concentrated solution boils at some 180°C) and as a binder. [11]

The hygroscopic properties of the material also cause a lot of problems when it comes to its use in thermal energy storage systems. Hygroscopy describes the behaviour of a material to adsorb and in turn absorb water from humid ambient air. Water molecules from vapour are adsorbed to the material's surface and condense. In a next step, the salt absorbs the water. If the relative humidity of the ambient air reaches a certain limit, the $CaCl_2$ absorbs so much water that it liquefies. The minimum level of relative humidity necessary for this phenomenon, called deliquescence, to occur is called deliquescence relative humidity. For $CaCl_2$, the value is 30%. [14, 15]

Due to a change in the water activity during the dissolution process, the material continues to absorb more water and the dissolution goes on until saturation is reached. If two or more deliquescent substances are present simultaneously, the deliquescence relative humidity is

lowered to the so-called mutual deliquescence relative humidity. The composition at which both substances dissolve completely simultaneously is called eutonic composition. **Illustration 2-7** shows the phenomenon described. [14]
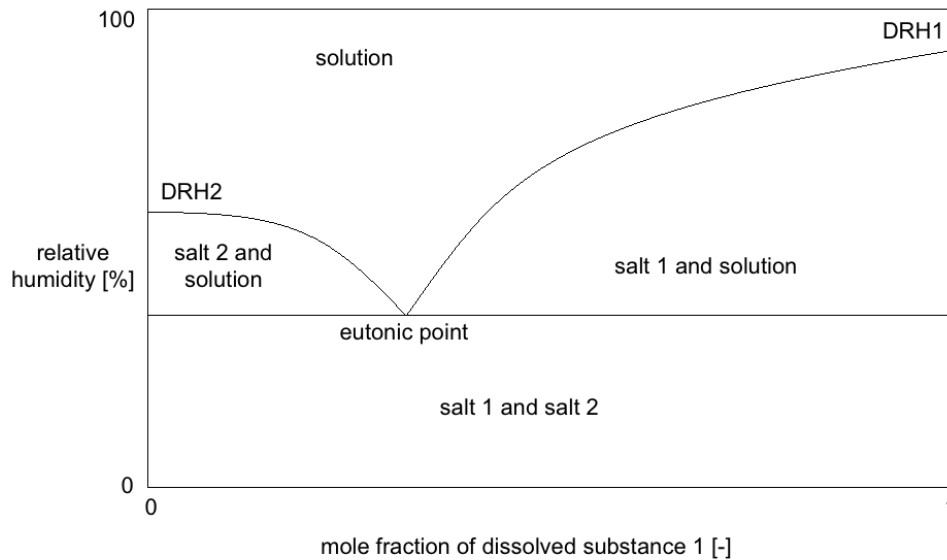
Illustration 2-7: Mutual deliquescence relative humidity and eutonic point.

Even though the salt might cause a lot of problems, it is used for a variety of reasons, as for instance its ample existence, low price, high thermal conductivity and non-toxicity. The most crucial and decisive feature tested in preliminary work in cooperation with the ISE Fraunhofer, Freiburg (Dr. Henninger), was the adsorption characteristic. **Illustration 2-8** shows the results of the experiments. Out of the materials tested, $CaCl_2$ showed the highest increase in loading with increasing relative vapour pressure. The labels of the axes are "Beladung", meaning "loading", for the ordinate and "relativer Dampfdruck", meaning "relative vapour pressure", for the abscissa. [16, 17]
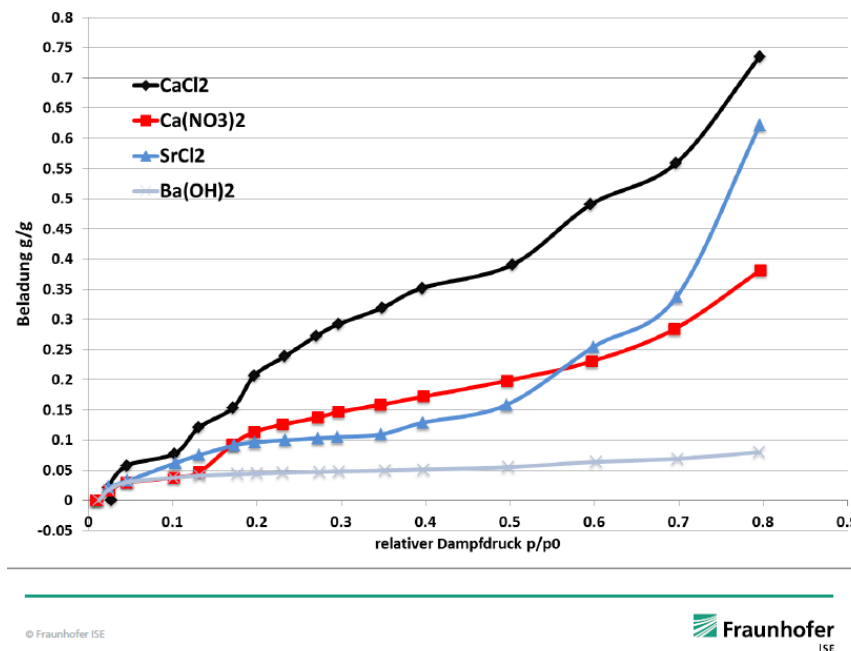
Illustration 2-8: Adsorption characteristics of different sorption materials. [17]

2.1.3 Composite Material

The composite material is a mixture of the clinoptilolite and the $CaCl_2$. The idea is that the salt coats the surface of the zeolite in order to enhance the energy storage capacity by adding hydration/dehydration processes to the sorption mechanism. In theory, the zeolite mainly offers structural stability and the manipulability of the particle size as well as an effective heat transfer. The salt alone is a powder. In the application described in this thesis, a powder would cause an immense pressure loss in the reactor and therefore cannot be used in a sensible way. This strengthens the role of the zeolite as a support material. Yet, it is an active support material for it contributes to the storage capacity due to its adsorptive properties. An example for a passive support material is ceramics. [18]

The general purpose of the hydrophobicity treatment is to stabilise the salt impregnation. Usually, mineral substances show polar forces that are bigger than the attractive forces between water molecules. Therefore, they are easily wettable. Without any protection, the salt would be washed off the zeolite surface very quickly. With the help of so-called hybrid molecules that possess both, a hydrophilic and a hydrophobic end, the surface of mineral substances can be protected against wetting. Mostly silane and siloxane (s. **Illustration 2-9** and **Illustration 2-10**) compounds are used for the purpose of hydrophobicity. Their hydrophobic ends protect the mineral surface from water. [19]
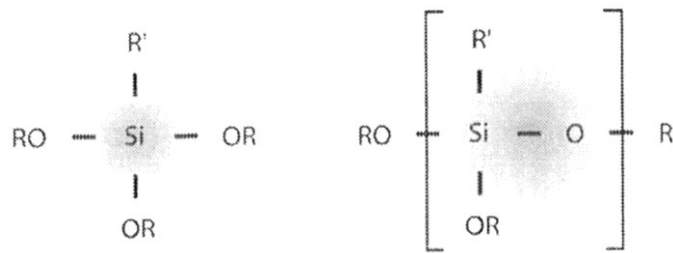
Illustration 2-9: Silane and siloxane groups. [19]
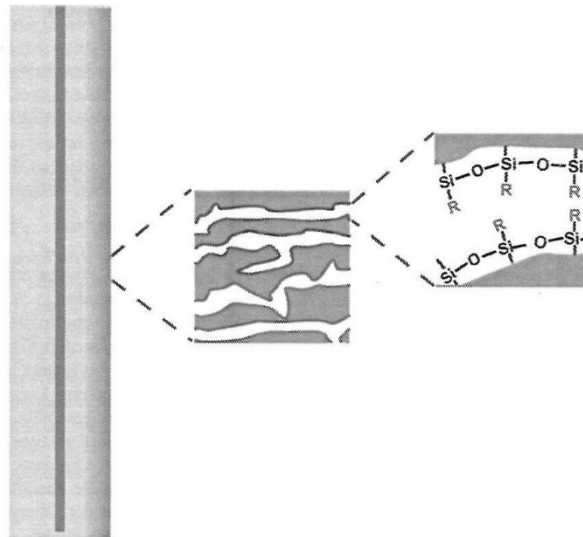
Illustration 2-10: Siloxane surface hydrophobicity. [20]

Next to the surface hydrophobicity there is the possibility of mass hydrophobicity. Instead of hydrophobising the respective materials after their production, the whole material is hydrophobised during its production already. This is done with the zeolites used in the course of the experiments for this thesis. The resulting material is therefore hydrophobic everywhere, not only on its surface. With construction materials like concrete, where hydrophobicity is often applied, this brings the advantage that the material is also resistant against moisture entering through cracks (s. **Illustration 2-11**). [21]
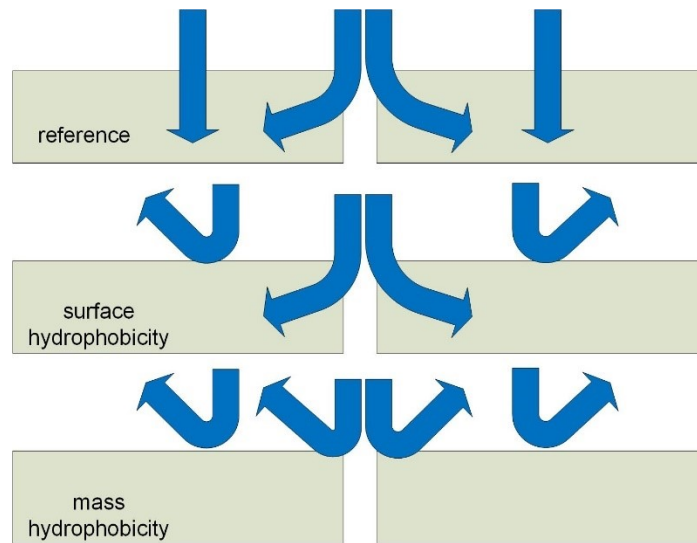
Illustration 2-11: Different types of hydrophobicity.

The composite material used is produced by the company Paltentaler Minerals GmbH (in the following called PM), situated in Lassing, Austria. In a first step, the zeolites are impregnated with the salt that is supposed to enhance the material's performance in sorption storage applications. Preliminary investigations of the adsorption behaviour (s. chapter 2.1.2) of several alkaline earth salts (for instance $CaCl_2$ and barium hydroxide) suggest that $CaCl_2$ performs better than the other salts tested. In order to stabilise chemical substances and the reaction behaviour within the zeolite matrix, the approach of coating the material with organic additives was chosen. By hydrophobising zeolite structures, molecules and ions shall be prevented from leaching out. **Illustration 2-12** shows the initial approach of the composite production. The individual images show the zeolite and its pore system, the salt uptake (yellow) and the hydrophobic modification (orange). [17]
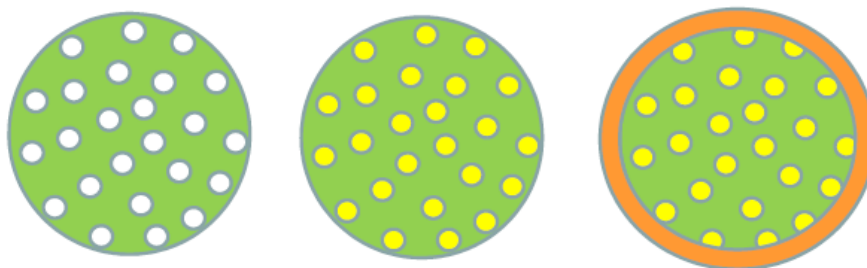
Illustration 2-12: General production of the composite material. [17]

The hydrophobic agent is a silane. 4% (w/w) are added to achieve optimised hydrophobic properties. Due to the strong cohesive properties of the salt, fine grinding becomes more difficult with higher salt loadings. Beyond 20%, the salt character of the composite prevails.

The optimisation work conducted by PM found that a loading of 19% (w/w) $CaCl_2$ and 4% (w/w) silane-modifier deliver the best cost-performance-ratio. With the loading amount optimised, the cycle stability was the major problem remaining. Experiments showed that salt ions quickly leave the zeolite matrix. Hence, in a further approach, the zeolite was first hydrophobised and then co-grinded with the salt. This process is depicted in **Illustration 2-13**. [17]
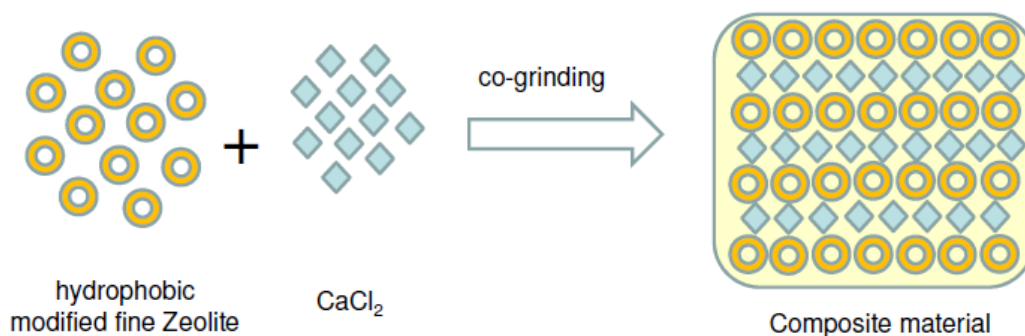
Illustration 2-13: Improved composite production process. [17]

The grinding is performed by an oscillating disc mill made of molybdenum carbide. Tests with the resulting, very fine material showed that only at very high salt loads of some 70% mobile salt phases started leaving the composite matrix. Due to the material's fine pore structure, the pressure loss in the loose bulk was significantly high. With coarse, impregnated zeolite that is crashed and not ground, salt ion mobility can be observed at much lower salt concentrations already. Hence, further research considered a second, inorganic coating before the material is hydrophobised. This inorganic layer, containing portlandite or ground blast furnace slag, proved not to be stable. In a different approach, pelletising showed severe problems with the binders used blocking the adsorption of water molecules. [17]

The final approach that delivers the material used in the experiments conducted in the course of this thesis combines the hydrophobicity and salt impregnation steps. The material is dried to a residual moisture of 5% and then ground. In parallel, a solution of $CaCl_2$ and the hydrophobising substance with different concentrations of $CaCl_2$ for the different composites is prepared. It is subsequently mixed with the zeolite at the ratio of 1:1. After twelve hours of contact, the material is dried until mass consistency is reached. [22]

Experiments by Meitner were conducted in order to analyse the effects of the hydrophobicity of the materials used by considering the ion exchange behaviour of the zeolites. She found that the ion exchange ability measured by the quantity of exchanged ions almost completely ceases due to the hydrophobicity treatment. 10 g of each, pure

clinoptilolite and hydrophobised clinoptilolite, were put into 150 ml of a 15% (v/v) $CaCl_2$ solution. After three, six and twelve hours, 50 ml of each solution were tested for cation species and quantity. The results can be found in **Illustration 2-14** and **Illustration 2-15**. The scaling has to be considered. [23]
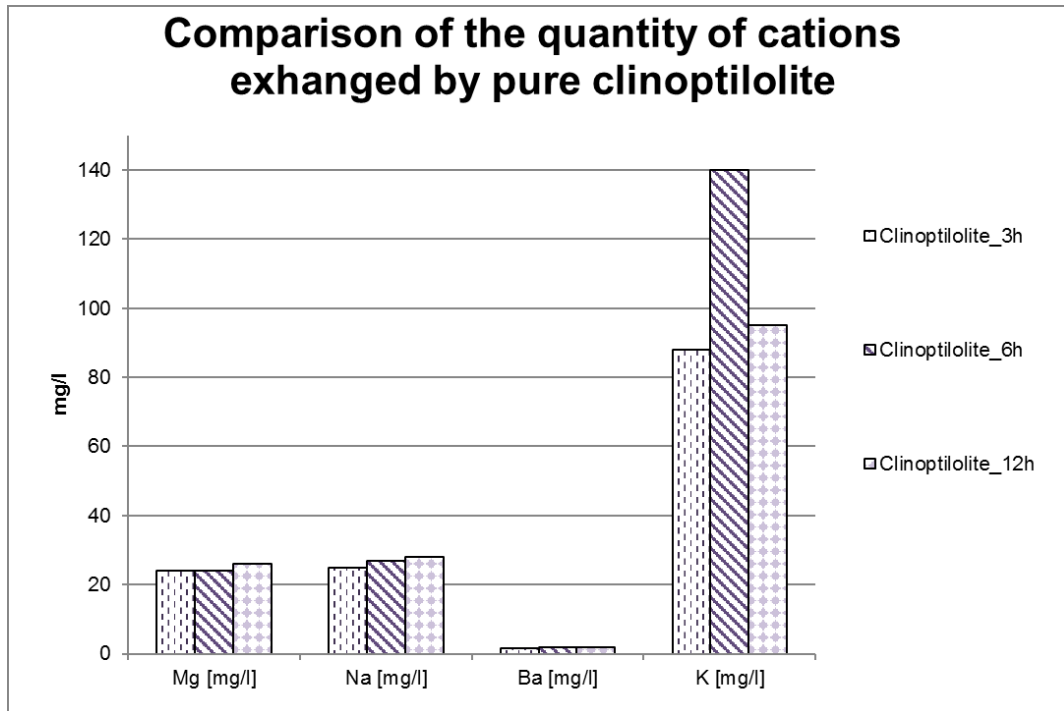
Illustration 2-14: Cations exchanged by pure clinoptilolite. [23]
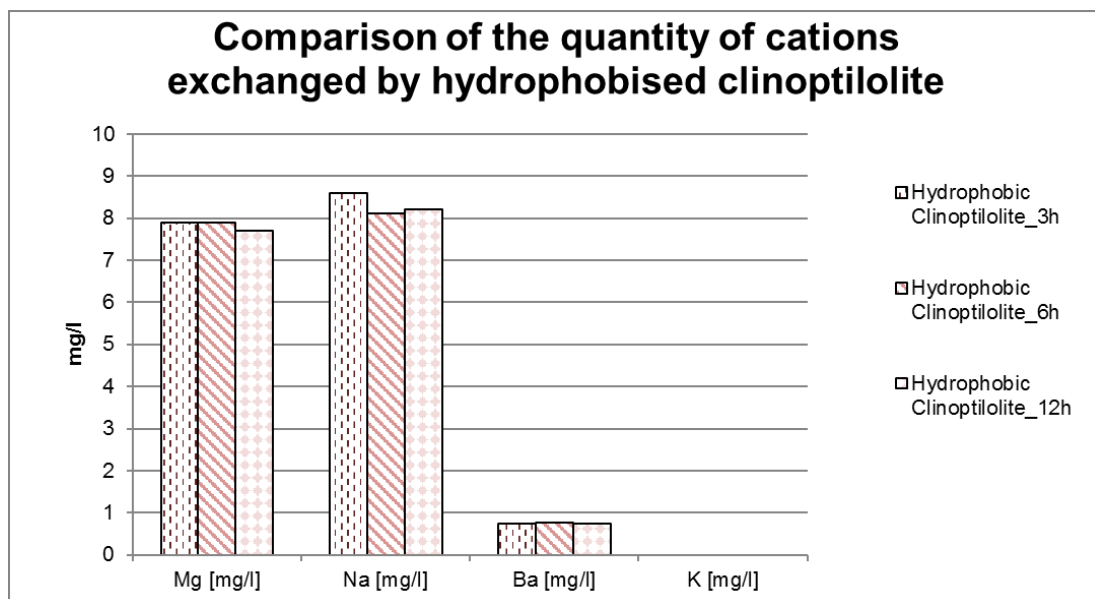
Illustration 2-15: Cations exchanged by hydrophobised clinoptilolite. [23]

It can be seen that the hydrophobicity treatment almost fully ceases the ion exchange activity of the zeolite. Therefore, it can be deduced that the zeolite surface is inaccessible for liquid water. The hydrophobicity stabilises the salt on the surface of the clinoptilolite but also causes problems like congested pores. Hence, it reduces the surface area available for adsorption and salt reactions. The overall effect is analysed by the experiments described later in this thesis. [23]

Also, it has to be considered that the pore sizes of natural zeolites are not all the same. In general, micropores, mesopores and macropores are defined. The classification is illustrated in **Illustration 2-16**. Based on the findings of the experiments conducted and described in this thesis, it is thought that the hydrophobicity treatment congests micropores and potentially a part of the mesopores. [15]
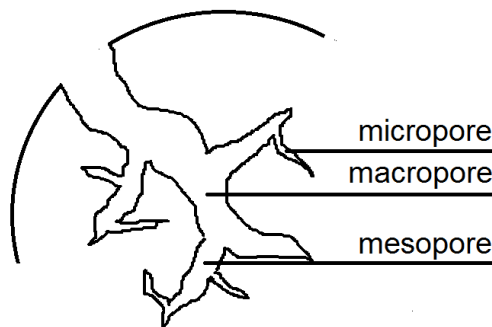
Illustration 2-16: Different types of pores.

Furthermore, the sorption properties are influenced by five important factors:

- Chemical nature of the salt
- Chemical nature of the zeolite
- Salt content
- Pore structure
- Synthesis conditions. [24]

As has been already mentioned, the zeolite is an active support material. Adsorption of water molecules to the zeolite surface contribute to the heat storage capacity of the system. However, experiments described in respective literature (for instance Aristov) suggest that with silica gel this contribution accounts for less than 5%. Hence, the zeolite's main purpose is to provide a large surface area for the salt to interact with the water molecules in the air. [24]

Experiments conducted by Wu et. al. confirm the huge influence of the salt impregnation when it comes to sorption capacities of silica gel. A way larger amount of water can be adsorbed with the help of the impregnation. The physical adsorption to the silica gel surface is complemented by the chemical absorption by the salt and the chemical hydrate reactions. It must be considered that a higher salt amount leads to a lower pore volume and therefore the salt content is limited. [25]

Illustration 2-17 and **Illustration 2-18** show microscopic images of Mono and Multi 5. The salt is clearly visible on the Multi 5 surface. It can be seen that the salt is not evenly spread over the surface. Due to the low salt amount, an unequal distribution occurs. Also, it appears that the salt can congest zeolite pores.
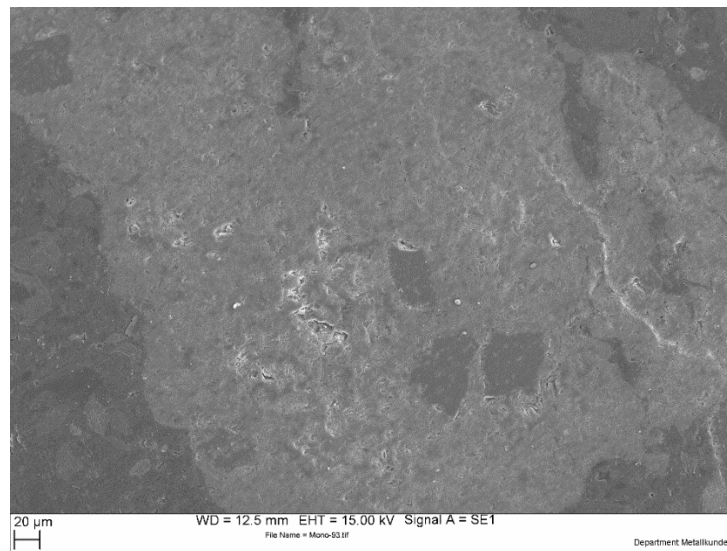
Illustration 2-17: Microscopic image of Mono.
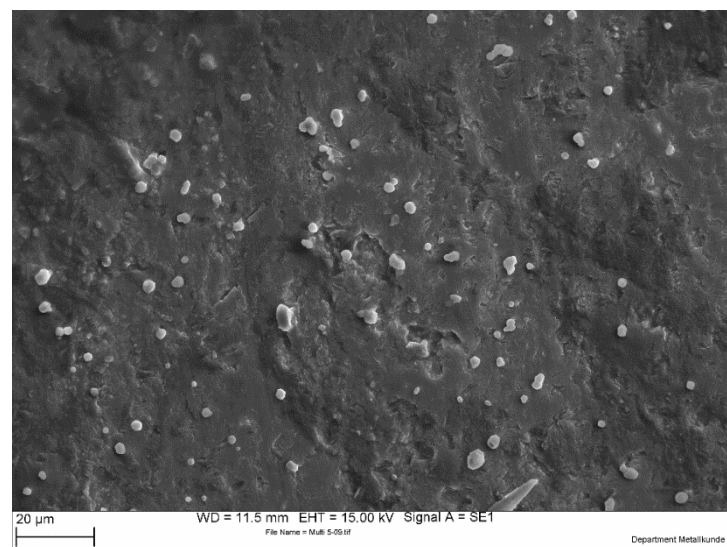
Illustration 2-18: Microscopic image of Multi 5.

To conclude, the salt impregnation has already been proven positively influential. Yet, there are many problems to be carefully observed. Therefore, this thesis focusses on the validation of the material's suitability for its use in low temperature energy storage systems on a laboratory scale.

2.2 Fundamentals of Thermochemical Energy Storage

Thermochemical energy storage has an important advantage over thermal energy storage systems. As they use the heat released by chemical reactions, there are no thermal losses over a long storage period. With sorption storage systems, the chemical reactions of the salt are supplemented by the adsorption of the water molecules. However, both mechanisms are reversible. Therefore, desorption – adsorption cycles can be used in energy storage applications. In order to understand these applications, transport phenomena have to be discussed. This chapter depicts the most important phenomena occurring within these thermochemical energy storage systems.

2.2.1 Diffusion and Flow Phenomena

In order to understand the interconnections of the mechanisms of the sorption process described in chapter 2.2.5, diffusion and flow phenomena in porous media have to be shortly discussed.

Diffusion mainly describes the movement of ions or molecules due to a concentration gradient. It is highly dependent on the prevailing temperature and pressure. These dependencies are highly complex. At this point, it is sufficient to know that diffusion is crucial for the sorption process in its function as the main transport mechanism of the water molecules in the air led through the sorption reactor. Also, the heat of adsorption is assumed to be released quickly. Therefore, when it comes to kinetics, the diffusive transport of water molecules makes for the limiting and rate-determining step. [26, 27]

For general momentum transport of molecules in porous media, three cases are distinguished. Free molecule flow occurs if the diameters of gas molecules are small and if the molecules hardly interact. If in addition the pore dimensions are small, the molecules interact with the inner pore surface by adsorption or through van-der-Waals forces. If the pore dimensions are big compared to the molecule diameters, general hydrodynamic flow patterns occur. A special flow type, called the slip-flow, occurs if the molecule's mean free paths and

the pore dimensions are similar to each other. Due to the different pore sizes present in natural zeolites, all three phenomena can occur. [27]

2.2.2 Sorption and Sorption Systems

Adsorption phenomena lead to an enrichment of at least one of the participating components if a fluid and a solid phase are in close proximity to each other. To describe the sorption mechanism, it is mandatory to clarify the sorption terminology. The solid media providing the surface on which the fluid phase is adsorbed is called adsorbent. The adsorbed component is called adsorbate. Before it is adsorbed, it is referred to as the adsorptive. **Illustration 2-19** provides a graphic overview of this terminology. [28]
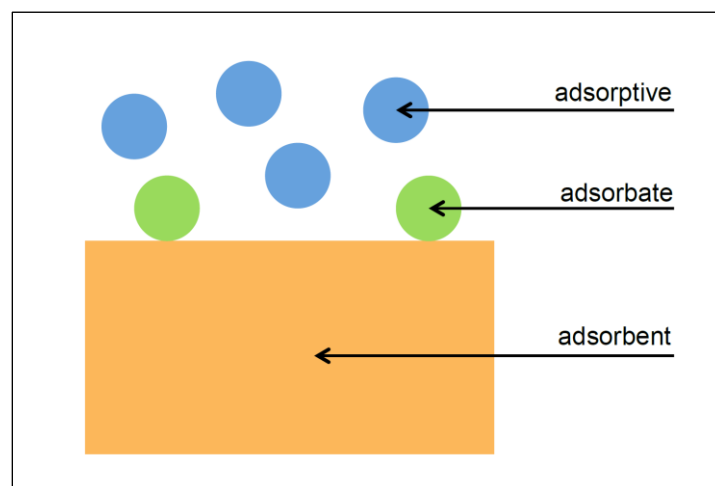
Illustration 2-19: Adsorption terminology.

In general, physisorption and chemisorption are discerned. Physisorption or physical adsorption is caused by physical interactions between the adsorbate and the adsorbent. The main force causing these interactions is the van-der-Waals force. This force can still cause adsorption even if the whole surface is covered by a single layer of adsorbate already. Therefore, especially if the pressure is increased, the formation of multilayers is possible. [28]

The driving force causing chemisorption is a chemical bond between the molecules of the adsorbate and the adsorbent. The necessary chemical link caused by a reaction of some kind leads to an end of the adsorption mechanism as soon as the whole adsorbent surface is covered by a monolayer of adsorbate. [28]

Chemisorption usually causes a higher change in energy than physisorption. The energy of chemisorption is about the same as if the underlying chemical reaction occurred elsewhere.

Physisorption energy changes are in the range of the vaporisation energy of the adsorptive. [26]

The sorption mechanism relevant to this thesis is the physical adsorption of the gaseous water molecules to the surface of the zeolite. Sorption thermodynamics can be described with the help of isotherms, which relate the adsorbent loading – in kilograms adsorbate per kilogram adsorbent – to the partial pressure of the adsorptive phase at a constant temperature. The different isotherm models (for instance Langmuir, BET, etc.) are all based on Gibbs' principles, who postulated the following assumptions:

- There is a thermal, chemical and mechanical equilibrium between all phases that are involved.
- The adsorbent is not changed by the adsorption.
- The adsorption does not influence the surface area and the volume of the adsorbent.
- The adsorptive type does not influence the loaded surface. [26]

Important types of isotherms are shown in **Illustration 2-20**.
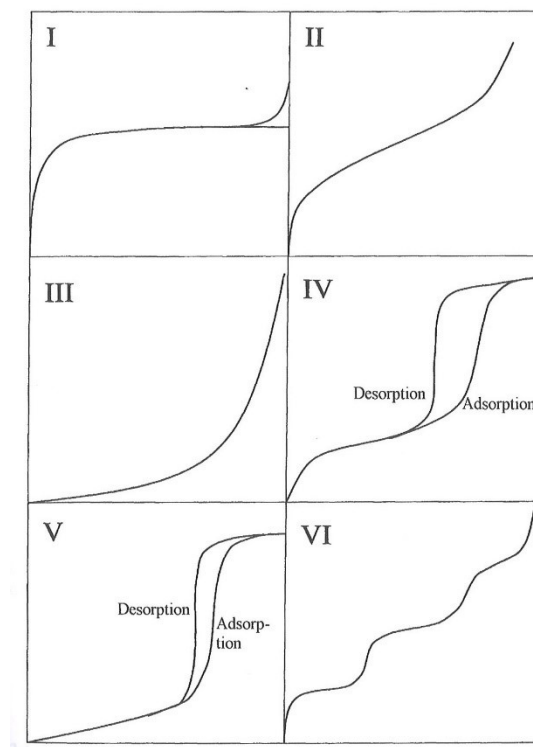
Illustration 2-20: Types of isotherms. [26]

A type IV isotherm has been observed with silica gel – water vapour systems. It can be assumed that zeolite – water vapour systems behave in a similar way. One way to describe this isotherm mathematically is the BET isotherm shown in **Equation (2.1)**. [26]

$$X_e(T) = X_{mon}(T) \cdot \frac{p_a/p_{tot}}{1 - p_a/p_{tot}} \cdot \frac{b(T)}{1 + [b(T) - 1] \cdot p_a/p_{tot}} \qquad \textbf{(2.1)}$$

The index e stands for equilibrium and the index mon refers to the state in which a monolayer of particles is coating the whole surface of the adsorbate. The indices a and tot refer to the partial pressure of the adsorptive and the total pressure in the gaseous phase. The term b(T) is a temperature-dependent coefficient that summarises a variety of other factors and coefficients. [26]

The BET-isotherm still fails to properly describe the hysteresis observed with water vapour – silica gel and water vapour – activated carbon (type V) systems. It is caused by capillary condensation. When the liquid between the capillaries of the adsorbate forms a curve at the top of the liquid column, a decrease in the vapour pressure in the boundary layer between the liquid and the gaseous phase occurs. Hence, the adsorptive can condensate and lead to an almost vertical slope of the isotherm. [26]

The reversed process of physisorption is called desorption. Chemisorption reversibility depends on the reversibility of the chemical reaction. However, since physical adsorption is the relevant mechanism to this thesis, further considerations shall happen with regard to physisorption. By putting heat into the material, the adsorbate is removed from the adsorbent's surface and becomes an adsorptive again. [29]

Desorption – adsorption cycles are used in thermochemical energy storage systems with sorption materials. There are closed and open sorption storage systems. Closed systems are also called evacuated systems. Such systems allow the regulation of the operation pressure of the fluid phase (**Illustration 2-21**). In open sorption systems, as applied in the experiments conducted in the course of this thesis, an air stream is led into a reactor and leaves it again. The air exits the reactor against the atmospheric pressure of the laboratory (**Illustration 2-22**). [29]
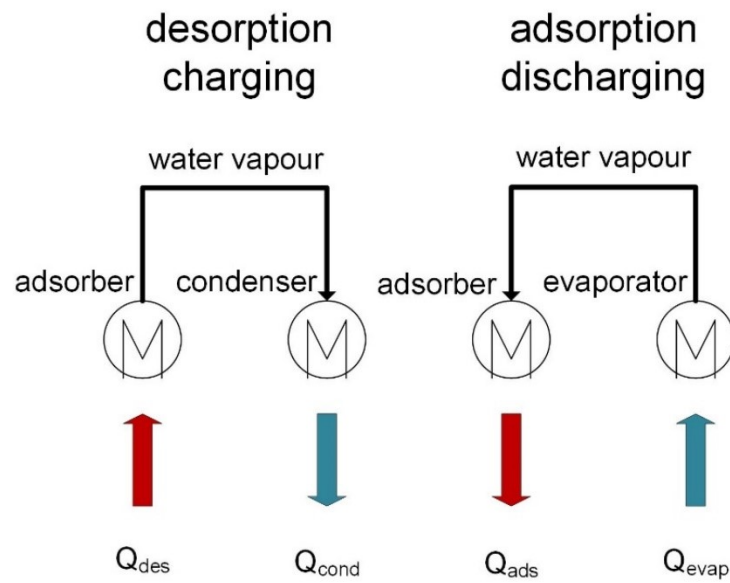
Illustration 2-21: Closed sorption system. [29]
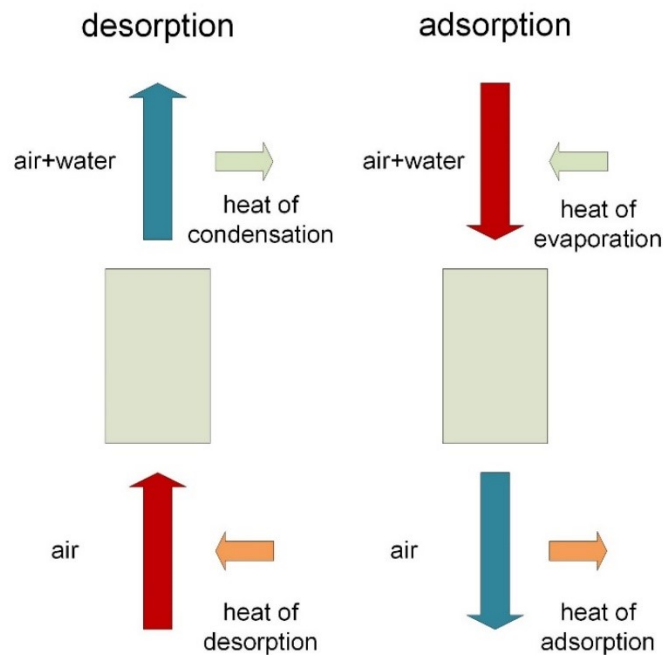
Illustration 2-22: Open sorption system. [29]

2.2.3 Hydration, Dehydration and Calcium Chloride Reactions

For thermal energy storage applications, physical processes like melting hardly exceed heats of some 15 kJmol^{-1} or 250 kJkg^{-1}. Evaporation of water on the other hand is not feasible for low or medium temperature applications in households. Therefore, reversible, chemical reactions in thermochemical energy storage applications have been considered. Levitskij et.

al. mention dehydration as the most promising reaction so far, especially because of its almost perfect reversibility. [30]

Hydration processes are usually exothermic. Water molecules are attached to the crystal lattice of a salt. Ion-dipole interactions or hydrogen bridge bonds cause the attachments. By supplying heat, the attached water can be removed again. [15]

Crystalline hydrates show very promising specific characteristics. $CaCl_2 \cdot 6H_2O$, for instance, has a specific heat of dehydration of 1061 $kJkg^{-1}$. Yet, they tend to liquefy due to their hygroscopic properties. This is also how the idea of hydrophobicity as a stabilising mechanism was born. **Formula (2-4)** and **Formula (2-5)** show a general dehydration step of $CaCl_2$ and, respectively, the complete dehydration of $CaCl_2 \cdot 6H_2O$, consuming +98.6 $kJmol^{-1}$.

$$CaCl_2 \cdot n\,H_2O \rightarrow CaCl_2 \cdot (n-m)\,H_2O + m\,H_2O \quad\quad \text{[30]} \quad\quad\quad \textbf{(2-4)}$$

$$CaCl_2 \cdot 6\,H_2O \rightarrow CaCl_2 + 6\,H_2O\,(l) \quad\quad\quad \text{[30]} \quad\quad\quad \textbf{(2-5)}$$
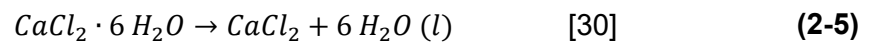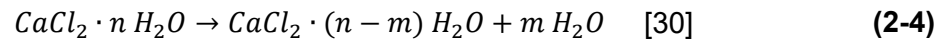
Even though this sounds very promising, numerous problems occur. Due to the dissolving process of the salt, the amount of salt changes. Therefore, the composition of the system within the pores, where liquid phases can and do occur, changes over time. In turn, different $CaCl_2$ species are present. The dehydration is not always complete. This thesis is thus an analysis of how promising the use of this composite is under laboratory conditions. [30]

2.2.4 Ion Exchange

During the ion exchange mechanism, ions are exchanged between a liquid and a solid phase. The concentration gradient between ions is not only balanced by diffusion, because the ions are charged, and, therefore, mere concentration balancing would affect electroneutrality. Usually, ion exchange materials possess ionogenic groups like -COO^- resins. If they are available for ion exchange, cations at the end of such groups are replaced during the process as shown in **Formula (2-6)** and **Formula (2-7)**. [8, 31]

$$z_B A^{z_A} + z_A \overline{B^{z_B}} \rightleftarrows z_B \overline{A^{z_A}} + z_A B^{z_B} \quad\quad\quad \text{[8]} \qu\quad\quad \textbf{(2-6)}$$

$$2Na^+ + \overline{Ca^{2+}} \rightleftarrows 2\overline{Na^+} + Ca^{2+} \qquad [8] \qquad \textbf{(2-7)}$$
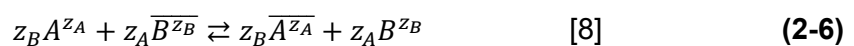
Zeolites do not possess these ionogenic groups. The cations exchanged in zeolites are the cations that can be found within the zeolite pores due to the electric field that occurs when trivalent Al is replaced by tetravalent Si, leaving the framework with a single, negative charge. The alkali and alkaline earth cations occupying the negatively charged positions are not fixed but free to move. The negative charges are therefore spread around the whole zeolite framework. [30]

These ion exchange abilities of the zeolite cause the aqueous salt solutions to change in their compositions during the sorption process. When the next desorption phase starts, the occurring solid salt hydrates are not only $CaCl_2$ hydrates anymore but also mixed crystals, containing, for instance, potassium chloride. This further complicates the whole process. [23]

2.2.5 Interconnections

Thermal heat storage by use of a salt-zeolite composite material is based on the principles of adsorption and desorption. However, no molecule can be adsorbed on the inner surface of the porous substance if it is not transported there first. Also, the occurring heat cannot be used if it is unable to leave the place of its origin. Hence, there must be some sort of interconnection between most of the phenomena described above. This chapter describes these interconnections as well as the influence of the properties mentioned before with the help of the process of thermal energy storage.

For the sorption and therewith the storage process to work, Bathen names seven steps from the transport of a molecule to the adsorbent to the transport of the occurring thermal energy, that is, heat, through the fluid medium. These steps are shown in **Illustration 2-23**. [26]
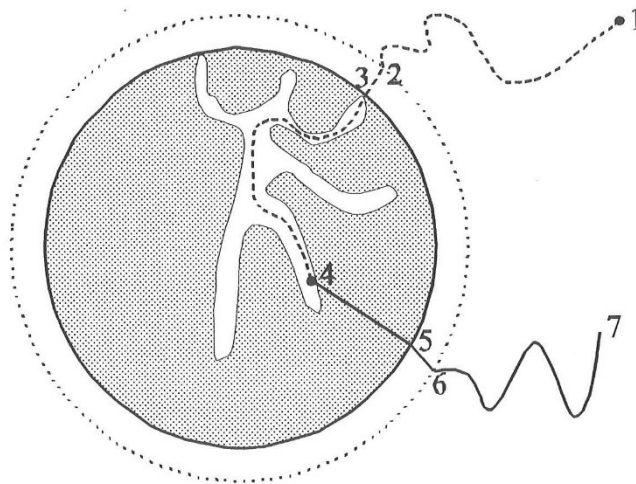
Illustration 2-23: Combined adsorption process. [26]

1. General momentum transport and continuum flow transport a molecule to the boundary layer of the adsorbent particle.
2. Diffusion mechanisms make the molecule to pass through the boundary layer. The kinetics of the diffusion processes are often the limiting factors for the whole heat storage process. Hence, the kinetics of the adsorption process itself (step four) are often neglected.
3. Depending on the molecule and the pore dimensions, certain diffusion mechanisms help the molecule to get to the spot where it is adsorbed to the porous substance's surface.
4. This step describes the actual adsorption process itself.
5. The energy released in step four is transported to the surface of the porous particle by heat conduction.
6. Heat has to get through the boundary layer of the particle just as the molecule does in step two. Just like with the diffusion mechanism, this transport through the boundary layer is simply the product of a model created to be able to describe these processes mathematically. The boundary layer does not actually exist.
7. Convection and heat conduction transport the heat away from the particle. [26]

These steps are complemented by the salt reactions. Hydration and dehydration reactions and $CaCl_2$ phase changes further complicate the overall mechanism. **Illustration 2-24** shows the combined process according to Aristov. [24]
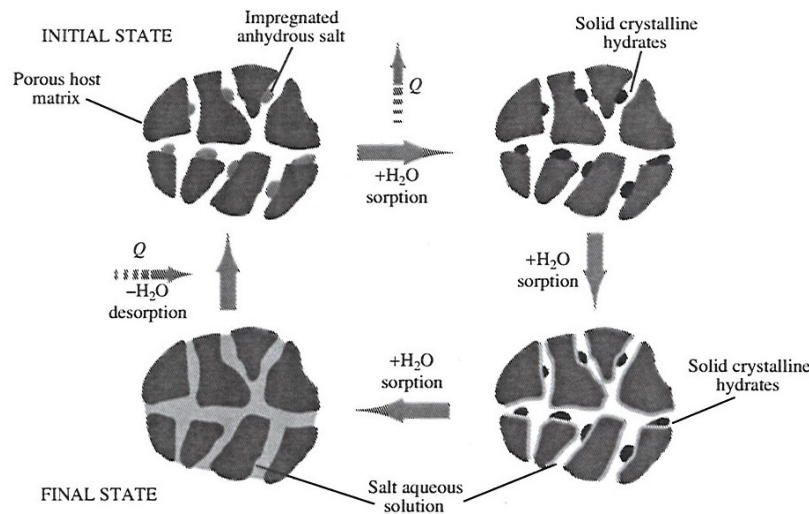
Illustration 2-24: Advanced interconnections. [24]

As complex as it already is, dissolving $CaCl_2$ and ion exchange phenomena are still not considered in **Illustration 2-24**. Therefore, the overall thermal behaviour of the material used in the course of this thesis is examined. The results can be found in chapter 4 of this thesis.

2.2.6 Key Parameters

In thermochemical energy storage systems, heat is brought into the system during the desorption process. Water is removed from the composite material in the reactor by the air that is led through the system. This is also called charging. As long as the material stays dry, no storage capacity is lost. During the adsorption process, humid air is led into the reactor and the resulting heat of adsorption warms up the air. [29]

In order to evaluate these sorption processes, key figures are needed. This thesis is to evaluate the materials' performance during the adsorption process. Therefore, all key figures are related to the adsorption only. The heat of desorption is not considered and, hence, no coefficients of performance are calculated. Also, usually the change in temperature of the air is considered. Since the reactor used is very small and the retention time of the air in the reactor is very short, it is assumed that the air would reach the temperature of the sorption material at the reactor exit, if the reactor was big enough. For all calculations, the upper material temperature is used and it is equated with the exit air temperature. This assumption was made under the advisement of Dr. Hauer. [32, 33]

The first important key figure is the temperature lift. It is the difference between the maximum air temperature reached during the adsorption phase and its starting temperature.

Furthermore, the so-called breakthrough curves are important for the description of the sorption processes. At the beginning of the adsorption phase, no water molecule leaves the reactor, because they are all adsorbed by the zeolite surface or interact with the salt. After a certain loading point, the first molecules can be detected by a humidity sensor at the reactor exit. The RH of the exiting air then starts to increase rapidly until it equals the inlet air composition. The breakthrough curve describes this temporal change of the exit air state. [33]

Other important parameters of these energy storage systems are the energy density and the usable heat. The energy density is a specific energy parameter describing the energy that can be stored per volume or mass unit of sorption material. In this case it is calculated via the air that flows through the reactor. Basically, the energy density defines how much air can be heated by how many degrees only due to the sorption and hydration mechanisms in the reactor. It is calculated as shown in **Equation (2.2)**. [33]

$$\rho_Q = \frac{c_{p,air} \cdot \dot{m}_{air}}{V_{sorb}} \cdot \int_{t_0}^{t_1} \Delta T(t) \cdot dt \qquad [33] \qquad \textbf{(2.2)}$$

In order to evaluate the data from the experiments easily, the integral is replaced by a sum as follows (**Equation (2.3)**). A more detailed description of the formula symbols used and the evaluation method applied can be found in chapter 5.

$$\rho_Q = \frac{c_{p,air} \cdot \dot{m}_{air}}{V_{sorb}} \cdot \sum_{i=0}^{n} \Delta T_{m,i} \cdot \Delta t_i \qquad \textbf{(2.3)}$$

This formula includes every single rise in temperature compared to the starting temperature. For most household applications of these systems, a certain temperature is needed to make the integration of such systems sensible. In Dr. Hauer's dissertation, a system is mentioned that integrates households into a district heating grid using sorption storage systems. For such systems, a temperature of 65°C is necessary. The results of the experiments presented in this thesis (chapter 4) suggest that an application of the materials observed cannot provide such temperatures. Therefore, a lower temperature of 40°C was chosen as a cut-off temperature for this thesis. The term usable heat of adsorption refers to the energy stored per volume unit

of adsorption material that delivers an exit air temperature above the cut-off temperature of 40°C. Its calculation is based on an equation found in the work of Dr. Hauer. The form used is shown in **Equation (2.4)**. Like with the energy density, the integral is replaced by a sum as shown in **Equation (2.5)**. [33]

$$Q_{use} = \frac{c_{p,air} \cdot \dot{m}_{air}}{V_{sorb}} \cdot \int_{t_0}^{t_1} \Delta T_{use}(t) \cdot dt \quad [33] \qquad (2.4)$$

$$Q_{use} = \frac{c_{p,air} \cdot \dot{m}_{air}}{V_{sorb}} \cdot \sum_{i=0}^{n} \Delta T_{m,use,i} \cdot \Delta t_i \qquad (2.5)$$

2.3 Humidity of Air

Air can only take up a certain amount of water vapour that is highly dependent on the prevailing temperature. For laboratory observations, it can be assumed that the pressure is constant at around 1 bar and for calculations it is sufficiently exact to assume that the water vapour as well as the dry air behave like ideal gases. [34]

There are a lot of ways to describe the amount of water taken up by a certain amount of air. The most common and the ones that are relevant to this thesis are the specific humidity as well as the RH, defined as shown in **Equation (2.6)** and **Equation (2.7)**. [34, 35]

$$\varphi = \frac{m_w}{m_w + m_{air}} \qquad (2.6)$$

$$f = \frac{e}{e_s} = \frac{m_w}{m_{w,s}} \qquad (2.7)$$

The latter offers the chance to describe the state of saturation of the air. When fully saturated, the amount of water taken up by the air is at its maximum and so is the water vapour pressure. At a certain temperature, this saturated vapour pressure cannot be exceeded. It is only dependent on the temperature and increases along with an increasing temperature. [34]

When a mixture of water vapour and air is cooled, the water starts to condense at a certain temperature, because the air cannot hold the existent amount of water anymore. This temperature is called dew point temperature (DPT). At DPT, the air is saturated with water vapour. [35]

Equation (2.8), the Magnus equation, provides an empirical attempt to mathematically describe the dependency of the saturated vapour pressure on the DPT. [34]

$$e_s(T) = 6{,}1 \cdot 10^{\frac{7{,}45 \cdot T}{235 + T}}$$ **(2.8)**

An effective way to set the relative humidity in an experimental setup as desired is the use of aqueous solutions of inorganic substances. Such substances, like sulphuric acid or various salts, lower the water vapour pressure above the solutions. [36]

In the initial experimental setup described in chapter 3.1, $CaCl_2$, sodium chloride and potassium carbonate solutions were used to set the relative humidity. Due to the temperature dependency of the water vapour pressure, there was no chance to counteract against seasonal changes in the room temperature. Even a slight change in temperature can lead to significant deviations from the desired relative humidity. Also, the small surface of the salt solution in the gas washing bottles used causes a problem, because the area of air – solution interaction is not big enough for an equilibrium adjustment. Later in this thesis, the effects and the occurring inaccuracies are described. [37]

The current experimental setup uses a method relying on the DPT explained above. With the help of a thermostat, deionised water in gas washing bottles is held at a certain temperature at which the air is saturated with water. Afterwards, the air passes through tubes that are long enough for the air to reach room temperature. While the maximum amount of water that can be taken up by the air increases, the actual water load does not change anymore, because there is no source of water after the gas washing bottles. Hence, according to **Equation (2.7)**, the relative humidity decreases from 100% to the desired value. [36]

3 Experimental Setup

This chapter shows the preliminary experimental setup and the amendments that were made in order to optimise the experimental execution. With the help of process flow diagrams, graphics and the results of exemplary experiments, the effect of the necessary amendments is illustrated.

3.1 Initial Setup

The initial experimental setup is shown in **Illustration 3-1**.
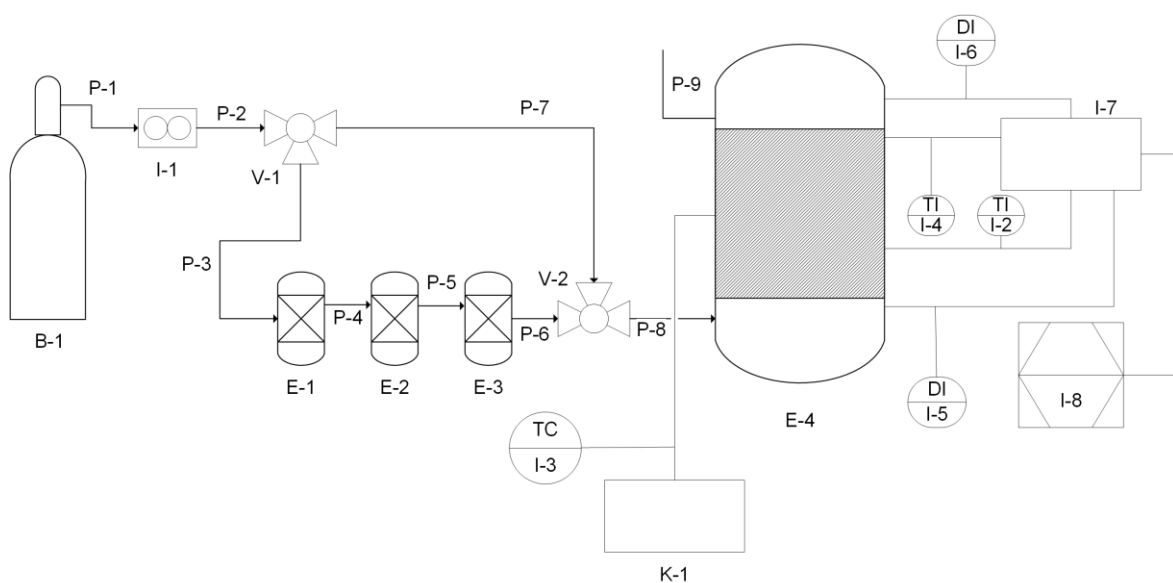
Illustration 3-1: Initial experimental setup.

In **Table 3-1** and **Table 3-2** the labels used in **Illustration 3-1** are explained.

Table 3-1: Basic symbol key to **Illustration 3-1**.

label	meaning
B	cylinder
DI	relative humidity indication
E	reactor
I	indication unit
K	control unit
P	pipe
TC	temperature control
TI	temperature indication
V	valve

Table 3-2: Detailed symbol key to **Illustration 3-1**.

label	meaning
B-1	cylinder with synthetic air
E-1 to E-3	gas washing bottles
E-4	reactor
I-1	flow meter
I-2 and I-4	thermocouples
I-3	temperature control by heater
I-5 and I-6	humidity sensors
I-7	case with electrical measuring system
I-8	computer
K-1	heater
P-1 to P-9, excluding P-7	pipes
P-7	heating tube
V-1 and V-2	cross valves

A more detailed depiction of the reactor can be found in **Illustration 3-2**.
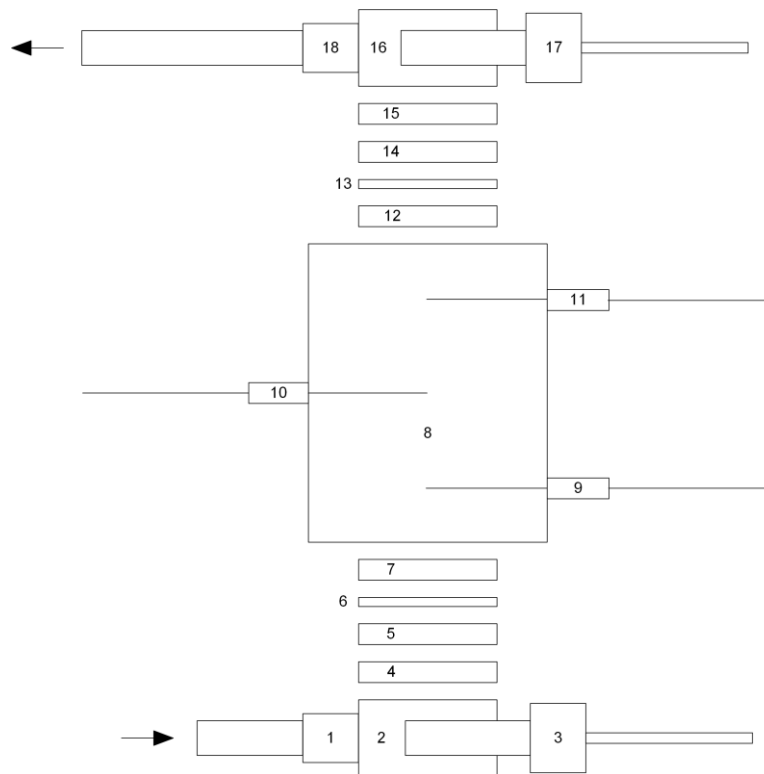
Illustration 3-2: Reactor composition.

Table 3-3 explains the numbering used in **Illustration 3-2**.

Table 3-3: Number key to **Illustration 3-2**.

number	meaning
1	air inlet
2	bottom seal
3	bottom humidity sensor
4	bottom inner gasket
5	bottom glass filter
6	bottom paper filter
7	bottom outer gasket
8	reactor
9	bottom thermocouple
10	thermocouple from heater
11	upper thermocouple
12	upper outer gasket
13	upper paper filter
14	upper glass filter
15	upper inner gasket
16	upper seal
17	upper humidity sensor
18	air outlet

The synthetic air used consists of 80% nitrogen and 20% oxygen. During the adsorption process (the exact execution is explained in chapter 4.1) it is led through the three gas washing bottles. The first one contains deionised water for cleaning purposes. The second as well as the third bottle contain salt solutions in order to set the relative humidity of the air as explained before. The temperature and humidity indication system signals are recorded by a measuring system and depicted with the help of a computer. The temperature is set by a heater that is connected to a thermocouple in the middle of the material bed. Even though there have always been two humidity sensors, the second one had to be tested and repaired due to malfunction. Hence, air was led through the empty reactor in a preceding experiment in order to determine the relative humidity set by the salt solutions. The relative humidity measured was about 55%, even though respective literature suggested 45% for the chosen settings, according to Meitner. Also, this value altered with the changing room temperature in different seasons with hardly any opportunity to change other parameters in order to counteract than changing the used salt. Therefore, the most significant amendment made is the different approach to set the relative humidity using vapour pressure tables and deionised water. [38]

Another problem was the justification of the heater. Unsuitable settings of the controller unit led to significant variations of the temperature during the experimental execution.

As a last change to the initial setup, the reactor was replaced by a bigger one in order to be able to work with more material and gain more significant data. After a certain time period the exit air temperature should approach the material temperature. Due to the small-sized reactor and the small heat exchange surface, this was not the case. Even the bigger reactor with a diameter of 4.3 cm and a height of 11 cm turned out not to be big enough. However, Dr. Andreas Hauer suggests that for calculations it can be assumed that the exit air temperature is the material temperature indicated by the second sensor. [32]

A single experiment with the synthetically produced zeolite 13XBF (particle size 1.6-2.5 mm) at a desorption temperature of 50°C delivered the results shown in **Illustration 3-3**.
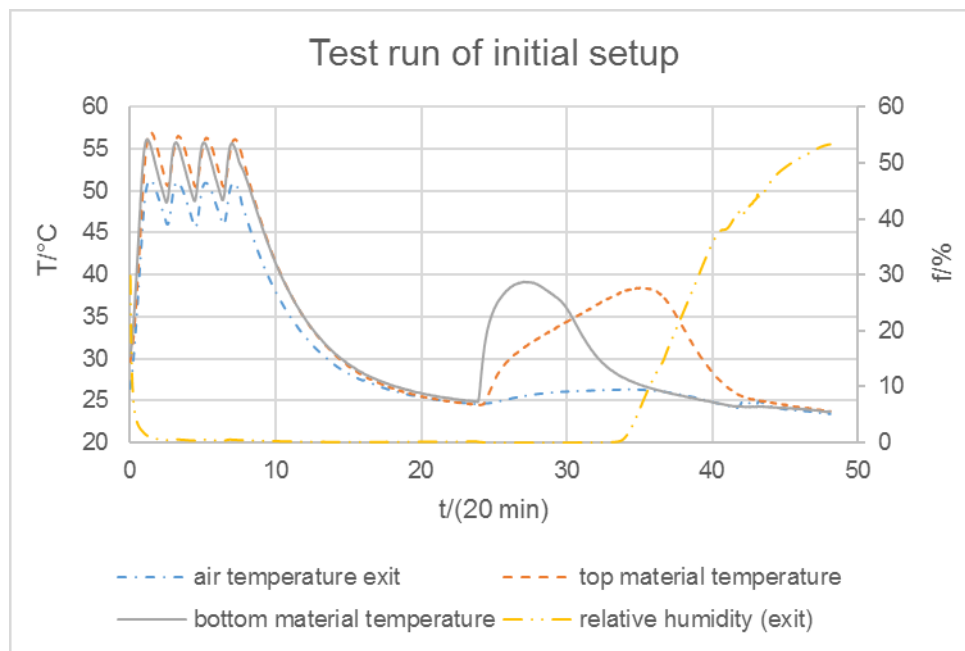
Illustration 3-3: Temperature behaviour of zeolite 13XBF in initial experimental setup.

The diagram in **Illustration 3-3** reflects the layout of all following diagrams regarding the sorption experiments. The experiment duration is plotted on the abscissa in 20 minute steps. Therefore, a value of nine means 3 h. The material and air temperatures are plotted on the primary ordinate on the left, the RH values on the secondary ordinate on the right.

The volume flow was held constant at 4 l/min during the whole experiment. The desorption happened at a temperature of 50°C. The variations of the temperature can be seen in **Illustration 3-3**. However, a difference of 5°C is basically acceptable. The influence of the variations of the temperature during the desorption process becomes more relevant at higher temperatures (s. **Illustration 3-4**). After letting the material cool down and reach room temperature, the adsorption process was initiated. The behaviour of the material resembles the description found in literature. The temperature lift was almost 15°C with a maximum temperature some 10°C below the desorption temperature. The whole experiment lasted 16 hours. After approximately eleven hours the first water molecules passed through the material and reached the second humidity sensor. It can also be seen that the air temperature at the exit hardly increased at all. This is because of the small reactor size and the resulting small heat exchange area. In theory, the maximum air temperature should approach the maximum material temperature.
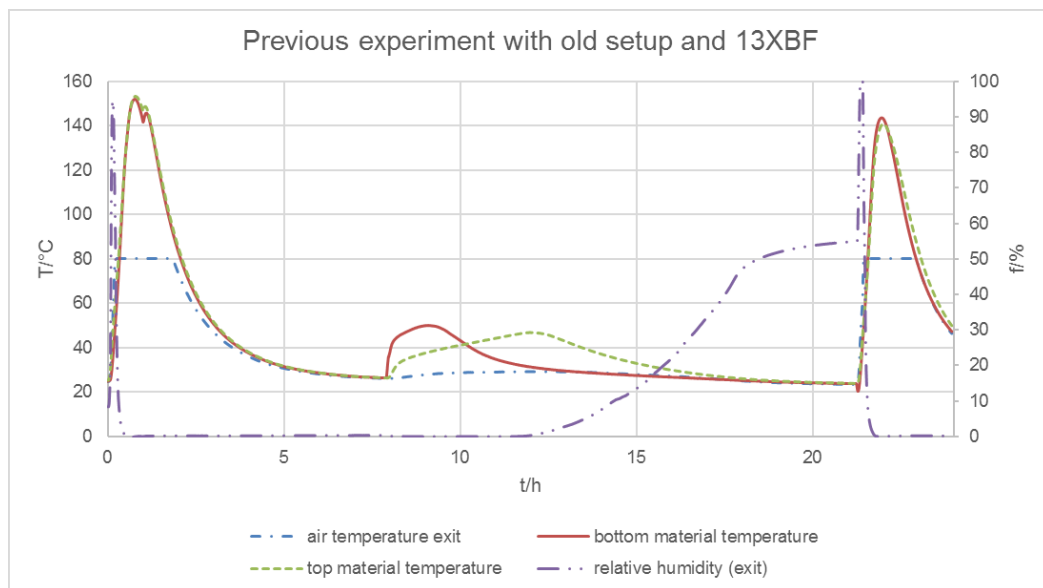
Illustration 3-4: 13XBF at 140°C desorption temperature. [38]

It can be seen that at higher temperatures the deviation from the desired temperature is far higher and the variations of the temperature are bigger than 10°C. [38]

3.2 Modification

The first step of the modification process was the disassembly of the existing setup in order to set the relative humidity. The gas washing bottles were cleaned and replaced, because only one of them had a frit assuring the distribution of the gas in the liquid. In avoidance of water getting into the pipes, only one bottle was filled with deionised water. The maximum water level at which no water could get into the pipes at a volume flow of 8 l/min was determined. Afterwards, the other bottles were filled accordingly. All pipe connections were renewed where necessary.

Secondly, the reactor was replaced by a larger one. Due to the limited length of the usable part of the heating wire used, the distance between the windings had to be increased. Also, the insulation of the heating wire showed severe damages. Therefore, the wire was replaced by a new, longer one. The windings are now closer together and an improved heat transfer can be achieved. The insulated wire is in direct contact with the reactor surface. It is covered by a layer of insulating wool, approximately 1.5 cm thick. The wool is fixed with the help of a layer of adhesive tape which has an aluminium layer on its other side.

Next, the gas washing bottles were put into the bath of a thermostat. Before, the thermostat had been emptied, cleaned and filled with new tempering liquid.

The temperature sensors were replaced by longer ones, so that they reach into the middle of the material bed. The second humidity sensor was re-installed and tested.

In order to tackle the problem of the temperature variations caused by the heater, its settings were adapted according to the user manual. **Table 3-4** shows the settings used.

Table 3-4: Explanation of heater parameters.

parameter	meaning	value
Pb	parameter for P-controller	1,5
Ti	reset time (I-controller)	70,0
Td	lead time (D-controller)	10,0
SP_L	lower limit of set point	79,0
SP_H	upper limit of set point	80,0
Lcb	low cutback (prevents overshooting)	6,5
Hcb	high cutback (prevents undershooting)	3,0
oP_H	upper heating power limit	16,0
operation	automatic or manual operation	auto

These settings allow the heater to operate in a way that the desired temperature is approached quickly but without severe overshooting. The variations of the temperature can be held low and a more accurate approach of the set point as well as a constant temperature can be achieved.

After the thermostat had been installed and the two gas washing bottles had been filled, the setting of the relative humidity could be tested. At first, random thermostat temperatures and volume flows were tested in order to discover general trends. The results of these tests can be found in **Table 3-5**.

Table 3-5: Setting the relative humidity with two gas washing bottles.

T [°C]	$\dot{V}$ [l/min]	f [%]
5	2	55
	4	45
	6	40
10	2	66
	4	56
	6	52

To assure that an equilibrium in the interaction between the air and the water is reached, a third gas washing bottle was installed. Subsequently, the resulting relative humidity at a room temperature of approximately 21°C was measured at different thermostat temperatures and volume flows. The results are shown in **Table 3-6**.

Table 3-6: Setting the relative humidity with three gas washing bottles at different volume flows and temperatures.

T [°C]	$\dot{V}$ [l/min]	f [%]
2	4	39
	6	35
	8	32
5	4	43
	6	40
	8	38
10	4	56
	6	52
	8	49
15	4	73
	6	71
	8	69

The values found in tables **Table 3-5** and **Table 3-6** are the mean values of both humidity sensors. At lower volume flows, the values differ significantly (4-6%). It is possible, that due to the low pressure in the reactor at a volume flow of 2 l/min, false air can reach the upper sensor, which in turn shows a higher value. Also, the air temperature in the reactor is not influenced by the temperature of the thermostat bath.

It can be seen that the minimum relative humidity is reached at low thermostat temperatures and high volume flows. The thermostat temperature has not been set below 0°C in order not to risk freezing of the water in the gas washing bottles. 8 l/min seems to be an appropriate value for the volume flow to achieve a low relative humidity without risking the breaking of the frits. Therefore, a table for different thermostat temperatures ranging from 0°C to 14°C at a volume flow of 8 l/min and a room temperature of approximately 24°C was created in order to set any desired relative humidity achievable with this setup. The results can be found in **Table 3-7**.

Table 3-7: Setting the relative humidity at a volume flow of 8 l/min and different thermostat temperatures.

T [°C]	f [%]
0	28,5
1	29,0
2	30,0
4	34,0
6	38,0
8	43,0
10	48,0
12	54,0
14	62,0

So as not to risk the breaking of the frits, the achievable minimum relative humidity at 0°C thermostat temperature and a volume flow of 10 l/min was determined and can be seen in **Table 3-8**.

Table 3-8: Minimum relative humidity achievable with the modified setup.

T [°C]	f [%]
0	28

In order to evaluate the accuracy and plausibility of these measurements, the Magnus equation was used to compare the measured humidity values to literature values (s. chapter 2.3). For every thermostat set point, the resulting relative humidity was measured three times. Subsequently, a mean value was calculated. These can be found in **Table 3-9**.

Table 3-9: Measured relative humidity per thermostat set point.

T_{th} [°C]	f_{meas} [%]	f_m [%]
2,5	32	31,00
	30	
	31	
12,0	56	57,00
	58	
	57	
18,0	85	83,00
	83	
	81	

For every temperature, the vapour pressure of the saturated air can be calculated with the help of the Magnus equation. If the results are put in relation to the vapour pressure of the saturated air at room temperature (s. **Table 3-10**), the calculated relative humidity can be obtained. Subsequently, the calculated values were put in relation to the measured mean values of three experiments. The findings and deviations can be found in **Table 3-11**.

Table 3-10: Vapour pressure of saturated air at room temperature.

T_r [°C]	22,50
$p_{s,r}$ [hPa]	27,31

Table 3-11: Deviation of the measured values from the calculation.

T_{th} [°C]	2,50	12,00	18,00
$p_{s,r}$ [hPa]	7,31	14,04	20,67
f_{calc} [%]	26,76	51,40	75,70
f_{meas} [%]	31,00	57,00	83,00
deviation [%]	13,68	9,82	8,80

With the mean relative humidity values, the actual air temperature in the gas washing bottles can be calculated with the same equation, only the other way around. The results can be found in **Table 3-12**.

Table 3-12: Actual air temperature in the gas washing bottles.

T_{th} [°C]	4,58	13,57	19,47
$p_{s,r}$ [hPa]	8,47	15,57	22,67
f_{calc} [%]	31,00	57,00	83,00
f_{meas} [%]	31,00	57,00	83,00
deviation [%]	0,00	0,00	0,00

It is highly plausible that the actual air temperature in the gas washing bottles is higher than the thermostat temperature, because there is not a lot of time or surface area for the air and the thermostat liquid to reach a temperature equilibrium. Also, the deviation is higher at low temperatures, which is also plausible due to the highest deviation from the room temperature at these conditions.

The comparison with calculated values and the previous tables also show that the third gas washing bottle does not change the resulting values. Hence, it can be assumed that an equilibrium state of air saturation is reached in the described setup. The following illustrations, **Illustration 3-5** and **Illustration 3-6**, summarise the stated results and depict the influence of the volume flow and the thermostat temperature on the relative humidity.
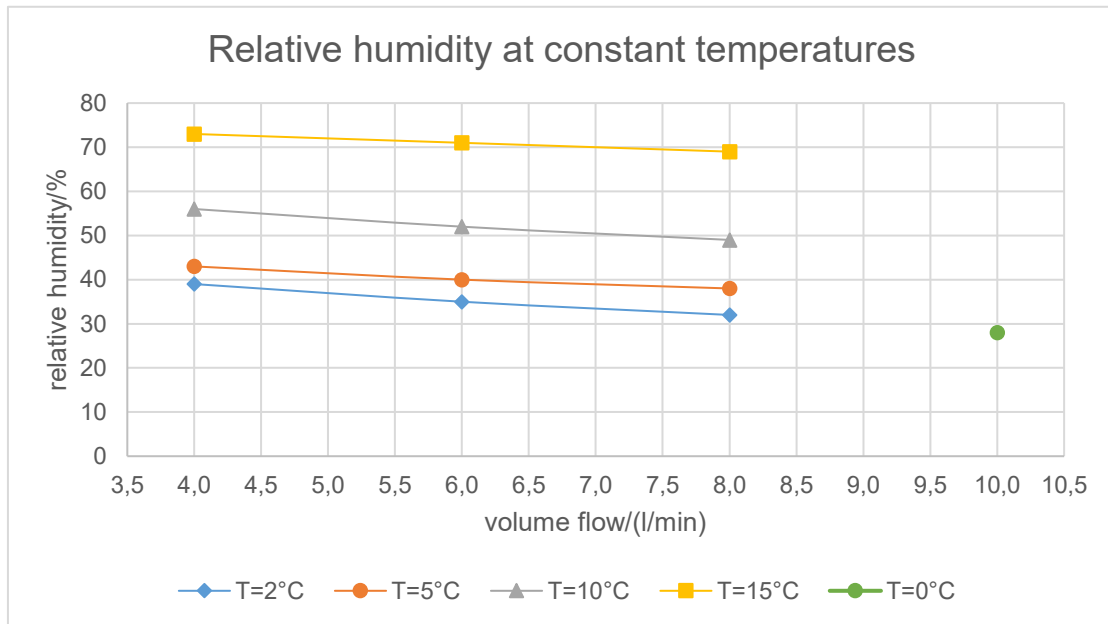
Illustration 3-5: Influence of the volume flow on the relative humidity.
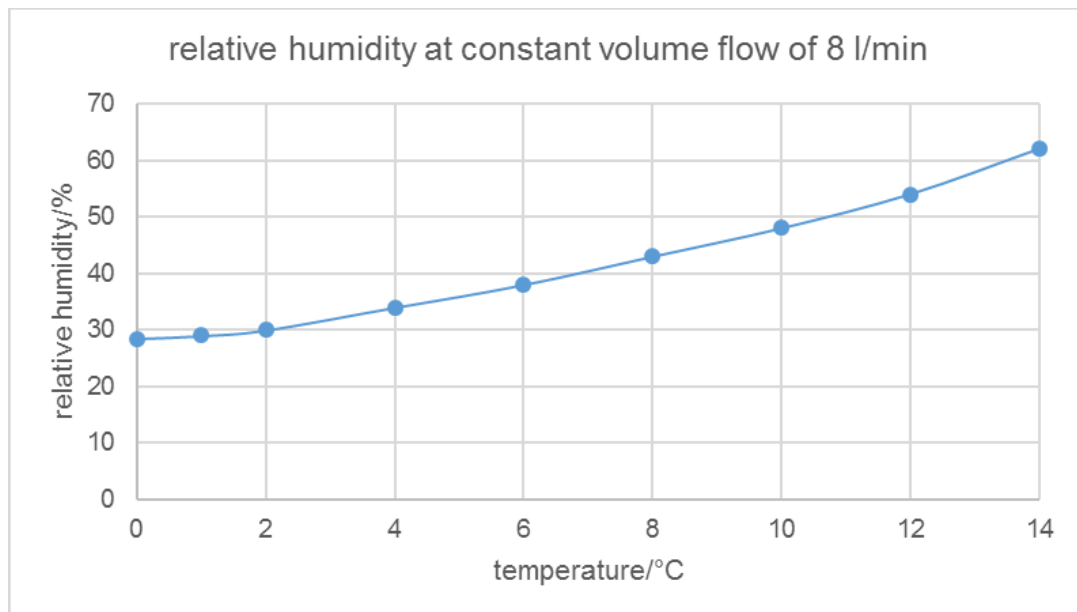
Illustration 3-6: Influence of the thermostat temperature on the relative humidity.

During the humidity measurements, it could be noted that it takes between 15 and 20 minutes for a new relative humidity value to attune and stay constant. Therefore, a third cross-valve was installed between the second cross-valve and the reactor in order to be able to lead the air from the gas washing bottles into the atmosphere for about 25 minutes before letting it flow into the reactor. By doing so, it can be assured that the adsorption process happens at a constant humidity throughout the experiment.

In order to determine the systematic fault of the humidity sensors, the air was led through the heating tube. This way it enters the reactor with 0% relative humidity, apart from minute deviations due to drops of residual water that cannot be removed. After some 90 minutes, the values were noted. The results can be seen in **Table 3-13** and in **Illustration 3-7**.

Table 3-13: Systematic fault of humidity sensors.

fault sensor 1 [%]	fault sensor 2 [%]
0,22	0,07
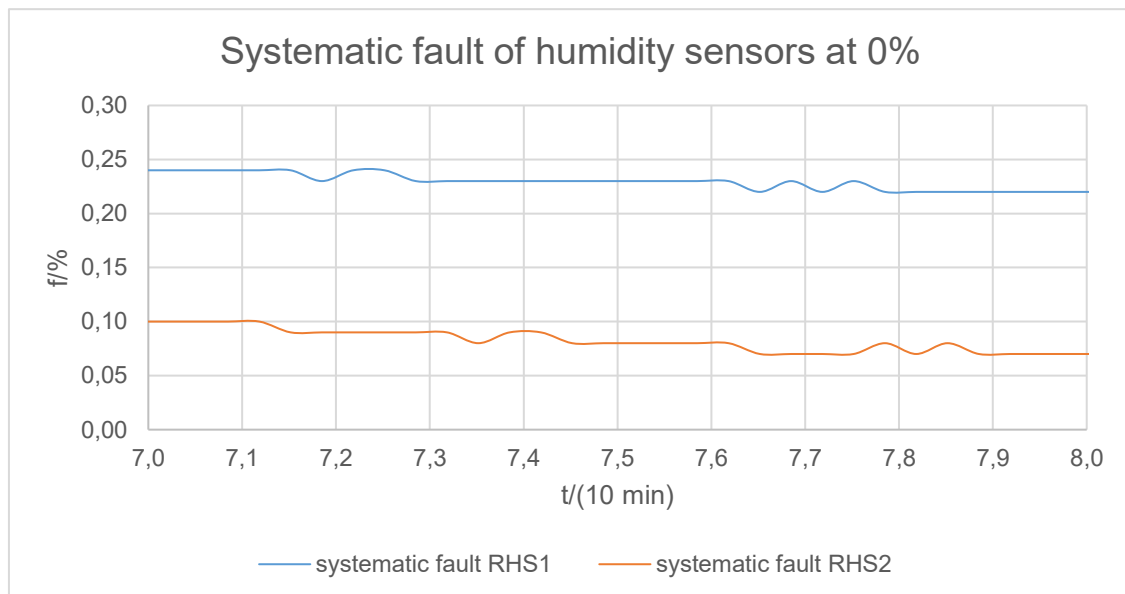
Illustration 3-7: Determination of the systematic fault of the humidity sensors.

3.3 Modified Setup

The modified setup is illustrated in **Illustration 3-8**.
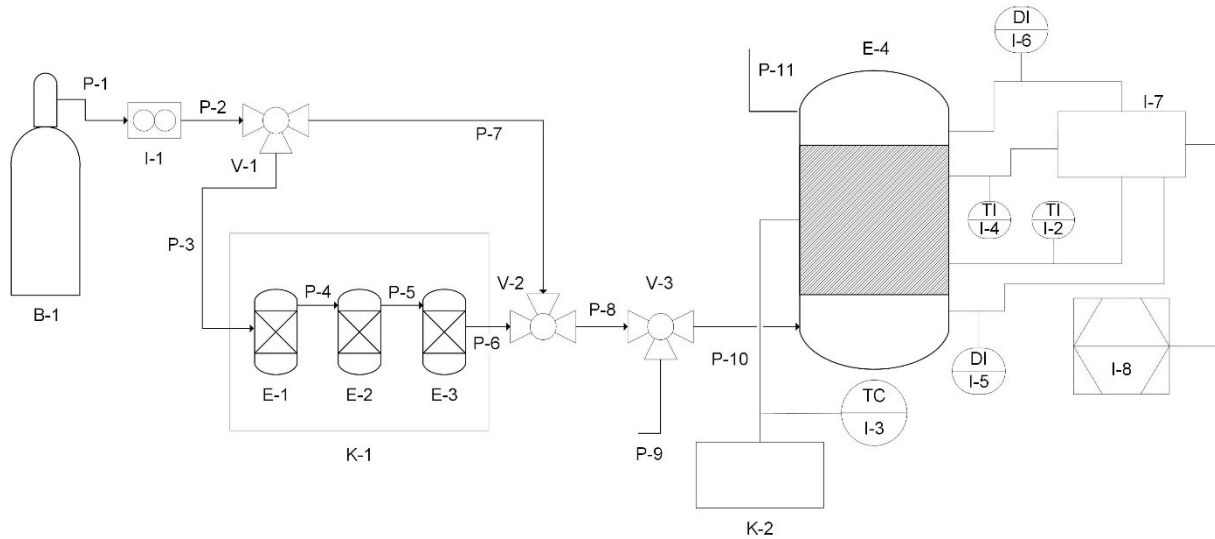
Illustration 3-8: Modified setup.

The symbol keys found in tables **Table 3-1** and **Table 3-2** are also valid for **Illustration 3-8** and **Table 3-14** shows the adapted symbol key including only amendments and additions.

Table 3-14: Symbol key for **Illustration 3-8**.

label	meaning
K-1	thermostat
K-2	heater
P-1 to P-11, excluding P-7	pipes
V-1 to V-3	cross valves

The following pictures, **Illustration 3-9** and **Illustration 3-10**, show the experimental setup and reactor used for the experiments described in this thesis. **Table 3-15** and **Table 3-16** show the respective number keys.

Illustration 3-9: Photo of experimental setup.

Table 3-15: Number key to **Illustration 3-9**.

number	component
1	air cyclinder
2	thermostat with gas washing bottles
3	reactor
4	heater
5	electrical evaluation unit
6	laptop with visualisation programme
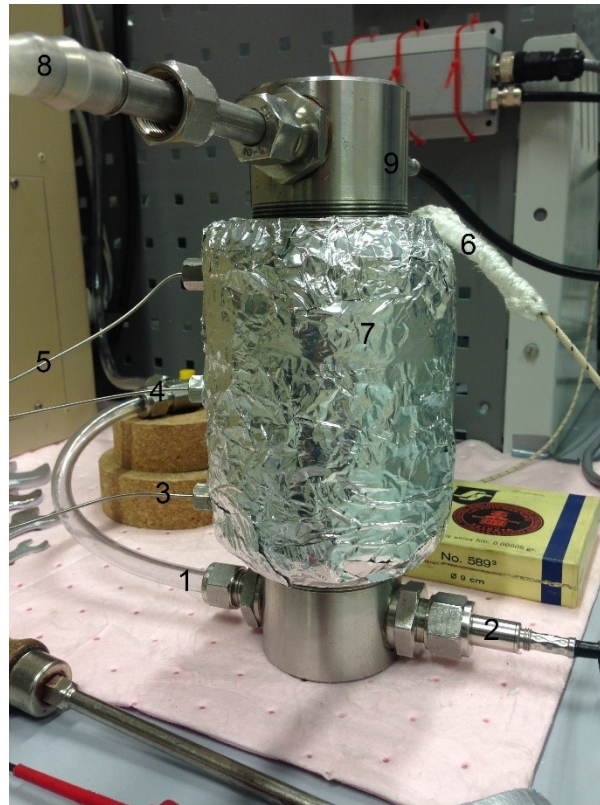
Illustration 3-10: Photo of reactor.

Table 3-16: Number key to **Illustration 3-10**.

number	component
1	reactor inlet
2	humidity sensor 1
3	thermocouple 1
4	thermocouple 2 (from heater)
5	thermocouple 3
6	heating wire (from heater)
7	insulation
8	reactor outlet
9	humidity sensor 2

In a first experiment with the synthetic zeolite 13XBF (1.6-2.5 mm) at a desorption temperature of 80°C and a volume flow of 8 l/min the new setup was tested. The results are shown in **Illustration 3-11**.
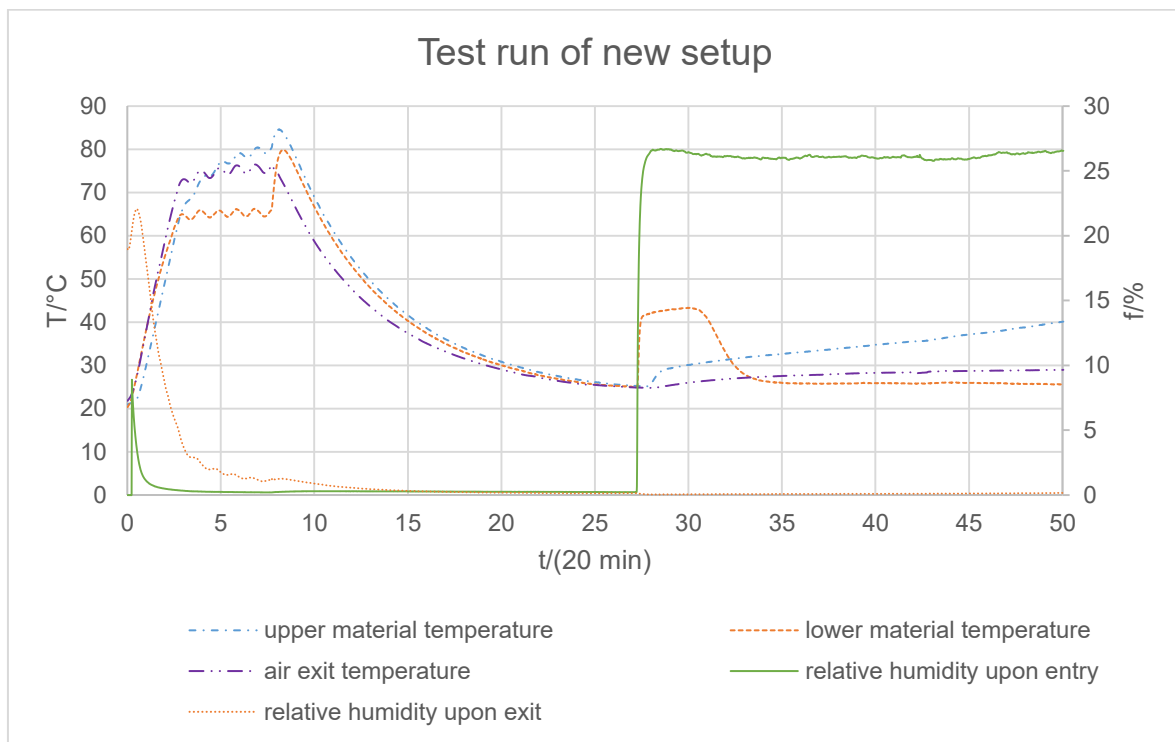
Illustration 3-11: Test run of new setup with zeolite 13XBF.

It can be seen that the heater works very exactly. The material temperature approaches the 80°C set point slowly and the overshooting is only some 4°C. What can also be seen is that the bottom material temperature does not exceed 65°C during the desorption process. This can be caused by the air entering the reactor. It seems not to enter at 80°C and therefore cools the material upon entry. As soon as the air flow is halted and the reactor is sealed so it can cool down, the material at the bottom of the bed reaches 80°C as well. Given that the thermocouple connected to the heater is located in the middle of the material bed and the upper thermocouple measuring the material temperature shows the desired 80°C, only a small part of the zeolite bed is influenced by the cooling effect of the entering air. However, this is a deviation from the desired condition and has to be considered. As the upper material temperature seems not to be influenced, it is chosen for further discussions.

Another deviation is caused by the remaining relative humidity of about 1.3% measured by the upper humidity sensor when the desorption process is over (constant humidity and temperature values for a minimum of 20 minutes). As soon as the reactor is sealed, the humidity at both sensors approaches 0% (0.2 and, respectively, 0.4%). The zeolite adsorbs the remaining water molecules when the cooling phase starts and therefore is not completely dry when the adsorption process begins.

The reason why the remaining 1.3% relative humidity cannot be removed might be that the air from the gas washing bottles (adsorption) and the air from the heating tube (desorption) have to pass through the same pipe system in order to reach the reactor (see **Illustration 3-8**). As these pipes and the cross-valve (V-3) do not reach a temperature that is significantly exceeding the room temperature, residual water can never be fully removed.

The constant values for the relative humidity during the cooling of the reactor indicates that the setup is sufficiently leak-proof.

The experiment was aborted before the breakthrough point. The abortion was caused by the low filling level of the air supply bottle. Yet, in order to discuss the success of the modification procedure, the experiment is sufficiently expressive.

What is remarkable is the setting of the relative humidity. For over 7.5 h the value of the relative humidity of the air entering the reactor was an almost constant 26% with a thermostat temperature of 2°C. This is 4% below the value stated in **Table 3-7**. It might indicate that during the humidity test runs, residual water in the reactor or a change in the room temperature increased the values by 3-4%. However, a relative humidity of 25% is seemingly achievable with the new setup.

Subsequent to the first test run, possible leaks were eliminated by winding a sealing film over potentially leaking connections due to the high air consumption. Also, the upper glass filter in the upper seal of the reactor broke. It was replaced by a second gasket of the same thickness. As the air flows used are not so high as that material could be carried out of the reactor, a paper filter at the top is enough. The bottom glass filter is intact and serves as a seating for the material bed. Afterwards, the air consumption was the same as before.

In conclusion, the modification was highly successful. The main aspects, the heat regulation and the setting of the relative humidity, both work exactly enough in order to continue with the explicit measurement of the thermal properties of the zeolite materials.

4 Measurement of the Thermal Behaviour

In order to determine the thermal behaviour of the materials described, they are all put through the same desorption-adsorption-cycle. Subsequently, the respective temperature lifts, energy density values and values for the usable heat of adsorption are analysed. This chapter describes the execution of the experiments and shows the results.

4.1 Experimental Execution

The experimental execution can be divided into three phases:

- Desorption phase
- Cooling phase
- Adsorption phase

These three phases are described in this chapter.

4.1.1 Desorption Phase

In the beginning of every experiment, the air outlet and the upper humidity sensor are dismantled and the reactor is filled with the sample, which has been weighed. After reassembling and sealing the reactor, the recording software is booted. The valves are brought into position so that the air passes through the heating tube. The heating tube and the heater are turned on and the logging software is started. The material is now gradually heated to the set point temperature of 80°C (or any other desired desorption temperature) and the heating

tube assures that the air is moisture-free. The relative humidity at both sensors ideally approaches 0%. As soon as the upper material temperature reaches the set point as well as the relative humidity reaches 0% and both values stay constant for at least 20 minutes, the air as well as the material are nearly free from any water molecules and the desorption phase is over.

4.1.2 Cooling Phase

After the desorption phase is finished, the reactor's air outlet pipe is sealed using a clamp and almost simultaneously the air flow is turned off and the cross-valve preceding the reactor is brought into the position where the air from the air source is led into the room. Ideally, no air from outside the reactor can get inside and the relative humidity values at both sensors are 0%. It takes about seven hours for the reactor and the sample to reach room temperature (between 20°C and 25°C). As soon as room temperature is obtained the cooling phase is completed.

4.1.3 Adsorption Phase

In order to assure that the relative humidity of the air that is led into the reactor for the adsorption phase is set as desired, the thermostat is activated when the material temperature is around 24°C. When the desired thermostat temperature is reached, the air flow is initiated. The air passes through the three gas washing bottles and is led into the room. With the help of the previous humidity tests it can be assumed that the desired relative humidity is reached after 25 minutes. This can be done parallel to the end of the cooling phase.

Subsequently, the cross-valve position is changed so that the air is now led into the reactor. Shortly after that, the clamp sealing the reactor's air outlet is removed. This chronology assures that no air from outside can get in through the air outlet in case of under-inflation in the reactor.

As the adsorption process begins, the material's temperature increases. At some point, the first water molecules pass through the material bed and the relative humidity at the upper sensor starts indicating an increasing value. When the exit relative humidity equals the entry relative humidity and the material temperature reaches room temperature, the adsorption phase is over.

The end of the adsorption phase is also the end of one experiment. The air flow is halted, the logging software is stopped and the data file can be obtained. After halting the air flow, the first gas washing bottle must shortly be opened in order to prevent water from rising into the

preceding pipe due to momentary under-inflation. In the case of the synthetic zeolite, the experiment could be repeated immediately. With the composite, the material has to be replaced first, because of the dissolving process of the salt. After the experiment, the material is weighed again. With a desorption temperature of 80°C and a volume flow of 8 l/min, the first phase takes about 2.5 h, the cooling phase some 7 h and the adsorption phase approximately 8 h with the zeolite 13XBF, depending on the parameters of the experiment, which makes for a total duration of about 17.5 h. With the natural zeolites, including the Multi 5-20 materials, the desorption phase is much shorter (1 h), while the cooling phase takes a little longer (8-9 h), probably due to the higher void volume and the resulting poor thermal conductivity. Due to the fact that most of the Multi materials don't reach the breakthrough point within 24 hours, the adsorption phase is only ended when the air cylinder is almost empty. On average, this takes some 16 h.

4.1.4 Deviations from the Described Execution

First of all, the desorption temperature is not 80°C throughout the whole loose bulk. After the air has left the heating tube, it still has to pass through some 30 cm of piping at room temperature. Hence, the material at the bottom of the loose bulk is cooled by the entering air and shows roughly 65°C. As soon as the reactor is closed and the air flow is halted, heat conduction heats up the cooler material as well. This is one of the reasons why the upper temperature value is chosen to evaluate the results, the other reason being that the exit air temperature is needed to calculate the energy density and it is assumed that it equals the top material temperature.

Depending on the material, the last percentage point of relative humidity is hard to remove. Sometimes, single droplets of water occur in the pipe system preceding the reactor. Also, the 13XBF materials always seem to retain a small amount of adsorbed water and take up even traces of available molecules. Due to the fact that one air cylinder is used for both the desorption and adsorption processes, the duration of the desorption phase is limited. Therefore, a remaining relative humidity of 0.2% to 1.5% is accepted.

Furthermore, the upper glass filter broke after several experiments while changing the material. A few experiments had been conducted without such a filter at the top of the material bed before it was replaced. Due to the limited air flow of 8 l/min, the paper filter was sufficient to keep the loose bulk stable and no influence on the results could be observed.

Sometimes, the material bed moves because of the air flow. The material can be loosened and set differently than before. The pressure conditions in the reactor can therefore change in

the beginning of the experiment and alter the volume flow. Hence, the experiment was regularly observed and the volume flow was adjusted when needed, especially during the first hour.

Lastly, at higher RH values, the humidity value at the entrance of the reactor is not stable. As soon as the adsorption phase begins, the relative humidity decreases. In the case of the 80% experiments, it even plummets to 65% and only slowly approaches 80% towards the end of the experiment. Due to the rapidly increasing temperature as soon as the zeolite adsorbs water molecules, the maximum saturated vapour pressure of the air also rises while the actual vapour pressure set in the gas washing bottles stays constant. This results in a lower relative humidity, whereas the absolute humidity is not influenced. For the comparable loading of the zeolite materials, the absolute humidity values resulting from temperatures set by the thermostat are held constant for the whole series of experiments. They reflect the relative humidity values of 30%, 55% and 80% based on an average room temperature of 22.5°C.

4.1.5   Reason for Choice of Experiment Parameters

In a complete system conception described by Dr. B. Mette, energy surpluses from photovoltaic installations can be used for the desorption of the composite material. Reasonable temperatures for household, that is low-temperature, applications obtained from a photovoltaic installation are in the range of 80°C. Therefore, this desorption temperature was chosen. [15]

The RH values are based on the deliquescence RH of $CaCl_2$, 30%, and an average room RH of 50%. In addition, the sorption behaviour at a relative humidity level exceeding these values by far was analysed. As a result, the three different, equidistant RH values of 30%, 55% and 80% were chosen.

4.2   Data and Observations

This chapter contains the data and results of all executed sorption experiments. Also, notable observations are described. **Table 4-1** gives an overview of all experiments conducted.

Table 4-1: Overview of conducted experiments.

thermal behaviour at different RH values			
material	f=30%	f=55%	f=80%
13XBF	Y	Y	Y
Mono	Y	Y	Y
13XBF H4	Y	Y	Y
Mono H4	Y	Y	Y
Multi 5	Y	Y	Y
Multi 10	Y	Y	Y
Multi 15	Y	Y	Y
Multi 20	Y	Y	Y
Multi 5 S	Y	Y	Y
cycle stability tests			
material	cycle 1	cycle 2	cycle 3
Multi 5	Y	Y	Y
Multi 5 S	Y	Y	N

4.2.1 Thermal Properties of Synthetic Zeolite 13XBF

Illustration 4-1 shows the thermal behaviour of the synthetic zeolite 13XBF at different relative humidity settings.
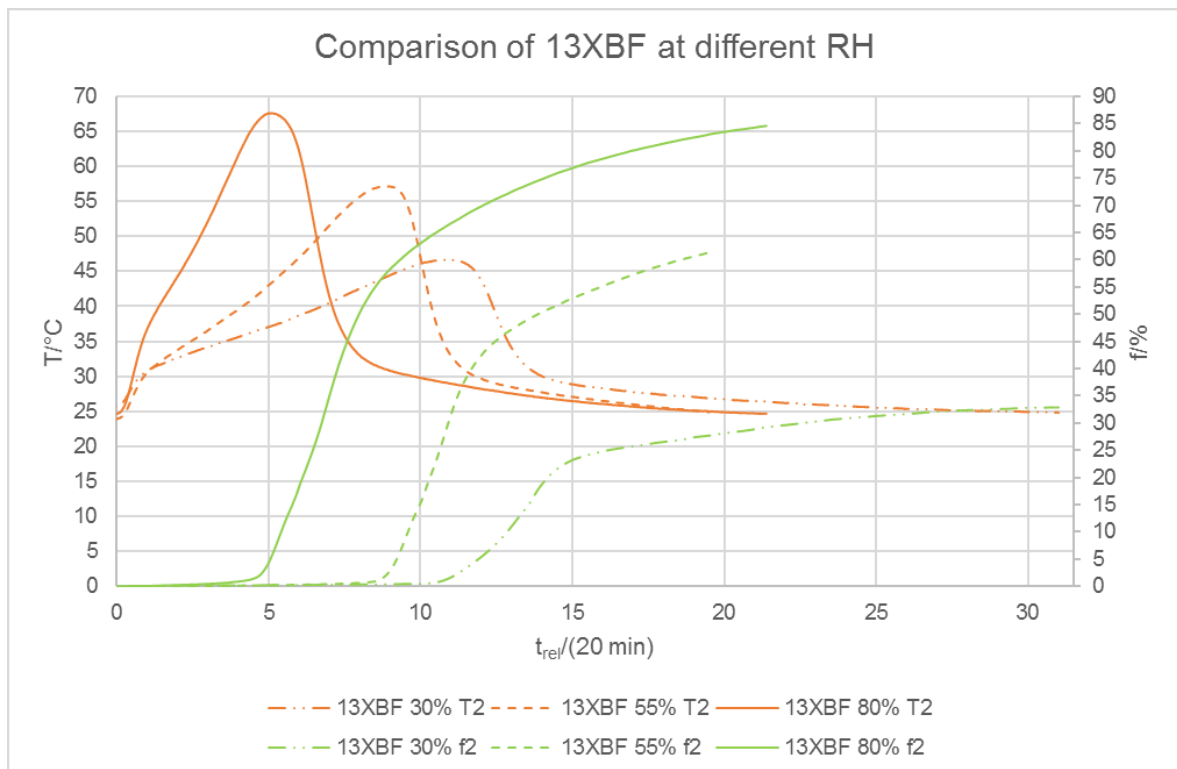
Illustration 4-1: Thermal behaviour of 13XBF.

Both the temperature and the RH (breakthrough curves) show a perfect trend as expected after the examination of respective literature. The steep slopes of the breakthrough curves suggest that every water molecule is adsorbed to a free spot of the zeolite surface. Due to the regular structure of the synthetic zeolite framework, the first water molecule can only leave the reactor when there are hardly any vacant spots left.

At higher RH settings, the experiment duration is lower than it is at lower RH values. The steepness of the breakthrough curves also declines with declining RH. Due to the higher absolute amount of water molecules at high RH, the whole zeolite surface is covered more quickly.

It must be mentioned that the final RH at the reactor exit exceeds the desired values of 30%, 55% and 80%. This is because the required thermostat set point temperature was unknown in the first experiments due to a change in the room temperature between the first RH measurements and the first experiments conducted.

The exemplary experiment with the modified setup shown in **Illustration 3-11** shows a very constant RH of roughly 30%. It has to be mentioned that at higher RH level, especially at 80% RH, the value is not as stable. Due to the immediate change in temperature at the bottom of the reactor, the maximum water uptake capacity of the air increases while the actual amount of water in the air flow stays the same. Therefore, the RH decreases. Yet, the effect on the experiment analysis is minute, because the upper RH sensor and thermocouple were used to evaluate all results. Also, the absolute amount of water per m³ of air that is available for adsorption is not influenced. Lastly, the effect of the rise in temperature on diffusion and other phenomena is a part of the overall energy storage process anyway. In order to illustrate the effects at different levels of RH, **Illustration 4-2** shows the development of the individual RH levels measured by the lower humidity sensor during the experiments with 13XBF.
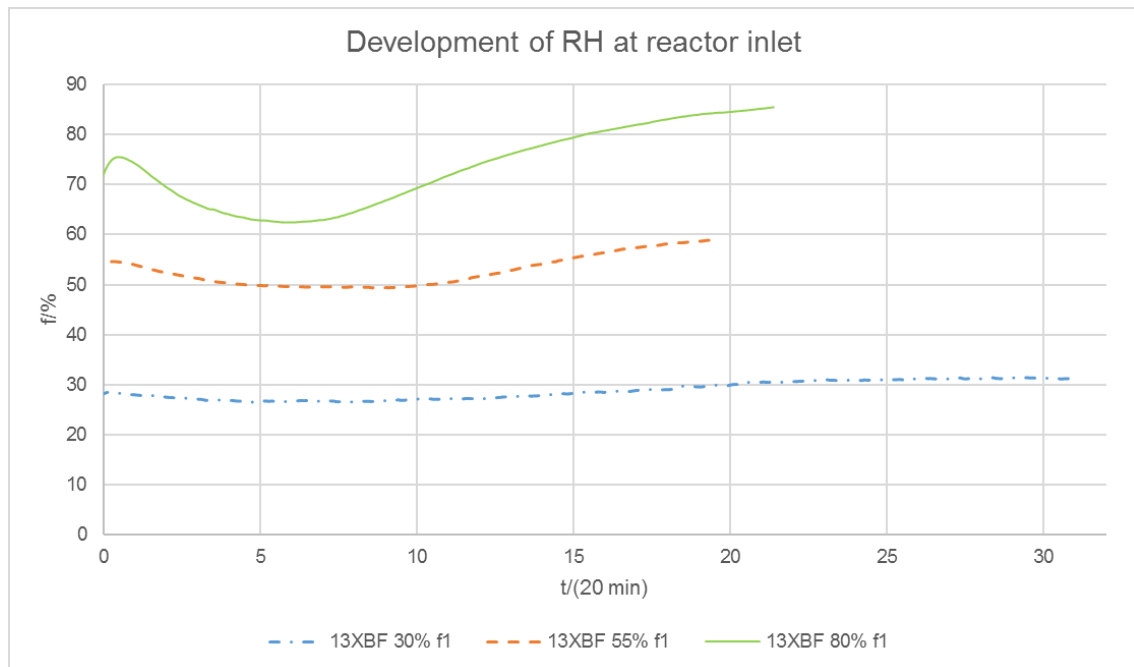
Illustration 4-2: Recordings of lower humidity sensor.

As a last point, it was observed that the water consumption in the first gas washing bottle was by far the highest of all three. Almost no water in the second and third bottle was consumed. This shows, that the saturation equilibrium of the air – water system could be reached easily.

4.2.2 Thermal Properties of Pure Clinoptilolite Mono

Illustration 4-3 shows the thermal behaviour of the pure clinoptilolite Mono.
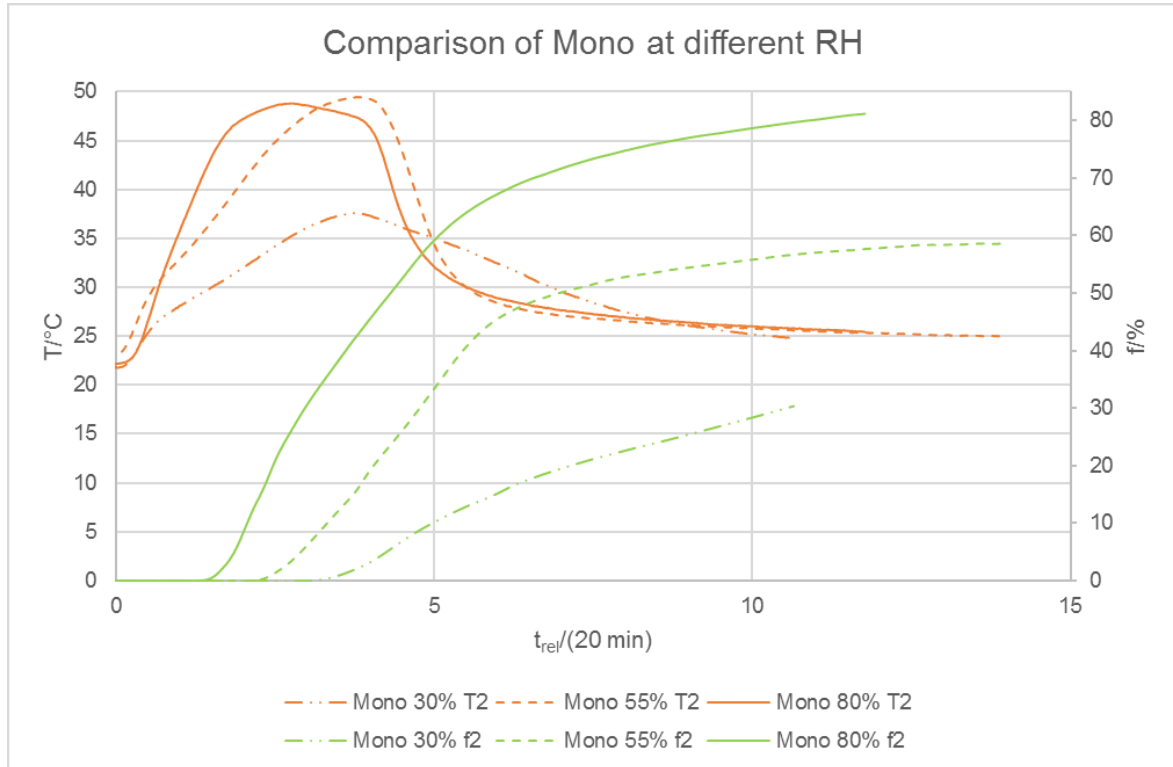
Illustration 4-3: Thermal behaviour of Mono.

At first sight it is noticeable that the slopes of the breakthrough curves are not as steep as with the synthetic zeolite 13XBF. Also, the temperature trend is by far not as distinct. Thirdly, the experiment duration is way shorter.

All three observations can be explained with the help of the difference in channel and cavity structure of the natural and the synthetic zeolites. The framework of the natural zeolite is irregular. Furthermore, the material bed looks very different. Natural zeolite grains are edgy and differ in shape and size. As a consequence, the material bed is not loaded with water molecules layer by layer but irregularly. If a certain spot on the surface is not easily accessible for water vapour, it is possible that it is occupied later than spots at the same height in the reactor.

Due to the lower number of surface spots occupied by water molecules simultaneously, the temperature lift is not as high as with 13XBF. This is thought to be changed by the $CaCl_2$ impregnation.

4.2.3 Difference Between the Synthetic Material and the Natural Zeolite

Illustration 4-4 shows the thermal behaviour of 13XBF and Mono in direct comparison.
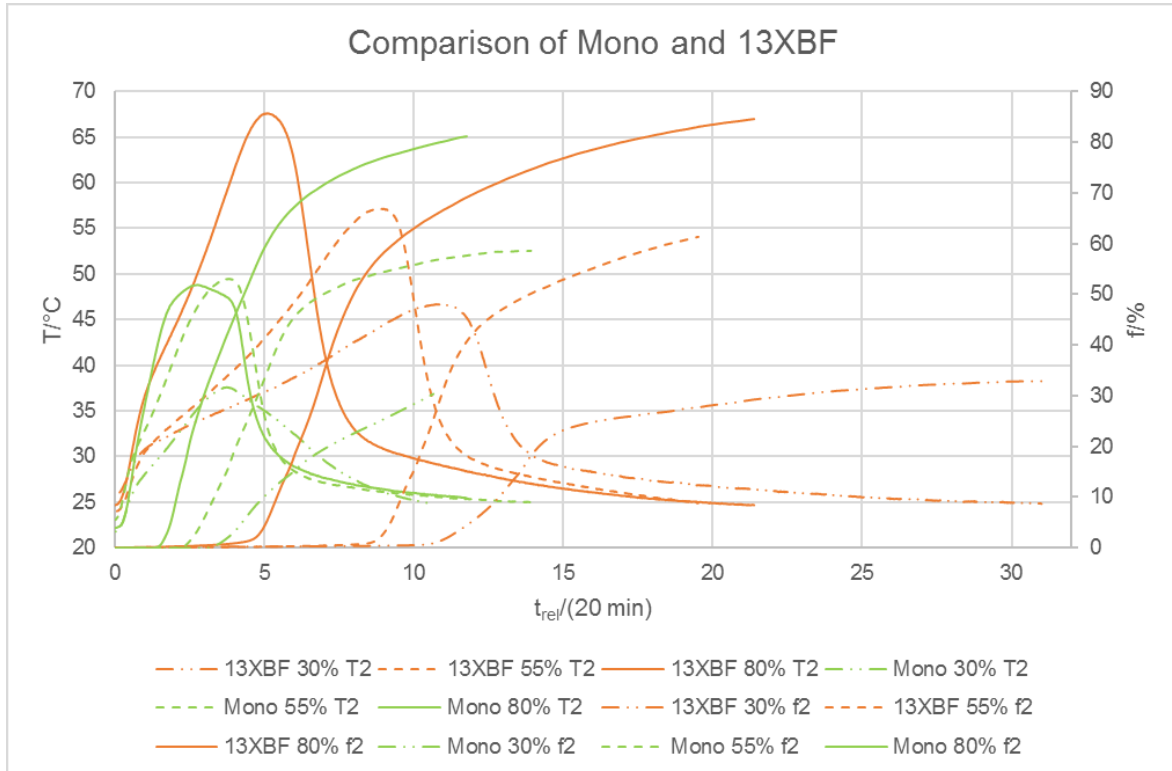
Illustration 4-4: Comparison of the thermal behaviour of 13XBF an Mono.

The individual materials have already been discussed above. In the following, the most important differences are shortly listed.

- 13XBF shows steeper breakthrough curves.
- 13XBF shows a distinct temperature curve trend.
- Mono's maximum temperatures are way lower than the ones of 13XBF.
- The experiment duration is longer with 13XBF.

4.2.4 Influence of Hydrophobicity on Synthetic and Natural Zeolites

The following illustrations, **Illustration 4-5** and **Illustration 4-6**, show the effect of the hydrophobicity on both, the synthetic and the natural materials.
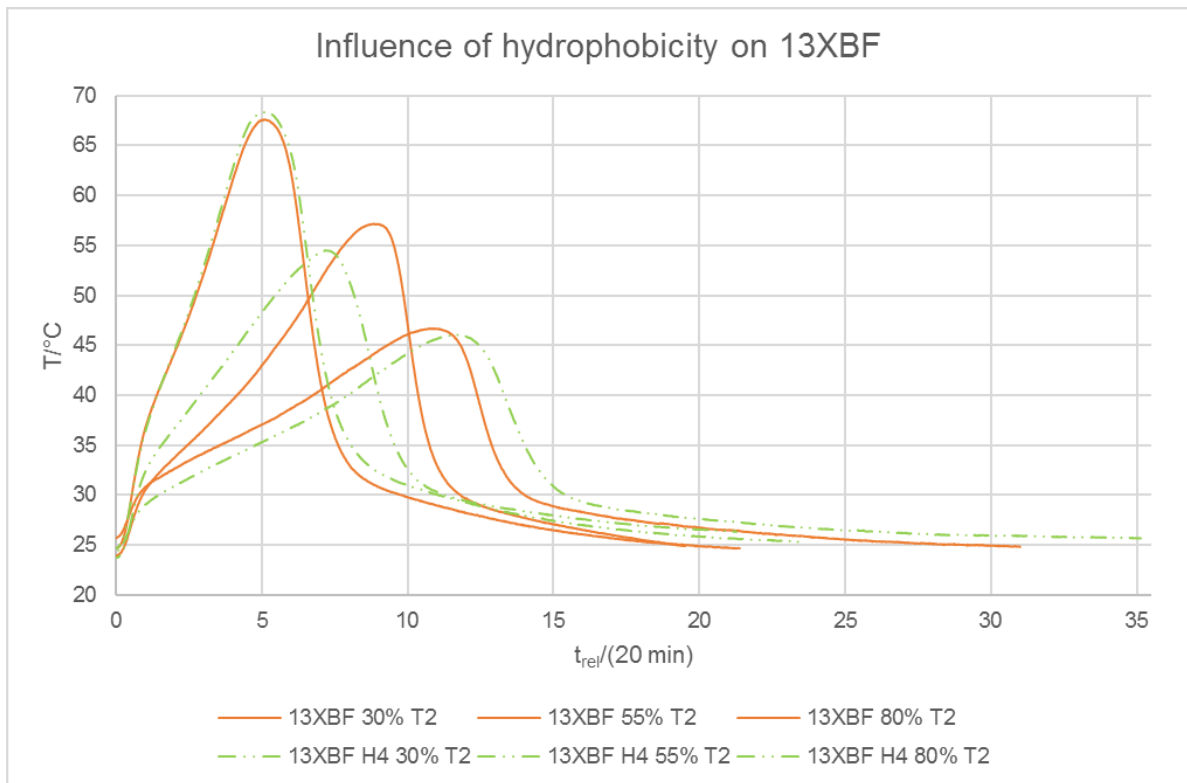
Illustration 4-5: Effect of hydrophobicity on 13XBF.
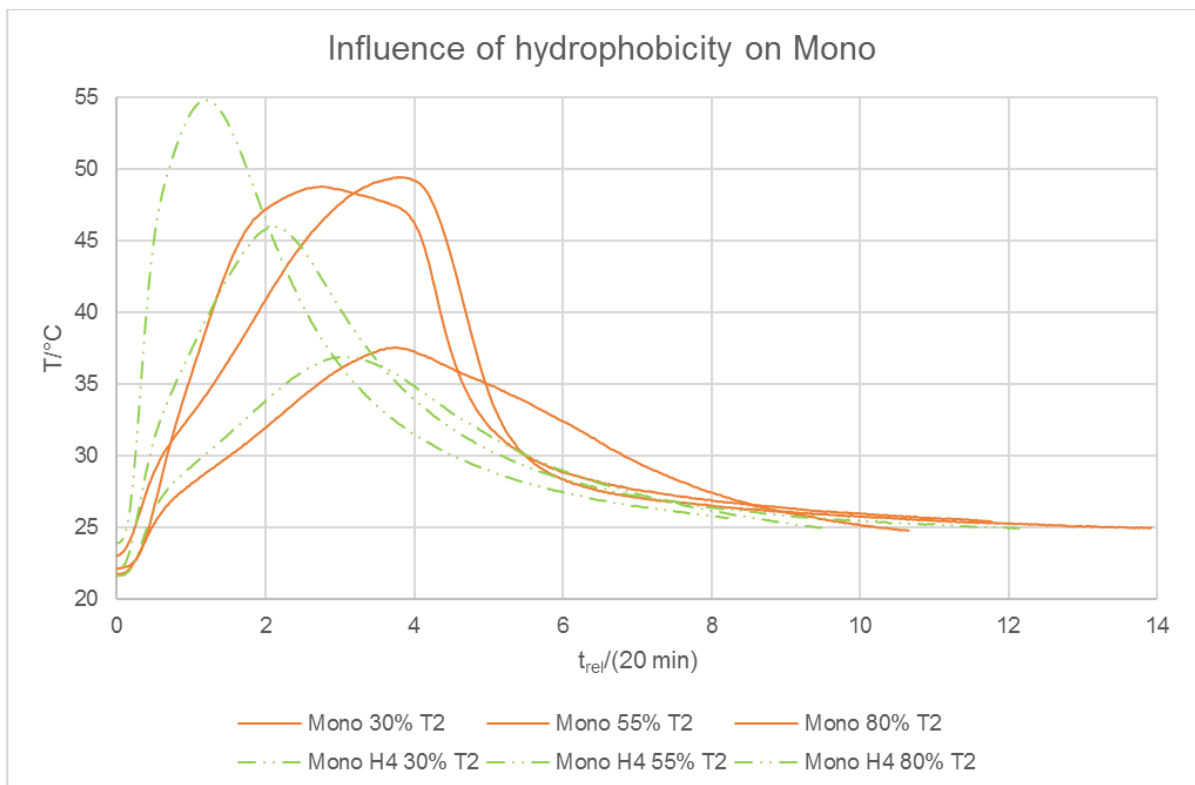
Illustration 4-6: Effect of hydrophobicity on Mono.

The experiments with the hydrophobised materials 13XBF H4 and Mono H4 illustrate perfectly what the hydrophobicity does to the materials.

In the case of the 13XBF zeolite, the effect is next to nought. The experiment duration increases slightly, whereas the maximum temperatures do almost not change at all. The peaks are shifted negligibly, which is most likely a random error, as the shift does not occur at all three RH levels tested and when it occurs, the shift direction is not always the same. The pore structure of 13XBF is already so regular that a thin layer of hydrophobic substances does not significantly change it.

The effect on Mono materials on the other hand is immense. Unlike 13XBF, Mono possesses micropores, which are most likely closed by the hydrophobicity treatment. Anomalies in the pore structure are smoothened. Therefore, the hydrophobised natural zeolite shows a trend in the temperature curves as distinct as the one of the synthetic material. The curves resemble the ones of 13XBF. Yet, the maximum temperatures are in the same range as the ones of pure clinoptilolite.

4.2.5 Thermal Properties of the Hydrophobised Composite Materials Multi 5-20

In this chapter, the results of the experiments with all Multi materials are presented. First, in **Illustration 4-7**, **Illustration 4-9**, **Illustration 4-10** and **Illustration 4-11**, the behaviour of the individual materials at different RH settings are illustrated. Later, all materials (Multi 5-20 and Mono) are compared to each other, always at a certain RH (s. **Illustration 4-14**, **Illustration 4-15** and **Illustration 4-16**).
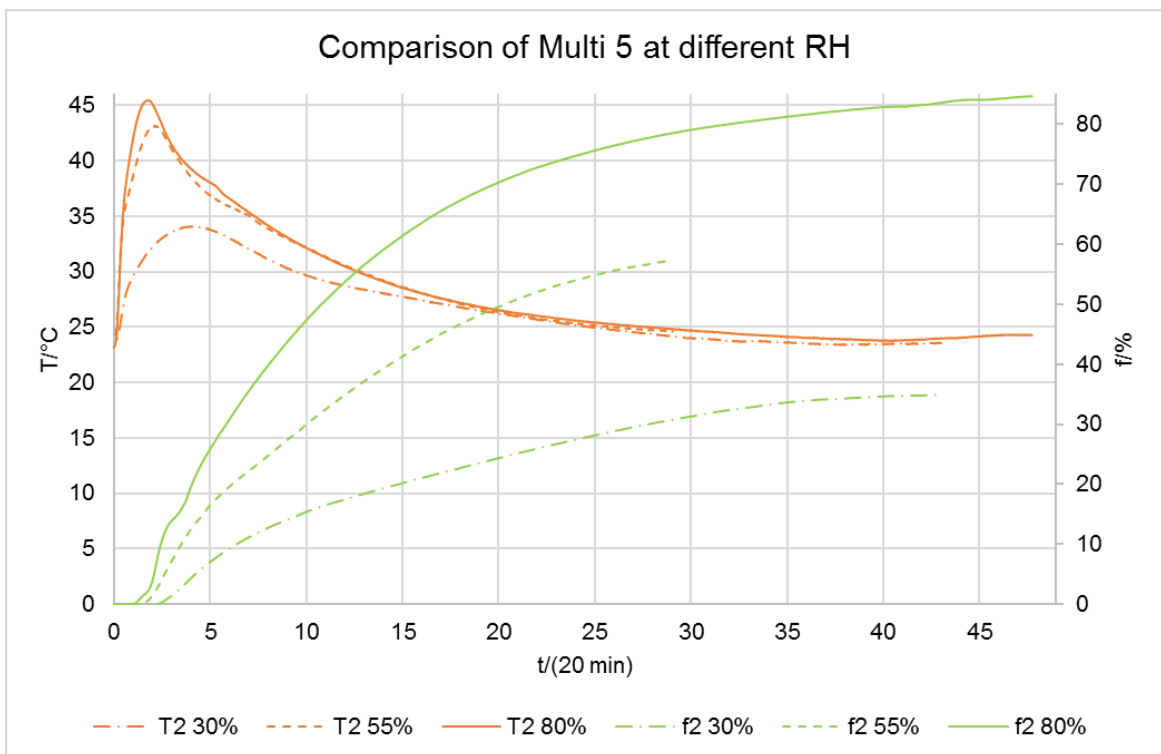
Illustration 4-7: Thermal behaviour of Multi 5.

At first glance, the temperature curves do show a pretty distinct trend. Yet, unexpectedly, the maximum temperatures are below the ones measured with the natural zeolite.

The most eye-catching, visual difference to the diagrams shown before are the slopes of the breakthrough curves. The first water molecules reach the reactor exit very early. The curves then slowly approach the RH at the reactor entrance. The inlet RH values are reached, but only after a very long time (adsorption phases of up to 16 h).

Due to the low amount of $CaCl_2$, the dissolution of the salt hardly occurs at 30% RH. After the experiments, the reactor and the material are dry. At 80% RH, the salt slightly liquefies and a small amount of the material adheres to the reactor (s. **Illustration 4-8**).
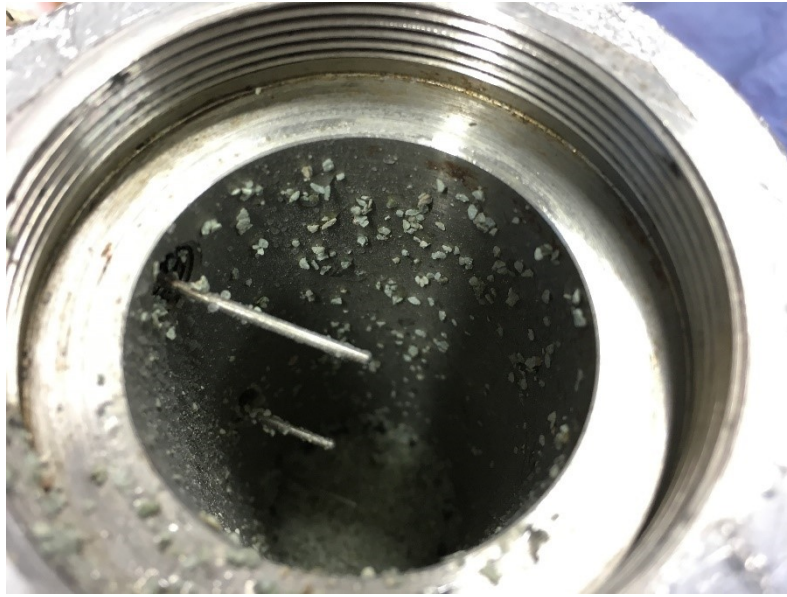
Illustration 4-8: Reactor after an experiment with Multi 5 at 80% RH.
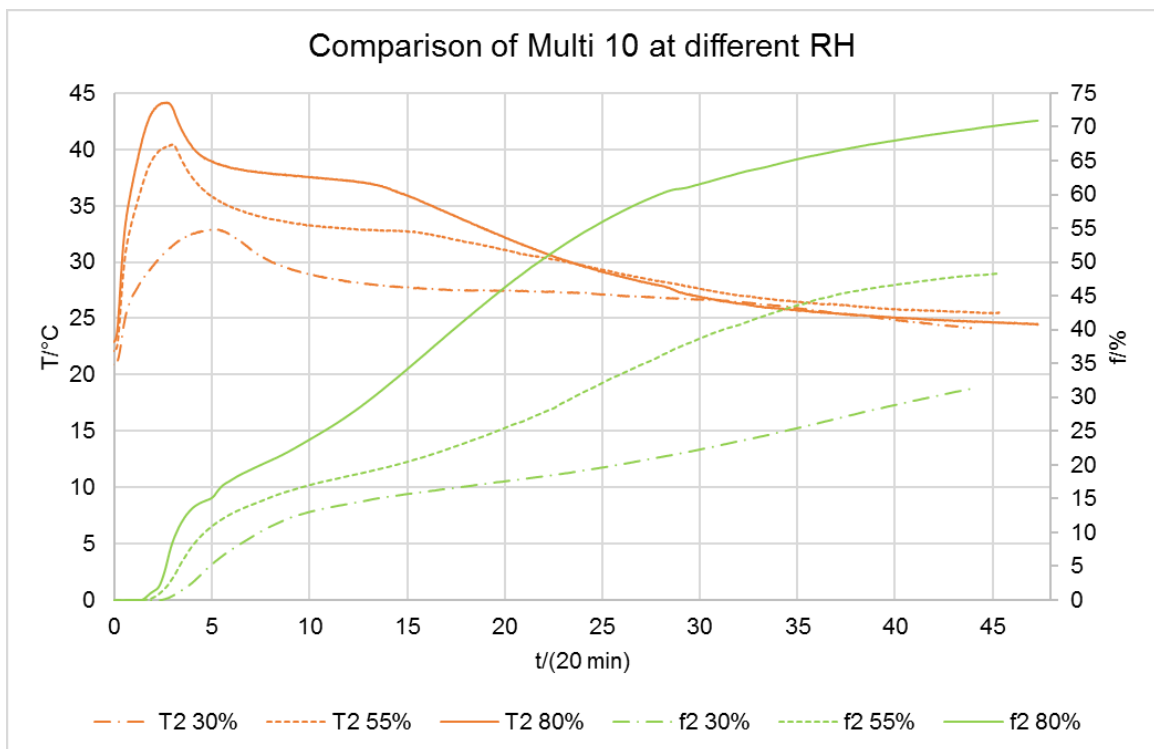
Illustration 4-9: Thermal behaviour of Multi 10.

At a higher $CaCl_2$ amount, all curves (temperature and breakthrough) show a saddle. Obviously, dissolution of the salt occurs. Due to the salt solution present, the pressure conditions in the reactor change. Also, ion exchange effects come into play. It is possible that ion exchange phenomena do already occur during the production of the composites. At this point, additional ion exchange mechanisms further change the material composition. Phase

changes, hydrate form transitions, salt dissolution, flow condition changes and ion exchange effects naturally have a huge influence on the thermal behaviour of the material. All in all, they seem to lower the suitability of the material for its application.
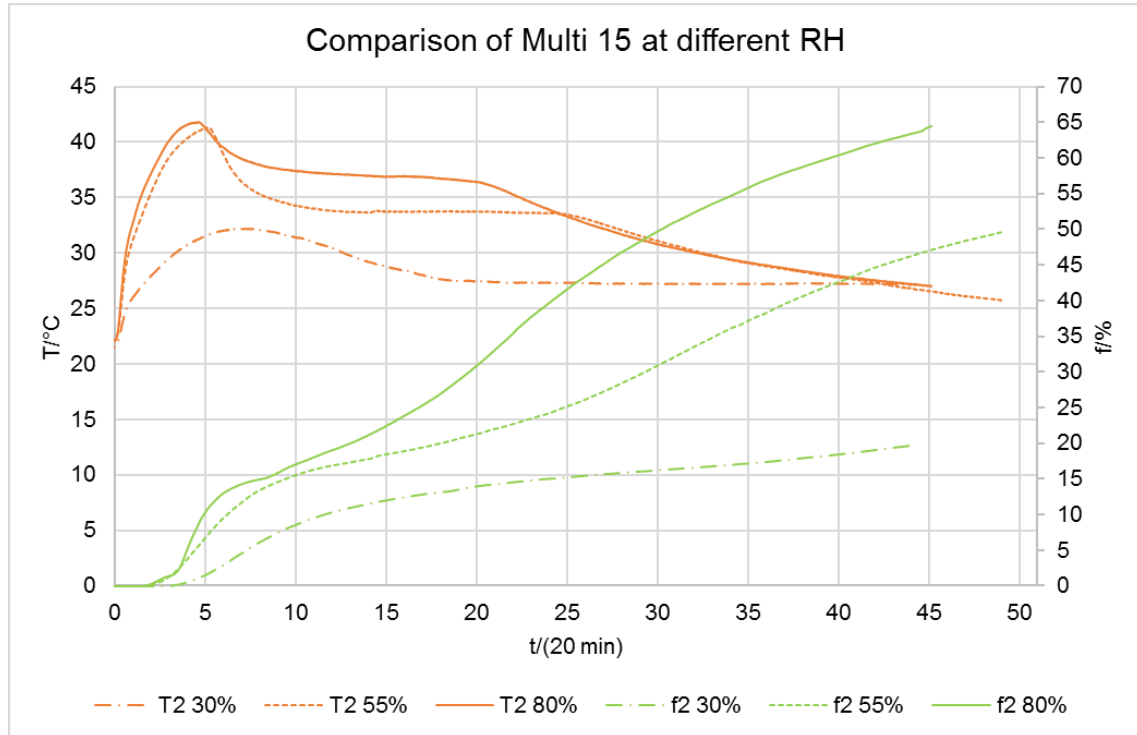
Illustration 4-10: Thermal behaviour of Multi 15.

The same effects as with Multi 10 can be observed.

Illustration 4-11: Thermal behaviour of Multi 20.

The same effects as with Multi 10 and Multi 15 can be observed. The higher the salt amount, the more salt dissolves and the more the results differ from the desired ones (s. **Illustration 4-12** and **Illustration 4-13**).

Illustration 4-12: Reactor after an experiment with Multi 20 at 80% RH.

Illustration 4-13: Multi 20 after an experiment at 80% RH.
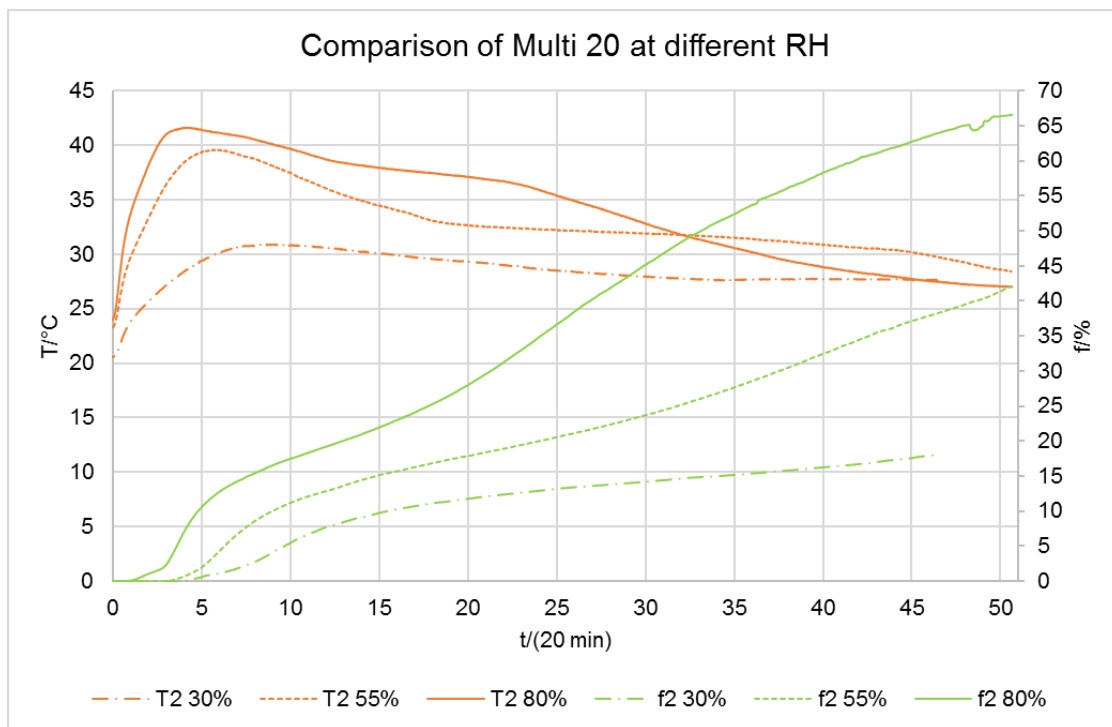
The overall optimisation problem regarding RH is that a higher RH level accounts for higher maximum temperature lifts but also increases the negative influence of salt dissolution mechanisms. As soon as the RH is below a critical limit, the resulting heat is below the level of usability.

Apart from the negative influence of the salt dissolution on the thermal behaviour, it also causes the corrosion of the reactor. After every experiment, the reactor has to be thoroughly cleaned.
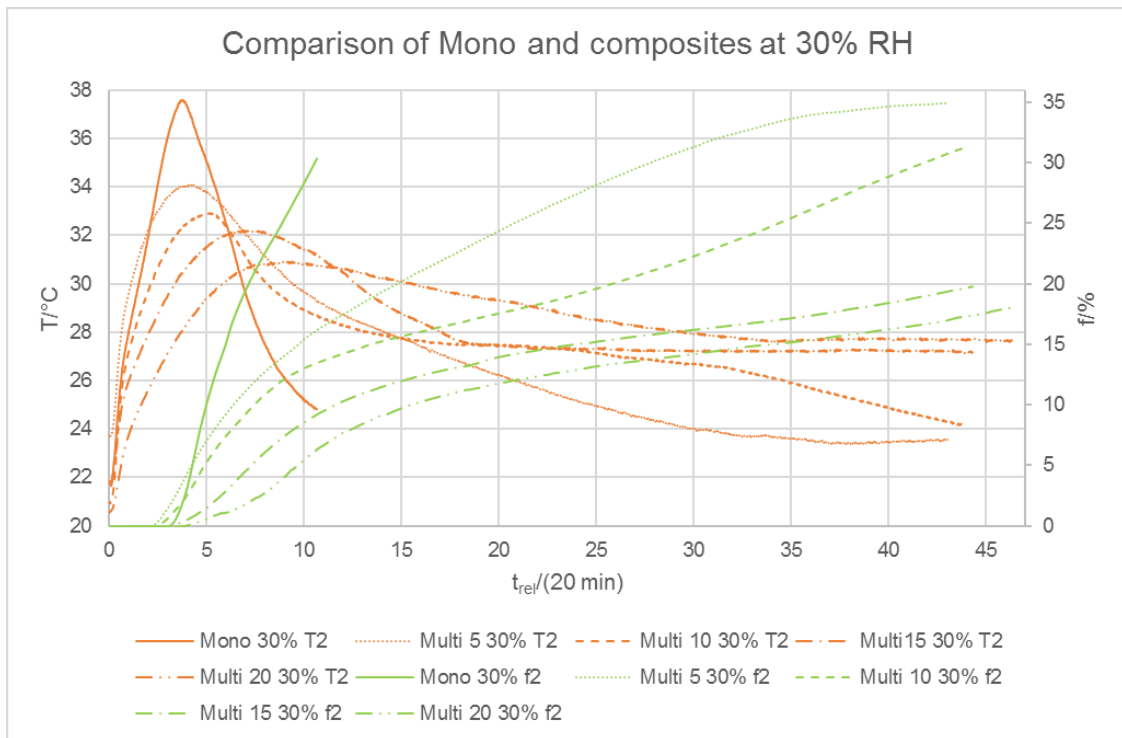
Illustration 4-14: Comparison of natural materials at 30% RH.

Illustration 4-15: Comparison of natural materials at 55% RH.
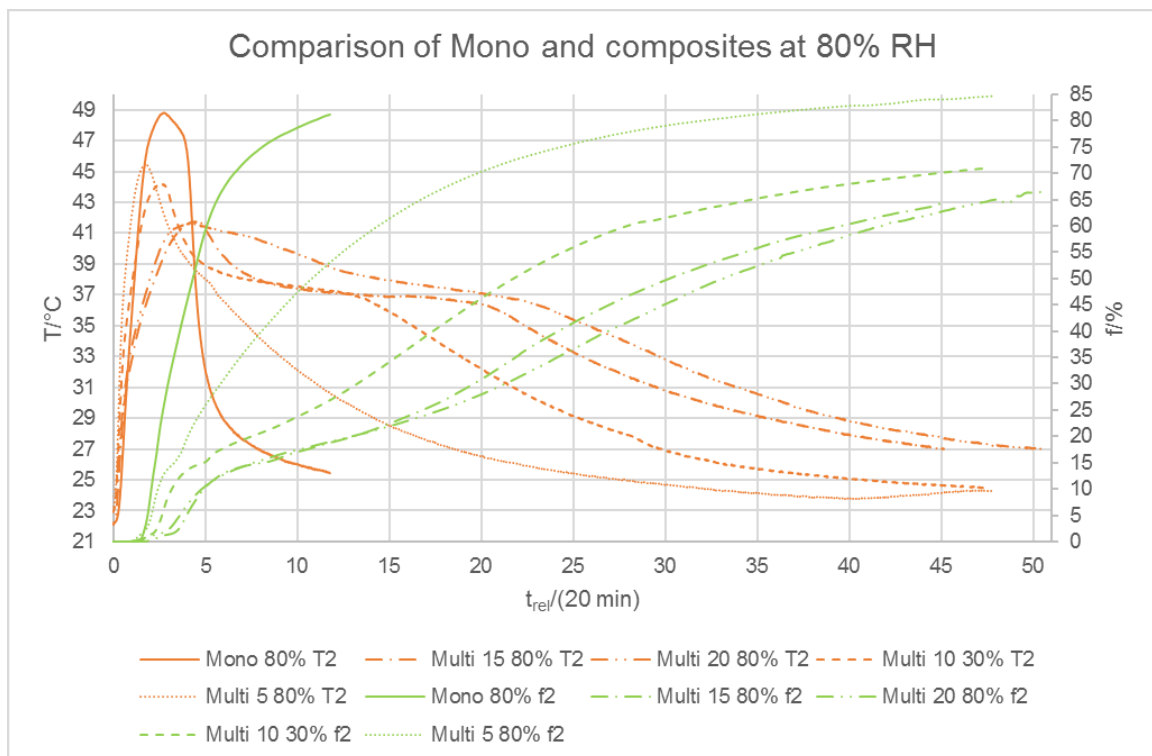
Illustration 4-16: Comparison of natural materials at 80% RH.

All three diagrams comparing all natural materials (pure and composite) show the same pattern and trend in the change of the maximum temperature lift, in the change of the breakthrough curve, in the extension of the experiment duration and in the time after which the maximum temperature is reached. Generally, the composite materials show a very sudden incline in temperature at the bottom of the reactor, while the temperature increase at the second thermocouple is a little more moderate.

In general, higher salt loads seem to intensify all the problems that come with the salt dissolution instead of increasing the suitability of the materials for thermochemical energy storage applications.

4.2.6 Thermal Properties of Multi 5 S

Illustration 4-17 shows the thermal properties of Multi 5 S at 30% and 80% RH.
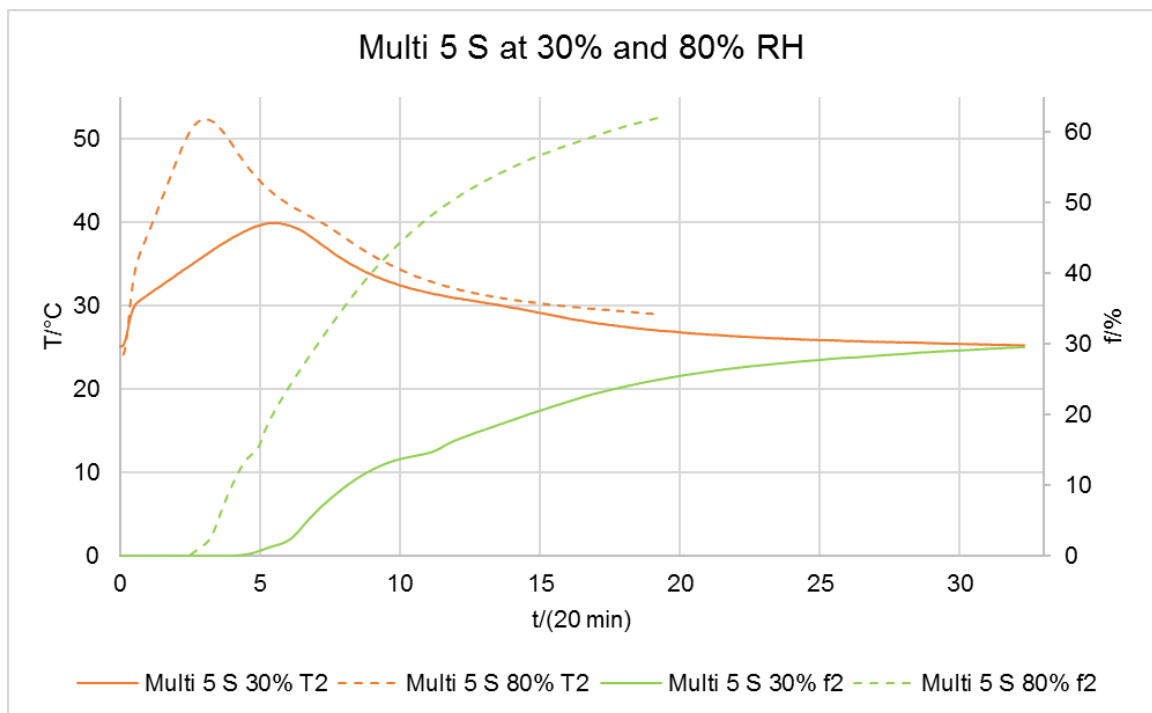
Illustration 4-17: Thermal behaviour of Multi 5 S.

The results are better than the ones with the hydrophobised Multi materials. Yet, the breakthrough curves are not steep either and the difference between these results and the ones of the Mono materials is minute. It seems that the salt alone does not cause as much pore congestion as the hydrophobicity treatment does. However, the salt is not stabilised and a lot of salt dust due to abrasion is clearly visible when filling the reactor already. (s. **Illustration 4-18**).

Illustration 4-18: Salt abrasion of Multi 5 S.

Furthermore, after the experiment, the height of the material bed in the reactor was reduced by roughly 1 cm. It seems that the salt was loosened from the zeolite matrix and filled the voids between the individual grains (s. **Illustration 4-19**).

Illustration 4-19: Material bed after an experiment with Multi 5 S.

It seems plausible that the results resemble those of the pure clinoptilolite. There is almost no salt component in the composite due to abrasion and the amount that is left does not properly adhere to the zeolite matrix.

4.2.7 Influence of Hydrophobicity on Composite Materials

The dissolution effects and the resulting negative influences on the thermal behaviour of the composites least affected Multi 5. Therefore, the non hydrophobised material Multi 5 S was also tested and compared to the hydrophobised composite. The results can be found in **Illustration 4-20**.
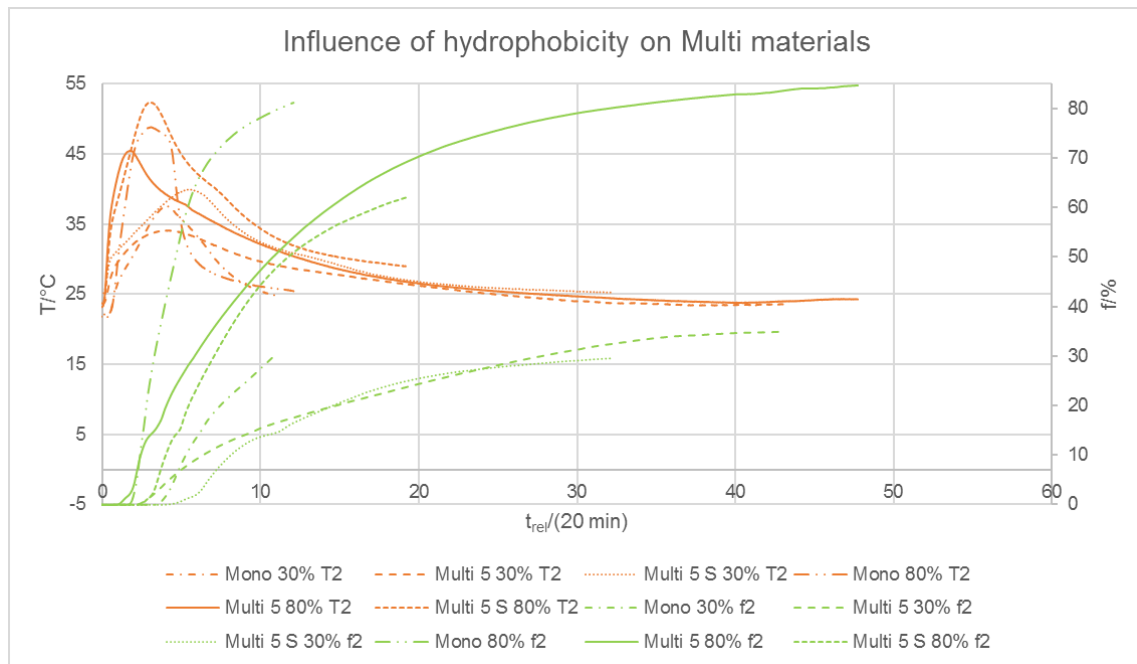
Illustration 4-20: Effect of hydrophobicity on Multi 5 S.

Again, even though the hydrophobicity treatment stabilises the salt effectively, congested pores or inaccessible surface area lower the beneficial effects of the Multi materials. The stabilising properties of the hydrophobicity can be seen in **Illustration 4-21**.
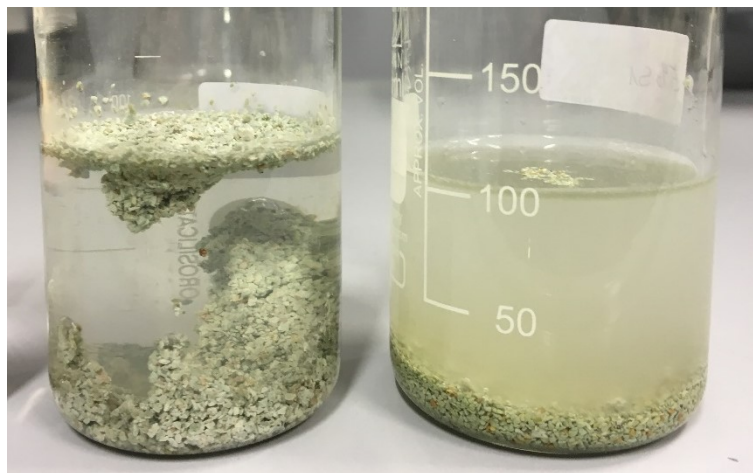
Illustration 4-21: Multi 5 (left) and Multi 5 S (right) in water.

4.2.8 Cycle Stability of Multi 5 Composite

In **Illustration 4-22**, the results of the examination of the cycle stability of Multi 5 can be seen. Cycle stability experiments with composites with higher salt amounts are unrewarding, because the dissolution is so distinct that cycle stability is foredoomed to failure.
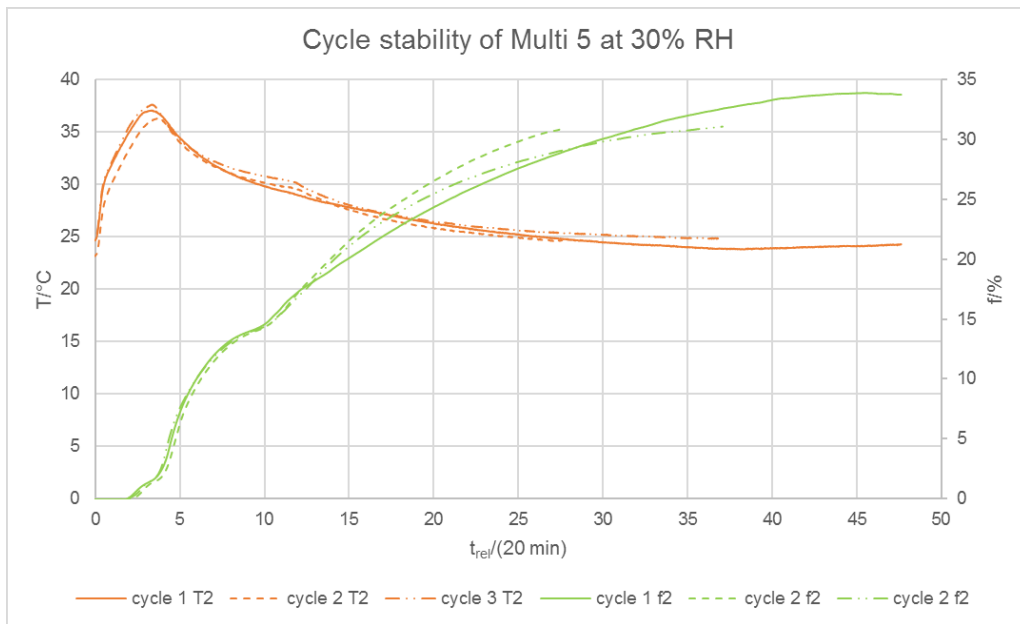
Illustration 4-22: Cycle stability test with Multi 5.

Cycle stability is given at low RH levels, because almost no salt liquefies. Yet, the heat is below the level of usability.

4.2.9 Cycle Stability of Multi 5 S Composite

Illustration 4-23 shows the results of the cycle stability experiments with Multi 5 S.
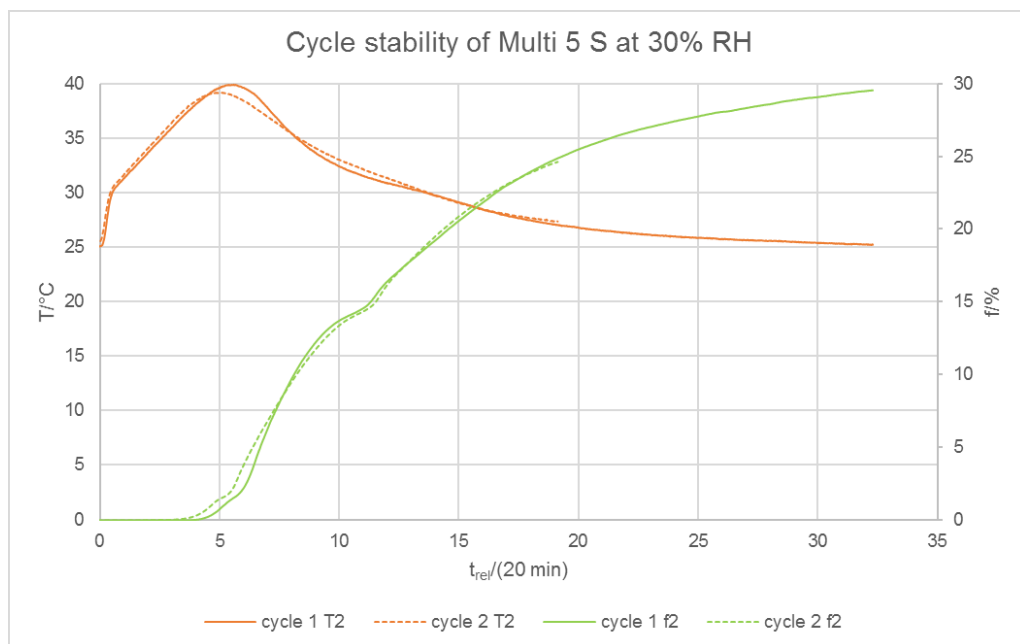
Illustration 4-23: Cycle stability test with Multi 5 S.

Again, cycle stability is given at low RH levels, because almost no salt liquefies. Yet, the heat is below the level of usability.

In this chapter, the thermal behaviour is described based on the slopes of the temperature and breakthrough curves as well as the temperature lifts. In the following chapter, the data is mathematically analysed and the key parameters energy density and usable heat are taken into consideration as well.

5 Data Analysis

The following chapter explains the methods used to evaluate the data registered by the evaluation unit in the experimental setup. In it, the determination and calculation of the characteristic parameters for the thermal properties of the sorption materials are explained.

5.1 Temperature Lifts

The electrical evaluation unit provides data in the form of Microsoft Excel .csv data sheets, which are converted into .xlsx documents. The results, one value every 20 seconds, are put into a single column, in which the individual values (temperature, RH, etc.) are separated by a comma. After separating the data, the column with the values from the upper temperature sensor (T2) are analysed. They start at room temperature, climb to some 80°C during the desorption phase and then drop to room temperature again. At some point, the temperature stays almost constant. When the air is led through the reactor and the adsorption phase begins, the temperature rises immediately. Therefore, it is very simple to pinpoint the start of the adsorption phase, that is, the baseline temperature value for the adsorption (t_{rel}=0) by hand. With the help of Microsoft Excel, it is a very simple task to find the maximum temperature that follows the adsorption starting point and subtract the baseline value. The results, the maximum temperature lifts, are shown in the following table and illustrations, **Table 5-1** as well as **Illustration 5-2**, **Illustration 5-3**, **Illustration 5-4** and **Illustration 5-5**. Before, the definition of the maximum temperature lift is shown in **Illustration 5-1**.
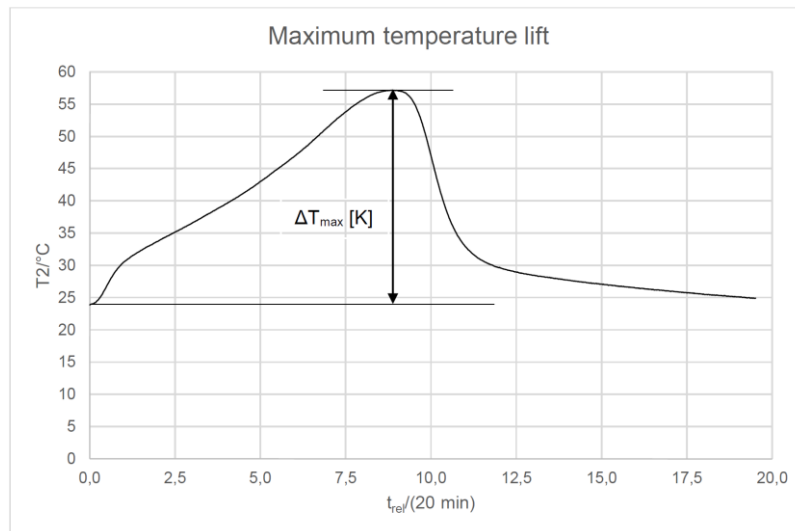
Illustration 5-1: Definition of the maximum temperature lift.

Table 5-1: Results – temperature lifts.

material	13XBF			13XBF H4		
f [%]	30	55	80	30	55	80
$T_{lift, 1}$ [°C]	18,60	29,54	41,53	18,04	28,27	39,52
$T_{lift, 2}$ [°C]	20,96	33,11	42,90	21,69	30,78	43,72
material	Mono			Mono H4		
f [%]	30	55	80	30	55	80
$T_{lift, 1}$ [°C]	16,08	24,30	35,48	14,32	24,05	33,24
$T_{lift, 2}$ [°C]	15,78	26,43	26,69	15,32	24,09	30,94
material	Multi 5			Multi 10		
f [%]	30	55	80	30	55	80
$T_{lift, 1}$ [°C]	15,25	25,95	27,43	15,16	25,22	30,65
$T_{lift, 2}$ [°C]	10,43	19,21	22,28	11,99	18,35	21,22
material	Multi 15			Multi 20		
f [%]	30	55	80	30	55	80
$T_{lift, 1}$ [°C]	16,31	24,98	33,43	15,86	25,36	25,40
$T_{lift, 2}$ [°C]	10,68	19,24	19,73	10,36	16,36	17,64

material/f [%]	Multi 5/30%			material	Multi 5 S	
cycle	1	2	3	f [%]	30	80
$T_{lift, 1}$ [°C]	15,43	15,89	16,13	$T_{lift, 1}$ [°C]	19,80	35,03
$T_{lift, 2}$ [°C]	12,40	13,12	12,77	$T_{lift, 2}$ [°C]	14,85	28,57

material/f [%]	Multi 5 S/30%	
cycle	1	2
$T_{lift, 1}$ [°C]	19,80	17,68
$T_{lift, 2}$ [°C]	14,85	13,70
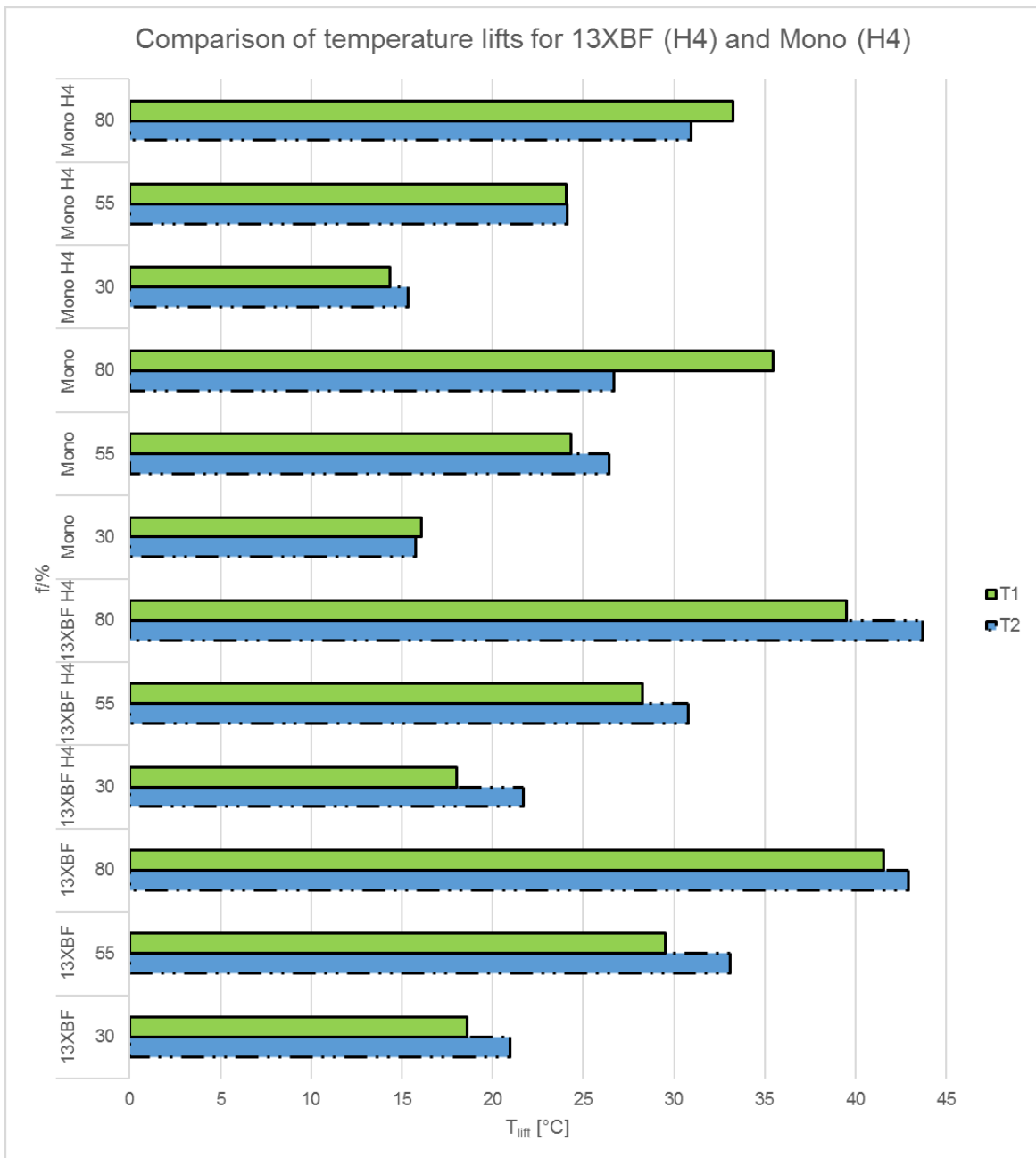
Illustration 5-2: Comparison of temperature lift results of the standard materials.

The layout of the result presentation as used in **Illustration 5-2** is also applied in the following graphs. The green columns represent the lower material temperature T1, the blue columns represent the upper material temperature T2. The different scaling of the graphs has to be considered.
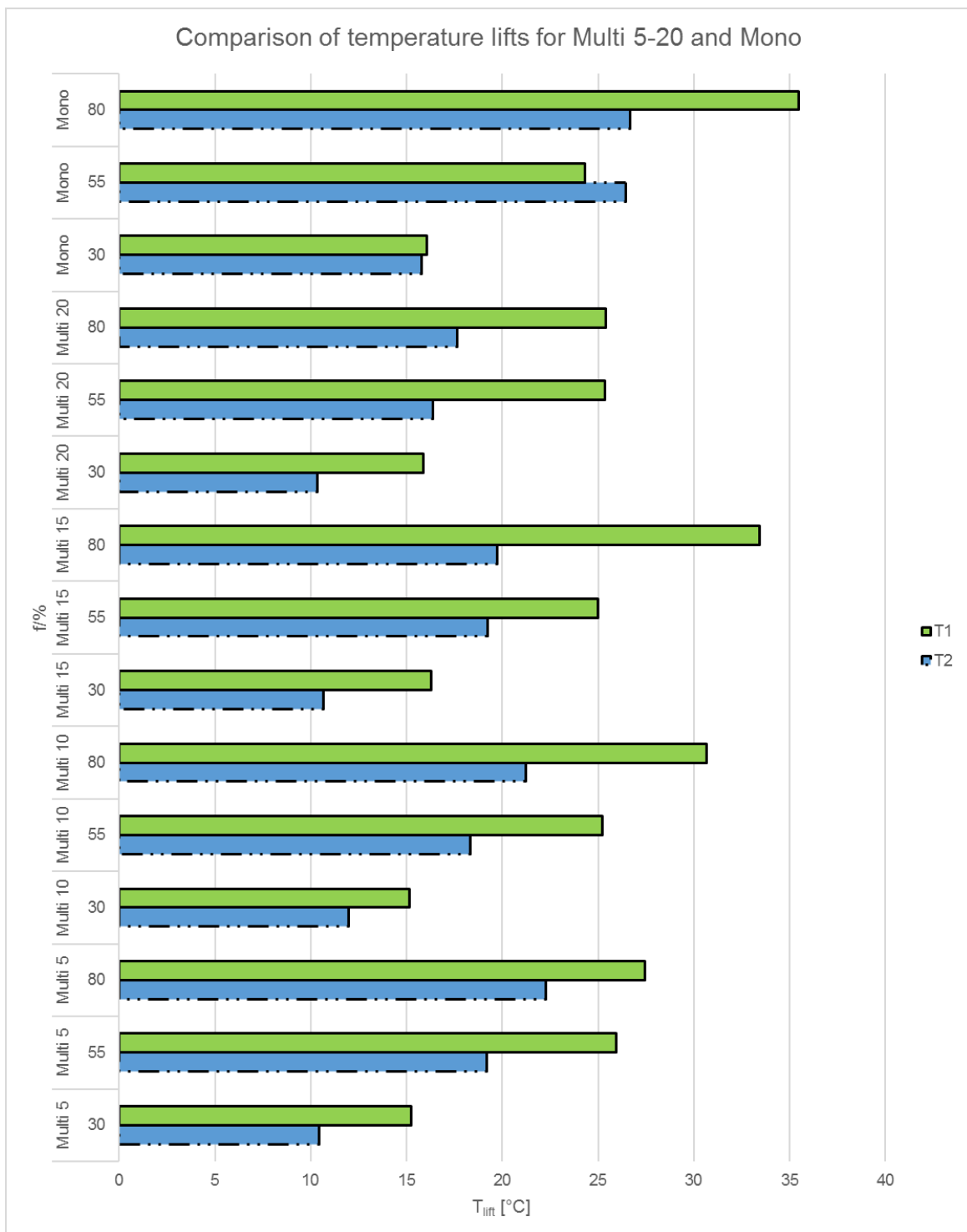
Illustration 5-3: Comparison of temperature lift results of composite materials.
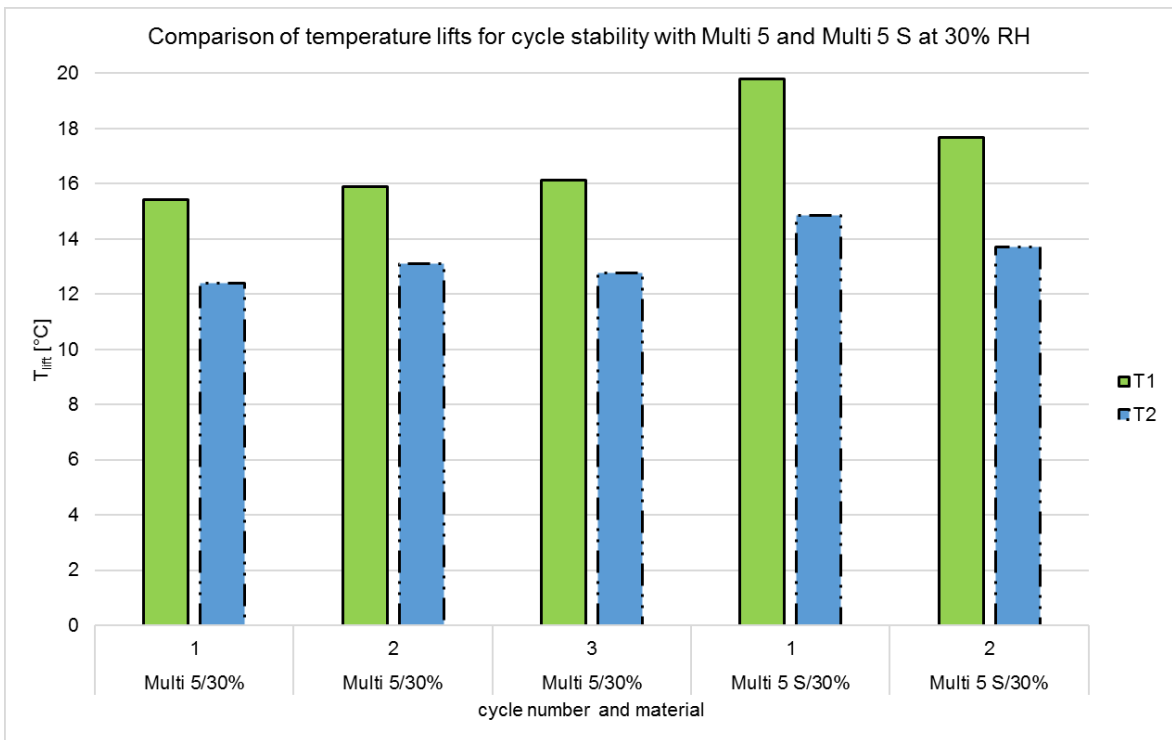
Illustration 5-4: Cycle stability – temperature lifts.
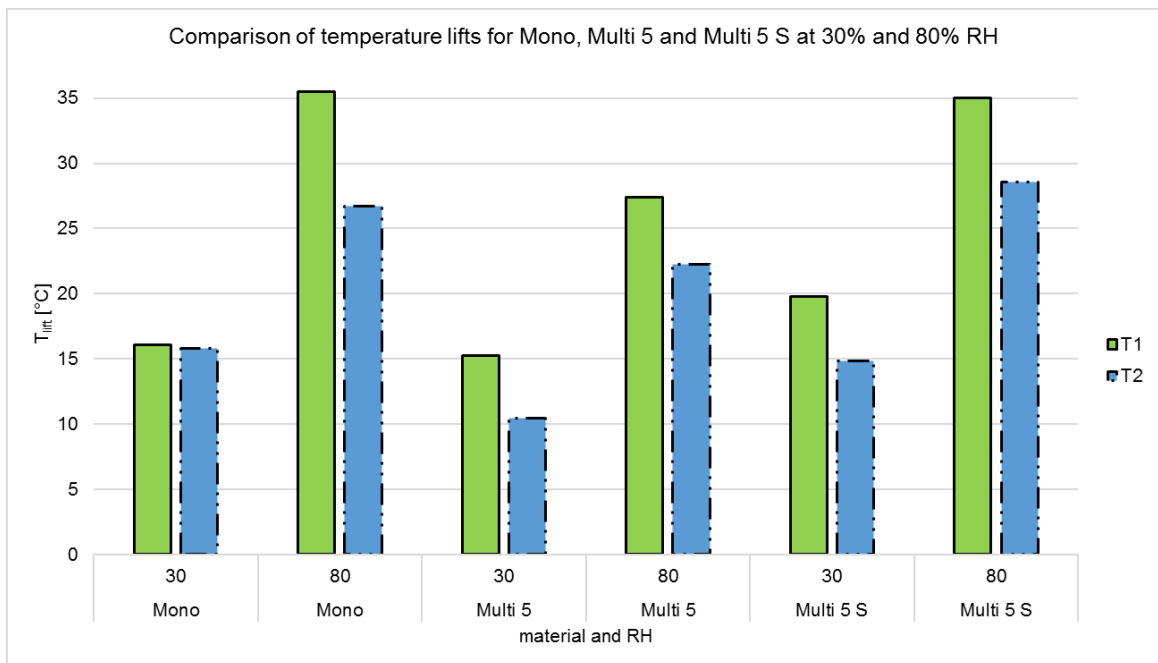
Illustration 5-5: Influence of hydrophobicity on temperature lifts.

The temperature lift trends resemble the graphic results of the temperature and breakthrough curves. At higher salt loads and RH values, the dissolution effects of the salt are

enhanced and the temperature lifts decrease. The performance of the Multi 5 S material lies in the range of Mono. For a more detailed description see also chapter 4.2.

5.2 Energy Density and Usable Heat

As explained in chapter 2.2, the energy density ρ_Q is an important indicator for the quality of energy storage materials. It represents the heat attainable by the air that is flowing through the reactor bulk. It is calculated as shown in chapter 2.2 grounded on basic heat engineering mathematics. In this case, the attainable heat in MJ is referenced to the bulk volume.

The electronic evaluation unit delivers values every 20 seconds, which is why the integral in the respective equations are replaced by a sum. For every time interval, the mean temperature is determined. The results of the multiplication are then summed up. The following illustrations, **Illustration 5-6** and **Illustration 5-7**, explain the process of determining the integral in the energy density equation.
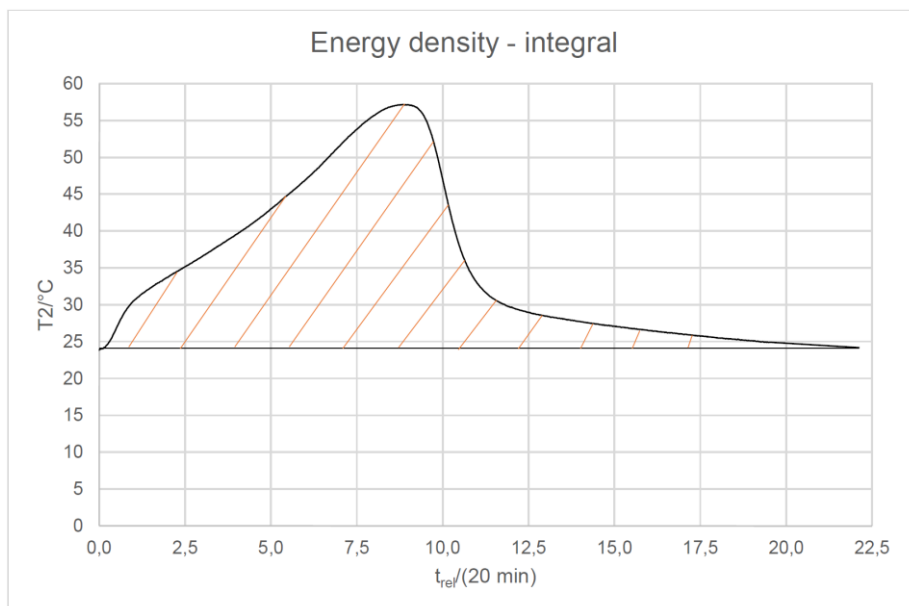
Illustration 5-6: Integral in the equation to determine the energy density.
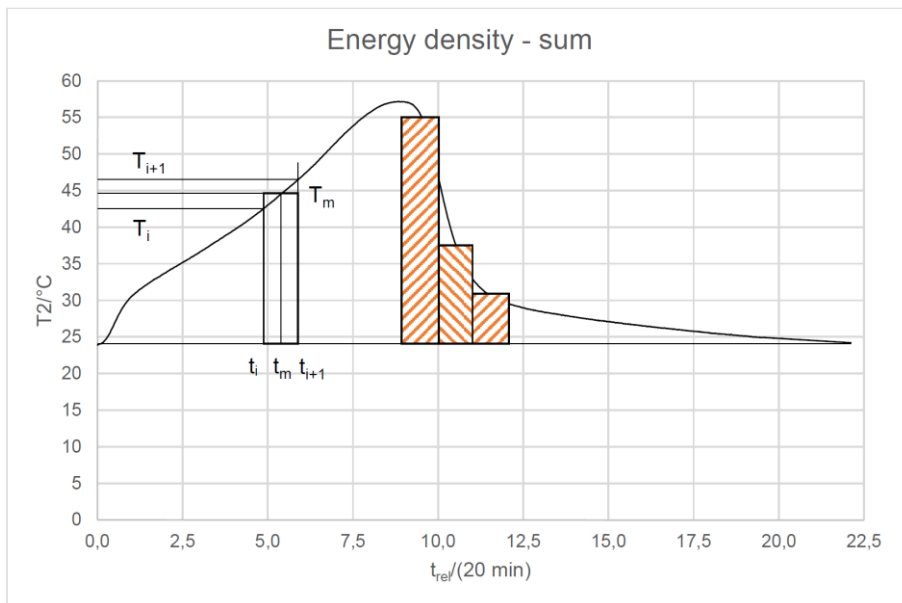
Illustration 5-7: Sum replacing the integral in the equation to determine the energy density.

The energy density indicator incorporates every temperature lift value. Yet, for reasonable technical applications, only temperatures over 40°C are usable. Hence, a second parameter, the usable heat of the adsorption Q_{use} is used to assess the value of the heat attained. Sometimes, the usable heat of the desorption is considered as well. In this case, the focus lies on the usable heat attainable by the materials and the heat produced through electrical heating is not considered. Its determination is based on the principle of the energy density determination, considering values over 40°C only. The evaluation principle is shown in **Illustration 5-8**.
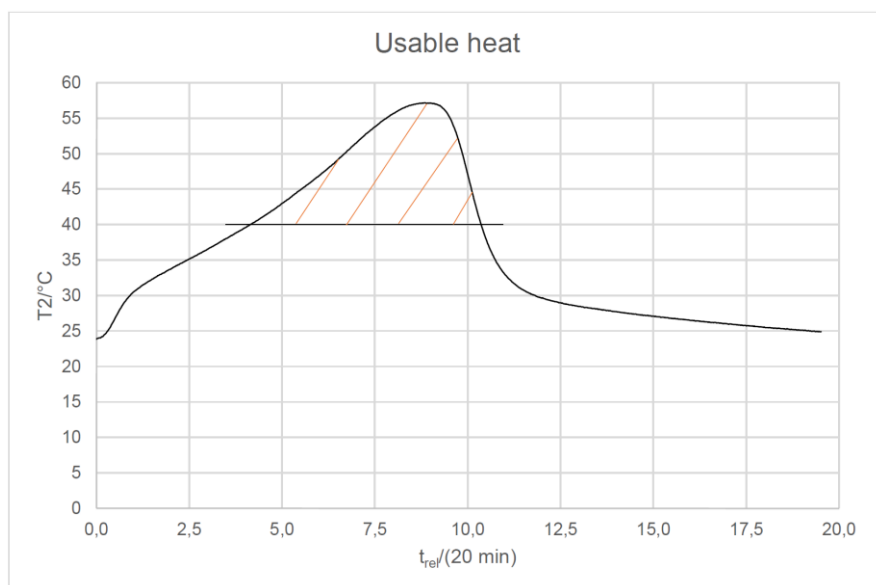
Illustration 5-8: Determination of the usable heat.

Just as with the energy density determination, the integral is replaced by a sum.

In most cases, the baseline temperature of the adsorption process is not the same as the final temperature. This can stem from altering room temperatures or a shortage of air and a consequent premature experiment abortion. Therefore, deviations from the actual energy density occur during the evaluation. Either the final temperature is higher than the baseline temperature or it is lower. The mistakes made in both cases are shown in **Illustration 5-9** and **Illustration 5-10**.
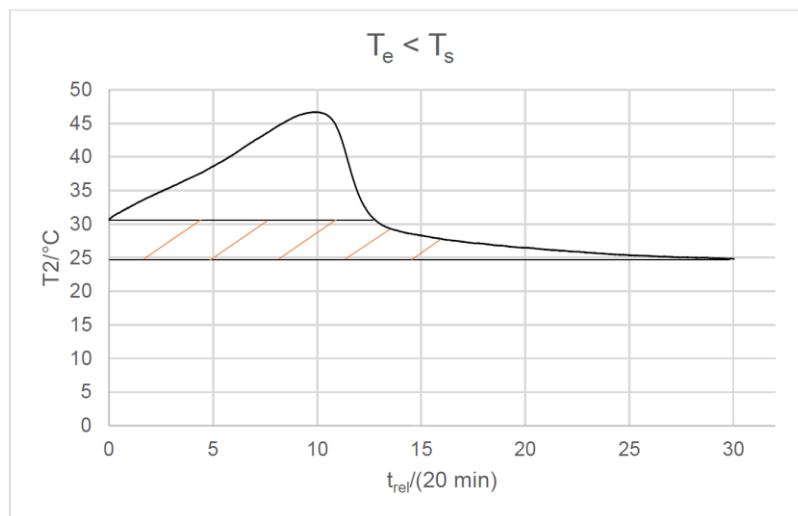
Illustration 5-9: Deviation from the actual energy density due to a final temperature lower than the initial temperature.
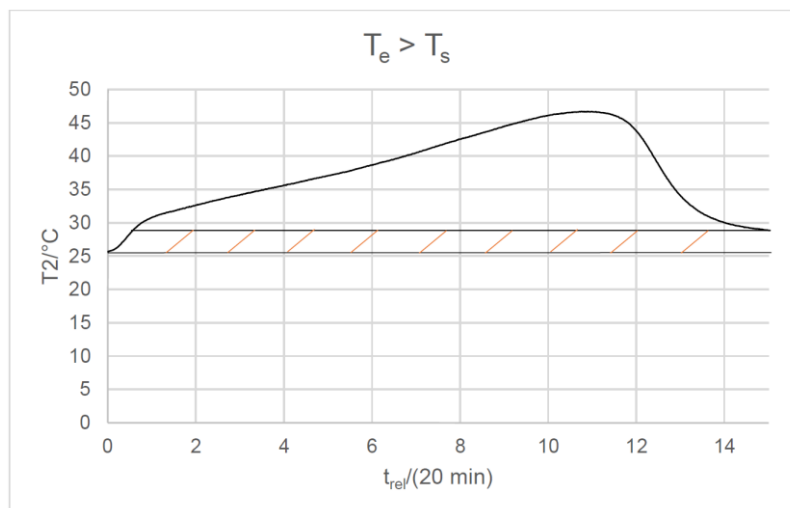
Illustration 5-10: Deviation from the actual energy density due to a final temperature higher than the initial temperature.

In all the standard materials the mistake made is usually low due to the minor difference between the baseline and final temperatures. With the composites at higher RHs, the mistake made is significantly higher due to the absent breakthrough (limited air supply per cylinder) and the shallow decline of the temperature during the end of the experiment. Yet, in order to illustrate the high energy densities obtainable compared to the almost non-existent usable heats with the composites qualitatively, the determination method is adequately exact. **Table 5-2** and **Table 5-3** show the evaluation method by the example of Multi 5 at 30%RH.

Table 5-2: Excerpt from the data sheet for the determination of ρ_Q for Multi 5 at 30% RH.

T2 [°C]	ΔT_m [K]	Δt [s]	$\Delta T_m \cdot \Delta t$ [Ks]	>0	$\Sigma (\Delta T_m \cdot \Delta t)$ [Ks]	ρ_Q [MJm^{-3}]
31,16	-	-	-	-	162524,99	147,39
31,19	7,52	21	157,82	157,82	-	-
31,22	7,55	20	150,90	150,90	-	-

Table 5-3: Excerpt from the data sheet for the determination of Q_{use} for Multi 5 at 30% RH.

T2 [°C]	$\Delta T_{m, use}$ [K]	Δt [s]	$\Delta T_{m, use} \cdot \Delta t$ [Ks]	>0	$\Sigma(\Delta T_{m, use} \cdot \Delta t)$ [Ks]	Q_{use} [MJm^{-3}]
31,16	-	-	-	-	0,00	0,00
31,19	-8,83	21	-185,33	0	-	-
31,22	-8,80	20	-175,90	0	-	-

The following substance properties and additional figures, listed in **Table 5-4** and **Table 5-5**, are needed in order to evaluate the experimental results.

Table 5-4: Required substance properties in order to calculate ρ_Q and Q_{use}. [39]

substance property	value	unit
$c_{p, air}$	1007,00	Jkg^{-1}K^{-1}
ρ_{air}	1,18	kgm^{-3}

Table 5-5: Additional figures needed in order to calculate ρ_Q and Q_{use}.

additional figures	value	unit
d_b	4,30	cm
h_b	11,00	cm
V_{sorb}	1,60E-04	m³
$\dot{V}_{air}$	8	lmin^{-1}
$\dot{m}_{air}$	1,57E-04	kgs^{-1}

ΔT_m describes the mean temperature lift between two temperature values. It results from the subtraction of the baseline temperature from the mean value of two T2 measuring points. $\Delta T_{m, use}$ does the same for the usable heat. In this case, 40°C are subtracted from every mean T2 value.

The columns captioned ">0" set all negative temperature lifts to zero. When the sum for all values $\Delta T_m \cdot \Delta t$ and $\Delta T_{m, use} \cdot \Delta t$, respectively, is determined, irrelevant data (mistake scenario two for the energy density and temperatures <40°C for the usable heat) is automatically not taken into account.

Table 5-6 as well as **Illustration 5-11**, **Illustration 5-12**, **Illustration 5-13**, **Illustration 5-14**, **Illustration 5-15** and **Illustration 5-16** show the results of the evaluations regarding energy density and usable heat.

Table 5-6: Results – energy density and usable heat.

material	13XBF			13XBF H4		
f [%]	30	55	80	30	55	80
ρ_Q [MJm^{-3}]	227,55	282,19	274,71	292,23	285,08	305,48
Q_{use} [MJm^{-3}]	27,92	72,64	106,27	24,14	41,70	115,24
material	Mono			Mono H4		
f [%]	30	55	80	30	55	80
ρ_Q [MJm^{-3}]	108,73	139,48	151,67	95,62	128,78	105,03
Q_{use} [MJm^{-3}]	0,00	20,96	24,52	0,00	7,78	23,10
material	Multi 5			Multi 10		
f [%]	30	55	80	30	55	80
ρ_Q [MJm^{-3}]	160,92	223,70	282,60	341,64	441,07	461,79
Q_{use} [MJm^{-3}]	0,00	4,93	10,04	0,00	0,24	8,43
material	Multi 15			Multi 20		
f [%]	30	55	80	30	55	80
ρ_Q [MJm^{-3}]	356,27	571,08	613,79	439,64	579,89	607,94
Q_{use} [MJm^{-3}]	0,00	1,80	3,64	0,00	0,00	7,66

material/f [%]	Multi 5/30%			material	Multi 5 S	
cycle	1	2	3	f [%]	30	80
ρ_Q [MJm^{-3}]	143,86	180,49	152,91	ρ_Q [MJm^{-3}]	184,08	158,56
Q_{use} [MJm^{-3}]	0,00	0,00	0,00	Q_{use} [MJm^{-3}]	0,00	43,32

material/f [%]	Multi 5 S/30%	
cycle	1	2
ρ_Q [MJm^{-3}]	184,08	165,33
Q_{use} [MJm^{-3}]	0,00	0,00

The layout used for the result presentation in the following graphs is always the same. The green columns always represent the energy density and the blue columns depict the usable heat values. The different scaling of the graphs has to be considered.
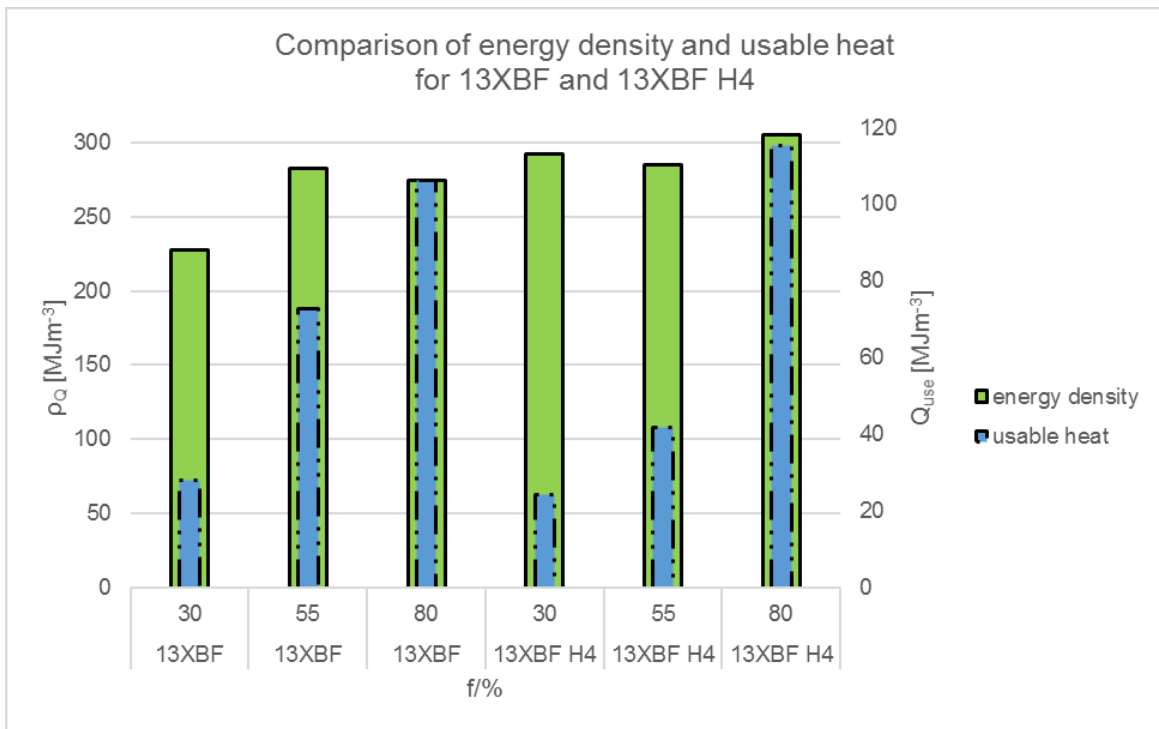
Illustration 5-11: Energy density and usable heat for 13XBF (H4).
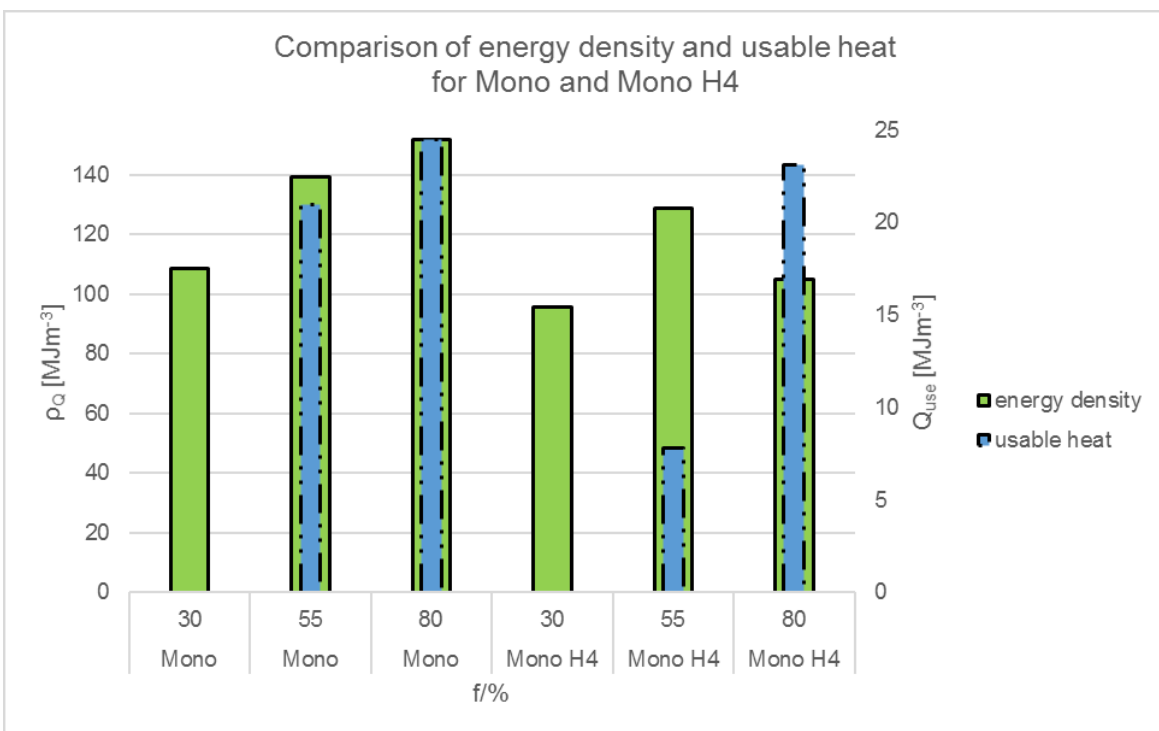
Illustration 5-12: Energy density and usable heat for Mono (H4).
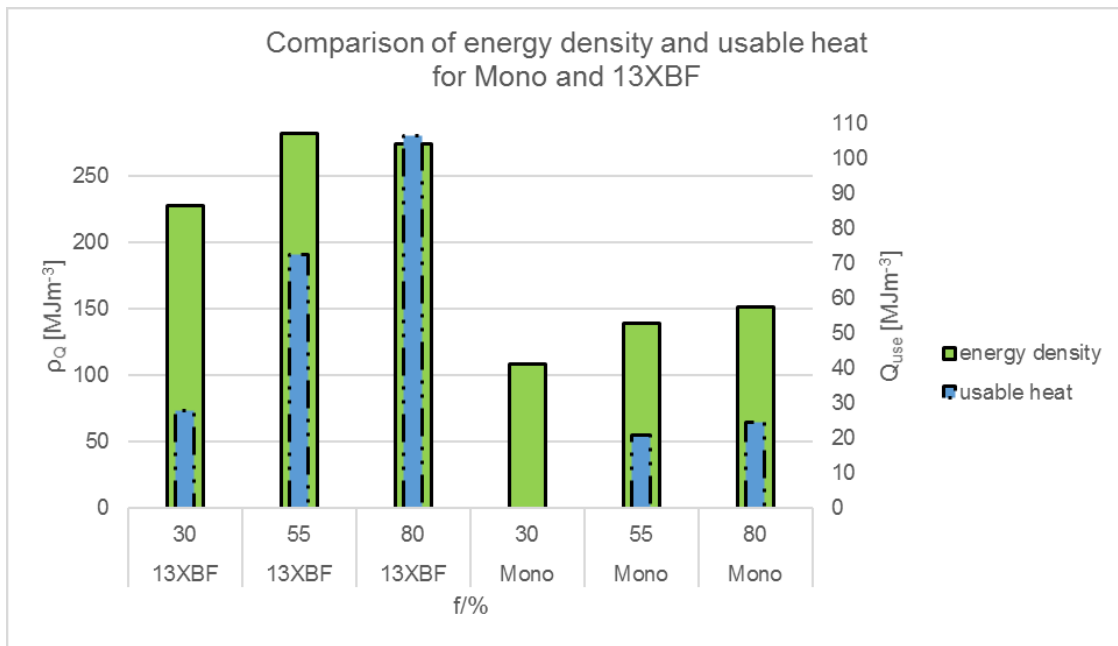
Illustration 5-13: Energy density and usable heat for Mono and 13XBF.
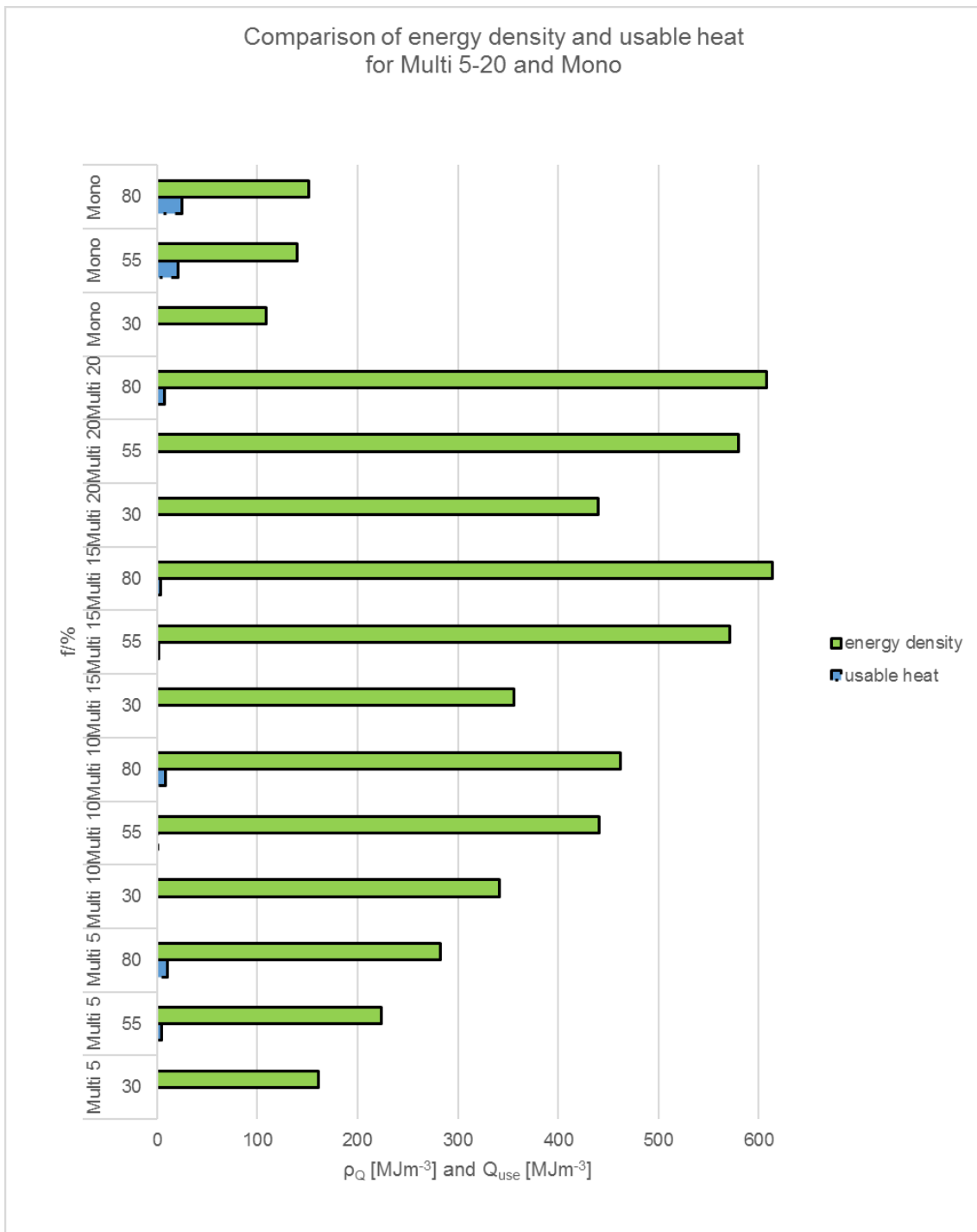
Illustration 5-14: Comparison of energy density and usable heat results of composite materials.
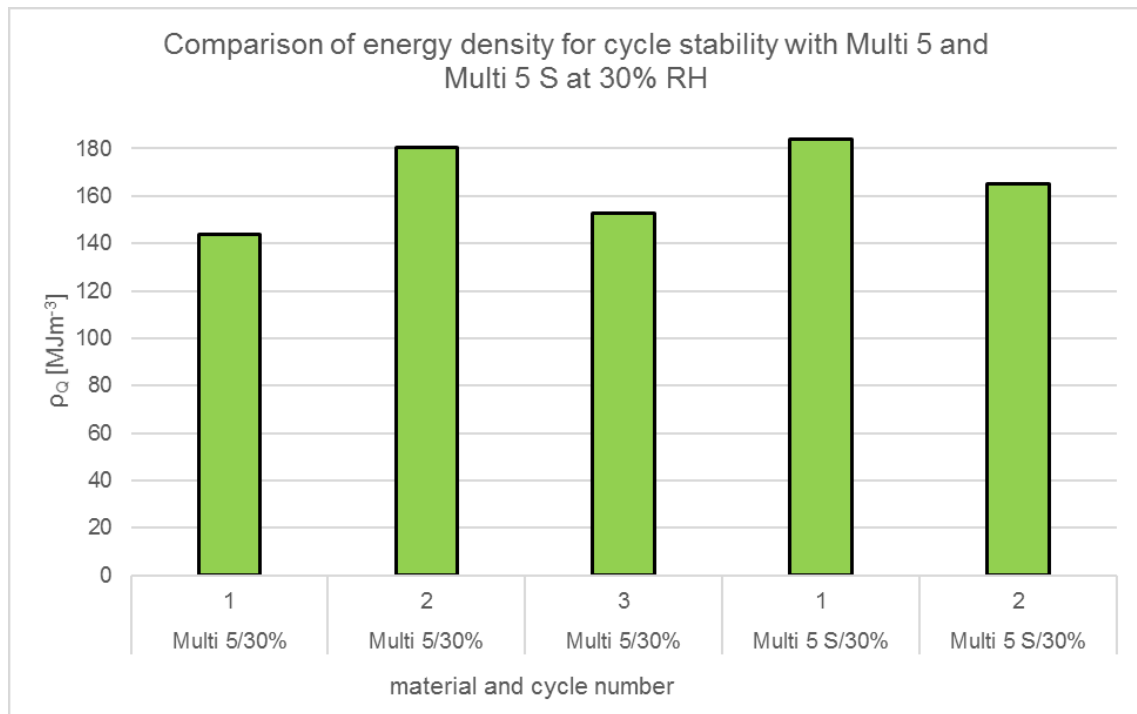
Illustration 5-15: Cycle stability – energy density and usable heat.
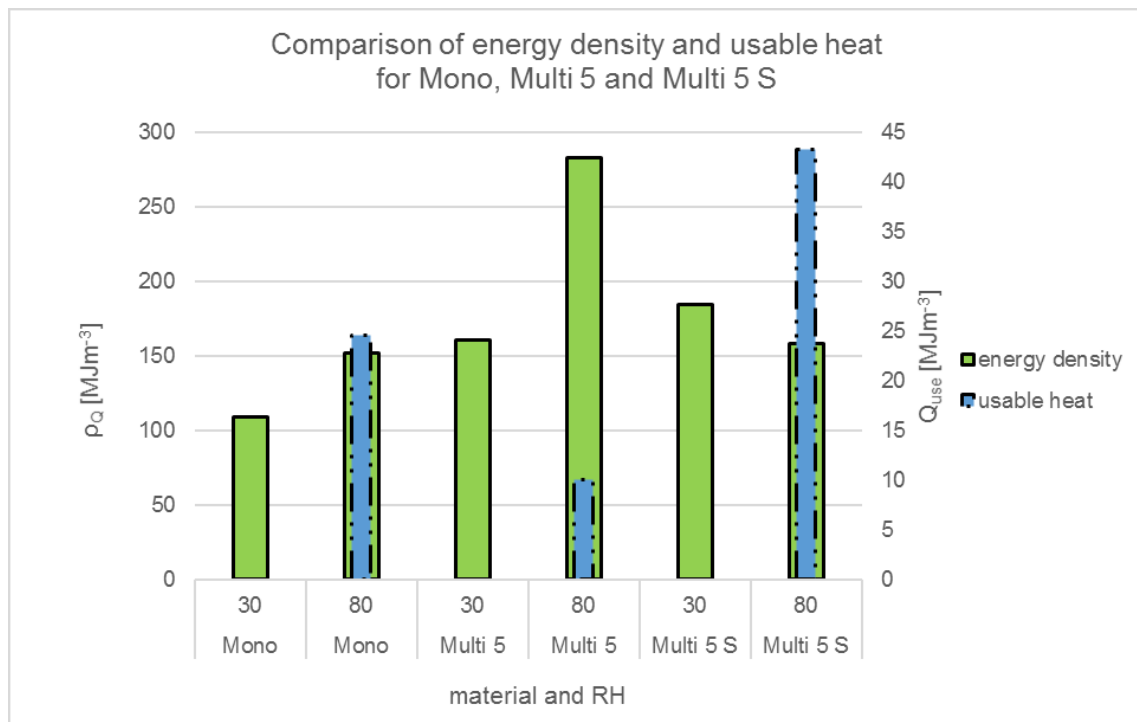
Illustration 5-16: Influence of hydrophobicity on energy density and usable heat.

The results for the energy density and usable heat of adsorption also resemble the graphic results of the temperature and breakthrough curves. The salt dissolution and the resulting effects prolong the adsorption phase but do not lead to high temperatures and a complete

breakthrough. Therefore, the calculated energy density values are extremely high whereas the usable heat values are almost non-existent.

At very low RH in the range of the deliquescence RH of the salt (30%), the dissolution effects are minor. Yet, the water molecule load of the air is so small that the sorption heat effects are nonviable. For a more detailed description also see chapter 4.2.

6 Interpretation and Conclusion

The aim of this thesis is to validate the suitability of a salt – zeolite composite material for its use in thermochemical energy storage applications. In order to achieve this aim, an appropriate experimental setup was established and used to investigate the thermal behaviour of several zeolite and composite materials. With the help of the conducted experiments, the research questions posed in chapter 1.3.1 can be answered sufficiently and adequately.

- How does the adjustment of the RH using gas washing bottles, deionised water and dew point temperature settings work?

With the help of literature research, analytical evaluation and laboratory experiments the initial method used to set the RH values using saturated salt solutions could be replaced by an application making use of the temperature dependency of the saturated vapour pressure. The results are extremely positive, for the RH value can be set as desired in a range between some 25% and 100%. The adjustment works very exact so that 5% steps are easily realised.

In fact, the experimental setup will be of further use to the Chair of Thermal Processing Technology in order to investigate the water uptake behaviour of bulk materials.

- How do the synthetic and natural zeolites (13XBF and Mono) behave during the adsorption process?

The 13XBF has an outstanding sorption behaviour reflecting the ideal concept that can be found in respective literature. Due to their regular structure, the materials adsorb the water molecules quickly and the zeolite bed is loaded layer by layer with almost no water molecule leaving the reactor before the complete material bed is loaded. As soon as the water uptake capacity is fully exhausted, the breakthrough curve shows a steep increase. High temperature lifts and in turn a high amount of usable heat can be achieved. This benchmark material proves

the enormous potential of the general long-term energy storage system that is widely investigated.

The natural Mono comes with irregularities in the pore structure and in a wide grain size distribution. As a result, the adsorption process does not happen as controlled as with the 13XBF. The breakthrough curves show a slope that is not as steep and the temperature lifts are lower. Yet, the mechanism is the same with a material that is way cheaper than the synthetic ones. It is only logical that the advancement of the natural material is investigated and that these investigations are sensible and promising.

The thermal behaviour of the 13XBF and Mono materials is well known. Still, the experiments conducted with them are important for the general understanding of the influence of the grain size and the pore structure on the sorption properties. For all further experiments, they serve as a benchmark.

- How does the hydrophobicity treatment influence the thermal behaviour of the zeolites Mono, 13XBF and Multi 5-20?

All Mono H4 and 13XBF H4 experiments again demonstrate the difference in the pore structure of the synthetic and the natural materials. While the influence on the synthetic materials is minute, the Mono materials are highly influenced. The irregular temperature curves are approximated to the regular ones of the 13XBF, but the temperature lifts as well as the energy density and usable heat values are decreased.

These results suggest that the hydrophobicity treatment does not affect the water uptake behaviour of the zeolite. The hydrophobic layer evidently does not impair the ability of the zeolite to adsorb water molecules. What it does to the natural zeolite, though, is that it seems to congest a part of the pores. Therefore, the total surface area available for the sorption process is reduced.

With the composite materials, the interpretation becomes more convoluted. Multi 5 S shows slightly better thermal properties than the Mono material (see the answer of the next research question on salt influence). Yet, the salt is not stabilised and cannot be held on the zeolite's inner surface. Therefore, cycle stability seems not to be within reach without any further treatment. This problem is tackled by the hydrophobicity treatment of the composite materials Multi 5-20 effectively. The visible salt abrasion when filling the reactor is minute. Also, the material does not create cloudy liquids if put in water. Cycle stability is therefore more feasible than without the treatment. Unfortunately, the pore congestion of the hydrophobicity treatment has such a huge impact on the overall performance that almost no usable heat can be detected

with the composites, even though the energy density values are extremely high due to the extension of the adsorption phase.

In conclusion, the used hydrophobicity treatment technique does not produce composite materials that are highly suitable for their use in sorption energy storage systems.

- Does the $CaCl_2$-impregnation improve the suitability of the natural zeolite to be used in sorption storage systems? If so, in what way? If not, why?

Multi 5 S shows a slightly better performance in the sorption experiments than Mono. In combination with the promising heats of hydration and chemical properties of the salt described in literature, it can be stated that the salt-impregnation does show a high potential of improving the performance of the natural zeolites. Chemical reactions do supplement the physical adsorption mechanisms in the resulting energy density and usable heat values.

Yet, the use of $CaCl_2$ does also raise a number of problems. First, the salt liquefies and causes corrosion. The presence of the liquid phase interferes with the whole sorption and reaction mechanism that is expected. With every sorption cycle, flow conditions change, ion exchange mechanisms occur and the salt composition is changed. Furthermore, the salt alone congests some of the pores of the zeolite, because it is not evenly distributed over the whole surface but can also form clumps. It has to be fixed for it does not firmly adhere to the zeolite surface. In the case of the used hydrophobicity treatment, even more pores seem to be congested.

All in all, the material is not yet suitable for its application. It can be summarised that the performed research was an eligible way to investigate the materials' sorption behaviour. It might seem that the results mar the utopic image of the material modification with salts. In fact, the conducted experiments immensely contributed to the understanding of the occurring phenomena in the sorption reactor. Based on the findings described, further research can be given direction in order to effectively and efficiently promote the development of long-term sorption energy storage systems and in turn emission-free and economical heating.

7 Outlook

In the introduction to this thesis, growth is mentioned – growth of the population, growth of the global economy and wealth, growth of the world's material consumption and a resulting growth of the planet's energy demand. If not common sense, legal restrictions force global research to focus on energy efficiency and low-emission technologies. Households are a suitable emission source to tackle for heating purposes add up to a huge part of said energy demand.

As a consequence, sorption energy storage systems integrated into the heating systems of houses are of enormous interest for research. They are not too good to be true. The underlying mechanism has continuously proven to work. Hence, their development will also be of interest in the future.

Based on the interpretation and conclusion in chapter 6, future research can be given direction. In the following, the two main aspects to tackle are commented.

- Salt selection

$CaCl_2$ shows a promising adsorption characteristic. In combination with its low price, it seems to be a suitable component of a composite sorption material. Nevertheless, it causes a lot of problems like corrosion. If the RH values used in the adsorption phase are so low that the salt does not liquefy, the water molecule load is so low that the achievable energy density and usable heat values are not sufficiently high. Further research might focus on the testing of the adsorption characteristics of different salts in combination with their deliquescence behaviour. A salt that is stable at RH values of some 55% that also shows reversible hydrate form transitions is desired.

- Stabilisation technique

The applied hydrophobicity treatment is highly successful when it comes to its effect on the stability of the salt on the zeolite's surface. However, it seems to congest micro- and mesopores. Its suitability is indisputable if its application is in systems where the material is exposed directly to liquid water. In the case investigated in the course of this thesis, it impairs the composite's suitability for the intended use.

If the problems found and described in this thesis can be tackled and solved, it is thinkable that the mentioned systems become applicable. In combination with an effective implementation in household heating systems, the achievable effect on carbon dioxide emissions is potentially massive.

8 Bibliography

[1]   World Bank, GDP per capita (current US$),
        http://data.worldbank.org/indicator/NY.GDP.PCAP.CD?display=graph, retrieved
        26.06.2016.

[2]   United Nations Population Division, World Population Prospects,
        https://esa.un.org/unpd/wpp/Graphs/Probabilistic/POP/TOT/, retrieved 26.06.2016.

[3]   Reichl, C., M. Schatz and G. Zsak, World Mining Data,
        http://www.wmc.org.pl/sites/default/files/WMD2016.pdf, retrieved 26.06.2016.

[4]   International Energy Agency, Key World Statistics 2015,
        https://www.iea.org/publications/freepublications/publication/KeyWorld_Statistics_2015.
        pdf, retrieved 26.06.2016.

[5]   Europäische Kommission, Europa 2020-Ziele, http://ec.europa.eu/europe2020/europe-
        2020-in-a-nutshell/targets/index_de.htm, retrieved 26.06.2016.

[6]   Umweltbundesamt Österreich, Energieeinsatz in Österreich,
        http://www.umweltbundesamt.at/umweltsituation/energie/energie_austria/, retrieved
        26.06.2016.

[7]   Aristov, Y. I., Current progress in adsorption technologies for low-energy buildings,
        Future Cities and Environment 1 (2015), 10.

[8]   Dyer, A., An introduction to zeolite molecular sieves, Wiley, Chichester, 1988.

[9]   Bish, D. L. and Ming, D. W., Natural zeolites, Mineralogical Society of America,
        Washington, DC, 2001.

[10] Mantell, C. L. and Hardy, C., Calcium metallurgy and technology, Reinhold Pub. Corp, New York, 1945.

[11] Falbe, J., Regitz, M. and Amelingmeier, E., Römpp Chemielexikon A-Cl, Thieme, Stuttgart, New York, 1989.

[12] Unterhalt, B., Pharmanorganische Chemie, Wiss. Verl.-Ges, Stuttgart, 2000.

[13] The Dow Chemical Company, Calcium Chloride Handbook, USA, 2003.

[14] Kwok, K., L. J. Mauer and L. S. Taylor, Phase behavior and moisture sorption of deliquescent powders, Chemical Engineering Science 65 (2010), 5639–5650.

[15] Mette, B., Experimentelle und numerische Untersuchungen zur Reaktionsführung thermochemischer Energiespeicher, Dissertation, Universität Stuttgart, Stuttgart, 2014.

[16] N'Tsoukpoe, K. E., Rammelberg, H. U., Lele, A. F., Korhammer, K, Watts, B. A., Schmidt, T. and W. K. L. Ruck, A review on the use of calcium chloride in applied thermal engineering, Applied Thermal Engineering 75 (2015), 513–531.

[17] Paltentaler Minerals GmbH, 2015, Report on sorption material development Deliverable 5.1. With assistance of Montanuniversität Leoben, Leoben.

[18] Kerskes, H., F. Bertsch, B. Mette, A. Wörner and F. Schaube, Thermochemische Energiespeicher, Chemie Ingenieur Technik 83 (2011), 11, 2014–2026.

[19] Meier, S. J., Grundlagen und Möglichkeiten einer Hydrophobierung von Betonbauteilen, Aedificatio-Verl., Freiburg Breisgau, 2002.

[20] Gerdes, A. and F. H. Wittmann, Hydrophobieren von Stahlbeton Teil 1: Transport und chemische Reaktionen silicium-organischer Verbindungen in der Betonrandzone, International Journal for Restoration of Buildings and Monuments 9 (2003), 1, 41–64.

[21] Meier, S. and M. Bäuml, Internal Impregnation of Concrete by Means of Silanes, Restoration of Buildings and Monuments 12 (2006), 1, 43–52.

[22] Leitner, H., 2016, Production process of hydrophobised composites, Telephone conversation to Daniela Meitner, Leoben, 19.04.2016.

[23] Meitner, D. and H. Raupenstrauch, 2016, Ion Exchanging Behavior of Composite Materials for Thermal Energy Storage, Montanuniversität Leoben, Leoben.

[24] Aristov, Y. I., New Family of Solid Sorbents for Adsorptive Cooling: Material Scientist Approach, Journal of Engineering Thermophysics 16 (2007), 2, 63–72.

[25] Wu, H., S. Wang and D. Zhu, Effects of impregnating variables on dynamic sorption characteristics and storage properties of composite sorbent for solar heat storage, Solar Energy 81 (2007), 864–871.

[26] Bathen, D. and Breitbach, M., Adsorptionstechnik, Springer, Berlin, 2001.

[27] Bird, R. B., Stewart, W. E. and Lightfoot, E. N., Transport phenomena, Wiley, New York, 2007.

[28] Rouquerol, F., Rouquerol, J., Sing, K. S. W., Llewellyn, P. L. and Maurin, G., Adsorption by powders and porous solids, Elsevier/Academic Press, Amsterdam, 2014.

[29] Paksoy, H. Ö., Thermal Energy Storage for Sustainable Energy Consumption, Springer, Dordrecht, 2007.

[30] Levitskij, E. A., Y. I. Aristov, M. M. Tokarev and V. N. Parmon, Chemical Heat Accumulators: A new approach to accumulating low potential heat, Solar Energy Materials and Solar Cells 44 (1996), 219–235.

[31] Inglezakis, V. J., The concept of "capacity" in zeolite ion-exchange systems, Journal of Colloid and Interface Science 281 (2005), 68–79.

[32] Hauer, A., 2015, Assumption regarding exit air temperature, Telephone conversation to Daniela Meitner, Leoben, 07.12.2015.

[33] Hauer, A., Beurteilung fester Adsorbentien in offenen Sorptionssystemen für energetische Anwendungen, Dissertation, Technische Universität Berlin, Berlin, 2002.

[34] Etling, D., Theoretische Meteorologie, Springer-Verlag Berlin Heidelberg, Berlin, Heidelberg, 2008.

[35] Dobrinski, P., Krakau, G. and Vogel, A., Physik für Ingenieure, Vieweg + Teubner, Wiesbaden, 2010.

[36] Hengstenberg, J., Messen und Regeln in der chemischen Technik, Springer, Berlin, 1964.

[37] Kutzelnigg, A. and F. Königsheim, Die Einstellung der relativen Feuchte mit Hilfe von gesättigten Salzlösungen, Materials and Corrosion 14 (1963), 3, 181–186.

[38] Meitner, D., 2015, Experiment with 13XBF, E-mail message to Christoph Ponak, Leoben, 02.06.2015.

[39] VDI-Gesellschaft Verfahrenstechnik und Chemieingenieurwesen, VDI-Wärmeatlas, Springer Bln, Berlin, 2006.